

ANALYSIS OF SIGNALING AND CODING SCHEMES FOR NON-COHERENT ULTRA-WIDEBAND SYSTEMS

Younes Souilmi

Thèse

Présentée pour Obtenir le Grade de Docteur
de l'École Nationale Supérieure
des Télécommunications (ENST)

Spécialité: Communication et Electronique

Date de Soutenance: 24 Juin 2005

Composition du Jury:

Président	Prof. P. Comon, I3S (Sophia-Antipolis, France)
Rapporteur	Prof. R. Kohno, YNU (Yokohama, Japan)
Rapporteur	Prof. H. Bolcskői, ETHZ (Zurich, Swizerland)
Examineur	Prof. G. Caire, EURECOM (Sophia-Antipolis, France)
Examineur	Prof. J. Boutros, ENST (Paris, France)
Directeur de Thèse	Prof. Raymond Knopp, EURECOM (Sophia-Antipolis, France)

Thèse réalisée au sein de l'Institut Eurecom

© Younes Souilmi 2005

AUTHOR'S ADDRESS:

Younes Souilmi

Institut Eurecom

Departement de Communication Mobile

2229, route des Crêtes

B.P. 193

06904 Sophia-Antipolis – France

Email: Younes.Souilmi@eurecom.fr

URL: <http://www.eurecom.fr/~souilmi>

Summary

Ultra-wideband (UWB) radio is a new emerging technology which promises to bring a real revolution in the field of local area wireless communications. UWB is based on a shift in spectrum management paradigm which consists on allowing users to transmit over a shared bandwidth of several GHz rather than allocating private bandwidth to each user. No significant interference is caused to other UWB users nor to other systems coexisting on the same frequency bandwidth thanks to the fact that the transmitted power is constrained to have a very low spectral density.

Given the huge bandwidth used by UWB systems, the latter operates in the low spectral efficiency regime. In our work we investigate the impact of UWB characteristics on the design of adequate signalling and coding schemes. Motivated by the fact that channel knowledge is not required to achieve channel capacity for vanishing spectral efficiency, we consider non-coherent type of detection. We first evaluate the performance of practical non-coherent schemes using on-off signalling. We then investigate the impact of channel estimation, made possible by channel stationary, on system performance and show at which extent practical coherent UWB systems can outperform non-coherent ones.

Later we introduce a multi-carrier UWB signalling scheme which generalizes the concept of on-off signalling to the time-frequency 2-dimensional signalling space. We analyze the performance of this signalling scheme by deriving lower and upper bounds on its achievable data rates over the set of all frequency taps correlation profiles.

We then consider UWB on-off signalling in the context of peer-to-peer multiple access networks. We propose a quantized threshold-based non-coherent receiver whose performance is shown to approach the performance of a genie aided receiver.

Finally we propose some practical channel code constructions that are specially designed for non-coherent UWB m -ary PPM systems. The code design uses an exit chart analysis. Code performance is then measured through simulations.

Resumé

La transmission Ultra large bande (UWB) est une nouvelle technologie qui promet d'engendrer une réelle révolution dans le domaine des réseaux locaux de communications sans fil. UWB est basée sur un changement de la philosophie de gestion du spectre de fréquence radio. La transmission UWB s'effectue sur une bande de fréquence partagée de plusieurs GHz contrairement aux systèmes de transmission classiques qui utilisent des bandes de fréquence étroites sur lesquelles ils bénéficient de l'exclusivité du droit de transmission. Ceci est rendu possible grâce à la contrainte, sur la densité spectrale de puissance transmise, imposée aux transmissions UWB et qui implique qu'ils ne génèrent aucune interférence, de puissance significative, ni aux autres systèmes radio avec lesquels ils coexistent ni aux autres utilisateurs UWB se trouvant aux alentours.

Étant donné les normes bandes de fréquence utilisées par la transmission UWB cette dernière opère dans le régime de transmission à très faible efficacité spectrale. Dans le cadre de cette thèse on explore l'impact des caractéristiques de la transmission UWB sur le design optimal de certains aspects de sa couche physique. Étant donné que, pour une efficacité spectrale égale à zéro, la connaissance de la réalisation du canal de transmission n'est pas nécessaire pour atteindre la capacité on considère dans le cadre de notre étude les schémas de détection non-cohérente. On commence par évaluer les performances des détecteurs non-cohérents pratiques associés à une transmission On-off. Par la suite on analyse l'impact de la connaissance partielle du canal, pouvant être obtenue grâce à la stationnarité du canal, sur les performances du système et on montre jusqu'à quel point cela permet d'améliorer les performances par rapport à celles d'un détecteur non-cohérent. En suite on introduit un mode de signalisation UWB utilisant des multi-porteuses qui correspond à une généralisation du concept de la signalisation On-off au cas bi-dimensionnel temps-fréquence. On analyse les performances de ce système en développant des bandes inférieure et supérieure sur les taux de transmission atteignables. En suite on s'intéresse à la transmission UWB On-off dans le contexte d'un réseau d'accès multiple peer-to-peer. On propose un détecteur d'énergie à seuil quantifié et on montre qu'il atteint des performances très proches d'un récepteur non-cohérent qui bénéficie d'informations sur les transmissions des interférents obtenues grâce à un oracle. Finalement nous proposons

quelques schmas de codage construits spcialement pour la transmission UWB PPM avec rcepteur non-coherent. Le design des codes est ralise grce a la technique des exit charts puis les performances values par des simulations.

List of Tables

List of Figures

I-1	FCC indoor UWB emission spectrum mask ([13])	7
II-1	CDF of total channel received energy	14
II-2	Example Eigenvalue Distribution: $T_d=50$ ns, $W=1$ GHz. Mean value indicated by a horizontal bar	15
II-3	Capacity versus SNR:different scattering environments. $T_d=25$ ns, $W=1$ GHz. The AWGN capacity is equal to $W \log \left(1 + \frac{P}{WN_0} \right)$	18
II-4	Capacity versus SNR:different bandwidths. $T_d=25$ ns	19
II-5	Multiband signaling: Capacity versus distance, different bandwidths. $T_d=25$ ns	20
II-6	Multiband signaling	21
II-7	Data rates versus E_b/N_0 . $T_d=25$ ns, $W=500$ MHz	22
II-8	Achievable data rates of <i>On-off</i> signaling versus m -ary PPM. $T_d=25$ ns, $W=1$ GHz	25
II-9	Channel matched non-coherent receiver	26
II-10	Mismatched non-coherent receiver	27
II-11	Comparison of the achievable data rates of the considered practical non-coherent receivers. A typical (i.e. $\alpha = 0.1$) scattering environment is considered. $T_d=25$ ns, $W=1$ GHz.	31

III-1 ML detection rule with orthogonal codebooks: upper bound on BLER versus the transmission data rate for a fixed block size $N = 10000$ and different number of blocks per codeword B . SNR=50dB, $T_d=25\text{ns}$, $T_p=1\text{ns}$	50
III-2 ML detection rule with orthogonal codebooks: upper bound on BLER versus the transmission data rate for fixed codeword length $BN = 200000$ and different block size values N . SNR=50dB, $T_d=25\text{ns}$, $T_p=1\text{ns}$	51
III-3 ML detection rule with orthogonal codebooks: upper bound on BLER versus the transmission data rate for fixed block size $N = 5000$ and number of blocks per codeword $B = 40$ and different SNR values. $T_d=25\text{ns}$, $T_p=1\text{ns}$	52
III-4 ML detection rule: orthogonal codebooks versus random codebooks. upper bound on BLER versus the transmission data rate for fixed block size $N = 5000$ and number of blocks per codeword $B = 40$ and different SNR values. $T_d=25\text{ns}$, $T_p=1\text{ns}$	53
III-5 ML detection rule with orthogonal codebooks: upper and lower bounds on the BLER versus the transmission data rate for fixed block size $N = 5000$ and number of blocks per codeword $B = 40$. The figure also shows the lower bound on the error probability of the pure non-coherent receiver. $T_d=25\text{ns}$, $T_p=1\text{ns}$	54
IV-1 OFDM- <i>on-off</i> signaling	57
IV-2 Impulsive FSK	58
IV-3 Achievable rates versus distance: $T_s = 0.5\mu\text{s}$, $T_d = 30\text{ns}$, $W = 1\text{GHz}$	63
IV-4 Capacity versus bandwidth: $T_s = 0.5\mu\text{s}$, $T_d = 30\text{ns}$, $SNR = 60\text{dB}$	65
V-1 Peer-to-peer Network	72
V-2 Quantized threshold receiver block diagramm	77
V-3 DMC equivalent channel model	77
V-4 Achievable data rates of genie-aided receiver. $T_d=50\text{ ns}$, $W=1\text{GHz}$. Number of interferers, from top to bottom: 1,5,10,20,50.	80
V-5 Achievable data rates of genie-aided versus quantized threshold receiver. $T_d=50\text{ ns}$, $W=1\text{GHz}$, 1 strong interferer $E_s' = 10E_s$	81

VI-1 Transmitter block diagram. 88

VI-2 Decoder block diagram. 88

VI-3 Transmitter block diagram:*m*-ary Accumulator 89

VI-4 Irregular repetition Tanner graph. 91

VI-5 Decoding Thresholds for IRA with an *m*-ary Accumulator 92

VI-6 Distance to Capacity 93

VI-7 Decoding simulations 94

Notations

For the sake of simplicity of the mathematical developments, we will use the same notation to denote a random variable and its corresponding realization. The differentiation can be made from the usage context.

z	Scalar variable
\underline{z}	Vector variable
\mathbf{Z}	Matrix variable

CONTENTS

List of Tables	vii
List of Figures	vii
Notations	xi
I Introduction	5
II <i>On-off</i> signaling for Non-coherent UWB Systems	9
A Motivation	9
B <i>On-off</i> signaling	11
C Channel Model	11
D Ergodic achievable rates	16
D.1 Constant received energy UWB channel	23
E Practical Non-coherent Detection Receivers	24
E.1 Channel-Matched Non-Coherent Receiver	26
E.2 Mismatched Non-Coherent Receiver	27
E.3 Achievable data rates	28
E.4 Numerical results	30
F Appendix	30
II.0.1 <i>on-off</i> :mutual Information computation	30
III UWB <i>On-off</i> Signaling With Imperfect Channel Estimation	33
A Models	34
B Sequence ML detection rule	35

B.1	Training sequence	37
C	Error Probability Upper-Bound	39
C.1	ML detection metric	40
C.2	Suboptimal ML detection metric	44
C.3	<i>Pure</i> non-coherent receiver	46
D	Error Probability Lower-Bound	48
E	Results	50
IV	Multi-carrier <i>On-off</i> signaling	55
A	System Description	56
B	Bounds on Mutual Information	60
C	Discussion	62
C.1	S-tone impulsive FSK	64
D	Conclusion	65
E	Appendix	66
IV.0.1	Average transmitted power	66
IV.0.2	Bounds on the mutual information of OFDM <i>on-off</i> signaling	66
IV.0.3	Proof of lemma 1	68
IV.0.4	Solution of the constrained minimization problem	69
V	Non-Coherent UWB Peer-to-Peer Networks	71
A	Multiple access channel model	73
B	Genie-aided receiver - Upper bound	74
C	Threshold detection - Lower bound	76
C.1	Quantized threshold receiver	76

C.2	Extreme case: 2-level threshold receiver	78
C.3	Ergodic achievable rates	78
D	Results	80
VI	Code Constructions for <i>On-off</i> Ultra-wideband Systems	83
A	Channel Model	84
B	Coding Schemes	85
B.1	BICM	85
B.2	Convolutional Code+Binary Accumulator	87
B.3	m-Ary Accumulator	88
B.4	Extension:IRA Codes With a symbol Accumulator	90
C	Optimization Results and Simulations	92
D	conclusion	92

Introduction

Ultrawide Bandwidth (UWB) represents a new paradigm in wireless spectrum management that aims to a better sharing of the latter. The classical approach, based on licensing, consists of assigning and giving the exclusivity of usage of specific spectrum bands to specific systems or users. The UWB approach allows unlicensed users to transmit over a large bandwidth and coexist in licensed bands by making their signals *invisible* and non-intrusive to other users. UWB signaling is loosely defined as any wireless transmission scheme that occupies a bandwidth of more than 500MHz and or with a fractional bandwidth greater than 0.2. The fractional bandwidth is defined by the expression $2(f_H - f_L)/(f_H + f_L)$, f_H is the upper frequency and f_L the lower frequency at the -10dB points. Like code division multiple access (CDMA), the signal is spread in the frequency domain. However, unlike traditional wireless communication techniques, the most common form of UWB employs very short pulses (e.g., nanoseconds) instead of continuous wave transmissions. The result is an ultra wide band, low average power spectral density, signal in the frequency domain. Short pulse signaling is more known as *Impulse Radio* and was historically the first form of UWB signaling to be used. Lately, other UWB signaling schemes were proposed such as UWB-OFDM. The bandwidths considered for UWB systems are much larger than for CDMA systems, such as UMTS, which has a 3.84 MHz spread bandwidth. By comparison, a UWB system operating at 2 GHz would have a bandwidth of at least 400 MHz which implies a potentially lower spectral efficiency than UMTS in some applications.

The origin of ultra-wideband (UWB) technology stems from work in time-domain elec-

tromagnetics begun in 1962 to fully describe the transient behavior of a certain class of microwave networks through their characteristic impulse response [1], [2]. The concept was indeed quite simple. Instead of characterizing a linear, time-invariant (LTI) system by the more conventional means of a swept frequency response (i.e., amplitude and phase measurements versus frequency), an LTI system could alternatively be fully characterized by its response to an impulsive excitation – the so-called impulse response. However, it was not until the advent of the sampling oscilloscope and the development of techniques for subnanosecond (baseband) pulse generation, to provide suitable approximations to an impulse excitation, that the impulse response of microwave networks could be directly observed and measured. Once impulse measurement techniques were applied to the design of wideband, radiating antenna elements [3], it quickly became obvious that short pulse radar and communications systems could be developed with the same set of tools [6], [9]. While at the Sperry Research Center, then part of the Sperry Rand Corporation, Ross applied these techniques to various applications in radar and communications. Intelligible voice signals were communicated over hundreds of feet without the need for synchronization and demonstrated to the government. In the 1970's efforts turned toward the communication of these signals [5], [4], [7], [8]. Through the late 1980's, this technology was alternately referred to as baseband, carrier-free or impulse the term "ultra wideband" not being applied until approximately 1989 by the U.S. Department of Defense. Work in radar continued in the 1990's with the development of synchronized arrays of short pulse sources. These systems were used for intrusion detection applications. Since the beginning of the 90's the work in communications was considerably expanded [11], [12], [10].

Interest in (UWB) transmission systems has intensified recently in the scientific, commercial and military sectors following a ruling by the US Federal Communications Commission (FCC) [13] concerning UWB emission masks. This ruling allows for coexistence with traditional and protected radio services and enables the potential use of UWB transmission without allocated spectrum. The restrictions on the emission power spectrum, aim to minimize the risk of possible interference with other wireless systems with overlapping spectrum bandwidth. At the physical layer (PHY) level, UWB communication systems operate by spreading rather small amounts of average effective isotropic radiated power (EIRP)– always less than 0.56mW (according to FCC mask)– across a very wide band of frequencies relative to its central frequency. This quantity is easily calculated from the imposed power spectral density limit of 75 nW/MHz (-41.3 dBm/MHz) between 3.1GHz and 10.6GHz, as per FCC mask shown in (I). The later is sensibly equal to the power spectral density of thermal noise, which means that interference from UWB transmitters, to other UWB users as well as other wireless systems sharing the same bandwidth, resembles thermal noise and thus do not have any significant impact as stated in [13]: *With appropriate technical standards, UWB devices can operate using spectrum occupied by existing radio services without causing interference, thereby permitting scarce spectrum resources to be used more*

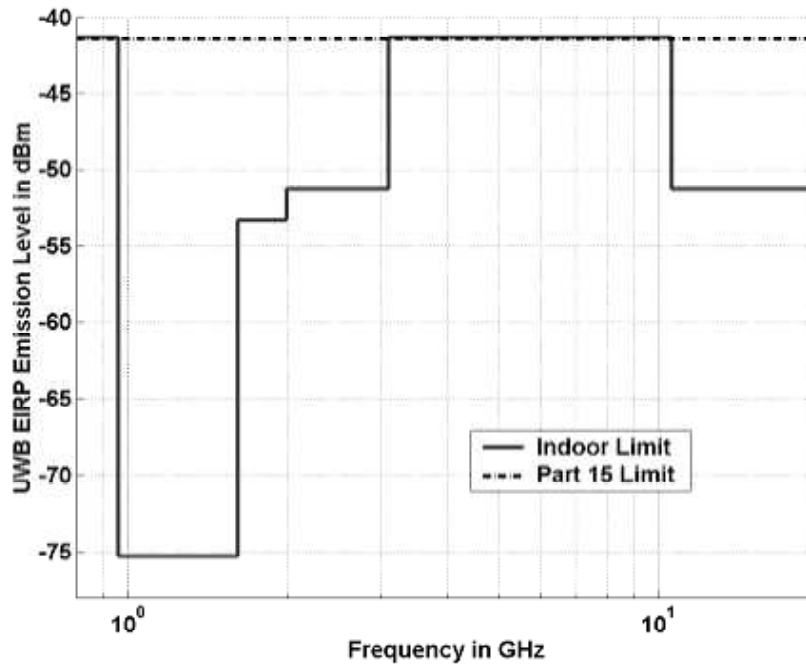


Fig. I-1. FCC indoor UWB emission spectrum mask ([13])

efficiently. The later statement may not hold any more if the density of UWB transmitters, within a certain area, increases.

The potential classes of UWB devices are many, ranging from imaging systems (ground-penetrating radar, wall-imaging systems, medical systems, and surveillance systems) to vehicular radar systems, and communications and measurements systems. They all have high spectrum efficiency potential in common. The technology offers significant potential for the deployment of short-range communication systems supporting high-rate applications and lower-rate intelligent devices embedded within a pervasive and personal wireless world.

The FCC-compliant UWB radio systems, using simple modulation and appropriate coding schemes, can transmit at information rates in excess of 100 Mbits/s over short distances. Alternatively, UWB radios can trade a reduced information rate for increased link range, potentially combined with accurate location-tracking capabilities. The two complementary operating modes are unique to UWB radio systems as they can be implemented based on very similar architectures with an unprecedented degree of scalability. UWB also has ap-

plications for military operations because it provides low probability of detection as well as anti-jam capabilities. Within the IEEE, two standardization groups have been created lately. The first one is the Task Group 3a (TG3a) [14] which focuses on the definition of a PHY alternative to 802.15.3 based on UWB signaling. This newly defined PHY will respond to consumer demands in the area of multimedia distribution and will work with an already designed MAC (802.15.3) to provide a unique combination of standard features and new technology. In parallel a new and complementary to IEEE 802.15.3a was recently formed within IEEE 802.15.4 (TG4a) [15] to analyze the potential and propose a standard specifying a low-rate, low power, offering localization capabilities, and low-cost WPAN technology based on UWB signaling.

UWB technology still faces some major technology challenges. Some of them exist in the areas of modulation and coding techniques suited for UWB radio systems. Originally, UWB signaling has been applied for military purposes, where achieving high capacity in terms of supported number of users was not necessarily a main objective. However, large multi-user capacity becomes very important in commercial applications. Coding and modulation are known to be some of the most effective means to improve on a system's multi-user capacity. Wide bandwidth provides fine delay resolution, and thus allows UWB systems to resolve a large number of propagation multi-paths. Therefore, in the case of fast pulse modulation techniques (i.e. PPM), the cost for realizing effective equalizers might be very high, in terms of both gate count and power consumption. This problem is much less pressing when using low pulse repetition systems (e.g., as in multiband approach), where the system complexity is instead challenged by the need for multiple parallel detectors or higher-order modulations. A particular challenging area at the PHY level today appears to be antenna design and implementation for UWB radio services. This is more challenging than for conventional narrowband systems given the large bandwidths, linearity requirements, and variable conditions of operation. A further aspect not yet fully investigated relates to the deteriorating effects of in-band interference in UWB receivers that originates from other radio signals, be they in near- or far- field proximity. This induces the necessity to identify methods for measuring prevailing noise levels and interference characteristics on the fly to be able to apply suitable interference rejection schemes. Finally, the use of new and advanced semi-conductor technologies in UWB system realizations need to be explored, such as micro-electromechanical systems (MEMS) and silicon on insulator (SOI) techniques as well as non-linear analog circuit and component design. These techniques could potentially provide interesting solutions to problems such as excessive clock speed, synchronization latency, and power consumption.

On-off signaling for Non-coherent UWB Systems

A MOTIVATION

Considering transmission in the wide-band regime, with a lack of channel state information at the receiver, it has been shown that the capacity of the infinite-bandwidth multipath fading channel is equal to, $C_\infty = \frac{P_R}{N_0 \ln 2}$ bits/s, the capacity of the additive white Gaussian noise channel with the same bandwidth and average transmitted power constraints. This holds irrespective of the amount of channel state information available to the receiver. Where P_R is the received signal power in watts, and N_0 is the noise power spectral density in watts/Hz. This well-known result was first proved by Kennedy [29] and Pierce [21] for Rayleigh statistics, and then generalized by Telatar and Tse [37] to arbitrary fading statistics. Both results are based on a constructive transmission scheme using frequency-shift keying which is set to be active at a vanishing duty cycle as the bandwidth goes to infinity. Though non-coherent detection (i.e energy detection) is optimal in the limit of infinite bandwidth (i.e. null spectral efficiency) it suffers some sub-optimality in the strictly non-null spectral efficiency regime. In [28] Verdu considers the trade-off between spectral efficiency and the minimum signal to noise ratio per bit needed for reliable communications $(E_b/N_0)_{\min}$, for a general non-coherent discrete-time multipath fading channel. He shows that the slope of the increase of spectral efficiency versus $(E_b/N_0)_{\min}$ is 0 at the origin which implies that extremely large bandwidths are needed in order to approach the optimal trade-off point. To get an idea of the loss incurred, consider a system with a 2GHz bandwidth and data rate

of 20 Mbit/s (this would correspond to a memoryless transmission strategy for channels with a 50ns delay-spread) yielding a spectral-efficiency of .01 bits/s/Hz. For a flat-fading Rayleigh channel, the loss in energy efficiency is on the order of 3dB, which translates into a factor 2 loss in data rate compared to a system with perfect channel state information at the receiver. Nevertheless the loss becomes less significant for lower data rates and/or higher bandwidths. The *near-optimality* of non-coherent detection in the low spectral efficiency regime thus motivates our interest in considering non-coherent detection for UWB systems. This choice is further motivated by the lower complexity of a non-coherent receiver with respect to coherent one, in particular in the context of UWB signaling. This aspect will be addressed in more detail later in this chapter.

The main issue that raises then, is the one of finding appropriate signaling strategies for non-coherent UWB systems. In the literature, this question has been raised in some similar contexts. In [20] Abou-Faycal and *al.* proved that the optimal input distribution¹ for a discrete-time memoryless Rayleigh-fading channel when channel realization is unknown to both the transmitter and the receiver, is discrete with a finite number of mass points including one located at the origin. They also showed, through a numerical analysis, that the number of mass points of the optimal input distribution increases for increasing SNR and that in the low SNR region it has exactly two mass points. Verdu in [28] proved that this holds in the vanishing spectral efficiency regime for discrete-time memoryless non-coherent(unknown channel realization to the receiver) frequency-selective channels with arbitrary statistics. Finding the optimal input distribution, subject to an average transmitted power constraint, is a very complicated task when considered for a general UWB channel or even for the more convenient case of Gaussian fading statistics. This issue is still unsolved even for simpler settings such as discrete frequency selective channels. Thus in our work we will not tackle directly the original problem but indeed give an insight into it by proposing some particular input distribution that we show to be near-optimal² in specific spectral efficiency regimes.

Motivated by the results in [20], [28], and [23] we first consider, in this chapter, *On-off* signaling, which is a two-mass points distribution including the origin. This signaling scheme is a generalization of *m*-ary *Pulse Position Modulation* which is the most commonly considered signaling scheme for UWB systems. We analyze the performance of this signaling scheme in terms of ergodic mutual information and consider some related issues such as practical non-coherent receivers. The use of ergodic mutual information as a relevant measure of performance will be motivated later by the specificities of UWB channels (see section (D)).

¹in terms of maximizing the average-power constrained capacity

²In the sens of approaching the capacity of the AWGN channel.

B *On-off* SIGNALING

The most common UWB transmission scheme is based on transmitting information through the use of short-term impulses, whose positions are modulated by a binary information source [16]. This can be seen as a special case of *On-off* signaling defined as any signaling scheme whose input distribution is of the following form. Terming u_k the k th transmitted symbol, we have that

$$u_k = \begin{cases} 1 & \text{with probability } \eta \\ 0 & \text{with probability } (1 - \eta) \end{cases} \quad (\text{II-1})$$

where $u_k = 0$ corresponds to not transmitting any signal (i.e. mass-point at the origin) while $u_k = 1$ corresponds to transmitting a pulse whose amplitude is proportional to $\sqrt{1/\eta}$ in order to maintain a constant average transmitted power for varying transmission probability η . In [28] Verdu introduces *flash signaling* which is defined as an *On-off* signaling scheme whose transmission probability η is chosen such that the amplitude of the transmitted pulses does not vanish for vanishing average transmitted power. In the following we will not restrict η to such a constraint.

C CHANNEL MODEL

We restrict our study to strictly time-limited complex signals, both at the transmitter and receiver. The time-limited and memoryless assumptions are made possible due to the virtually unlimited bandwidth of UWB signals. Baseband representation is used for all the considered signaling models since envisaged realizations will be passband above 3GHz.

The transmitted pulse, of duration T_p , is passed through a linear channel, $h(t, u)$, representing the response of the channel at time t to an impulse at time u . We assume that the impulse response of the channel is of duration $T_d \gg T_p$. The channel is further assumed to be a zero-mean process.

The received signal bandwidth W is roughly $1/T_p$, in the sense that the majority of the signal energy is contained in this finite bandwidth. The received signal is given by

$$r(t) = \int_0^{T_p} x(u)h(t, u)du + z(t) \quad (\text{II-2})$$

where $z(t)$ is white complex Gaussian noise with power spectral density N_0 . The channel

is further assumed to satisfy

$$\int_0^{T_d+T_p} \int_0^{T_p} h^2(t, u) dt du < \infty \quad (\text{II-3})$$

which rules out impulsive channels and practically models the bandlimiting nature of analog transmit and receive chains.

The finite-energy random channel may be decomposed as

$$h(t, u) = \sum_{i=1}^{\infty} \sum_{j=1}^{\infty} h_{i,j} \theta_j(u) \phi_i(t) \quad (\text{II-4})$$

where $h_{i,j}$ are the projections of the channel on the the input and output eigenspaces, $\{\theta_j(u)\}$ is the set of eigenfunctions (for $L^2(0, T_p)$) of the transmit pulse and $\{\phi_i(t)\}$ is the set of eigenfunctions (for $L^2(0, T_p + T_d)$) of the received signal. Since the input in equation (II-2) is one-dimensional, the most appropriate choice for $p(t)$ is the one which maximizes the expected energy of the channel output

$$p(t) = \operatorname{argmax}_{f(t)} \mathbb{E} \int_0^{T_d+T_p} \left(\int_0^{T_p} h(t, u) f(u) du \right)^2 dt = \theta_1(t) \quad (\text{II-5})$$

where $\theta_1(t)$ is the eigenfunction corresponding to the maximum eigenvalue, μ_1 , of the input cross-correlation function

$$R_i(u, u') = \mathbb{E} \int_0^{T_s} h(t, u) h(t, u') dt = \int_0^{T_s} R_h(t, t; u, u') dt \quad (\text{II-6})$$

and $R_h(t, t'; u, u') = \mathbb{E} h(t, u) h(t', u')$. The use of this input filter is conditioned on the emmission requirments of UWB systems, and thus it may not be possible to satisfy the maximal energy solution in practice.

Within the framework of this thesis we do not consider the impact of the shape of input filter on system performance. Instead of the general time-varying channel model, for the rest of the work we consider a block fading channel model so that the channel impulse response is time-invariant in any interval of $[kT_c, (k+1)T_c)$, where T_c is the *coherence-time* of the channel. We denote the channel in any block by $h_k(t)$. The received signal is

$$r(t) = \sum_{k=0}^N s(u_k) p(t - kT_s) * h_k(t) + z(t) \quad (\text{II-7})$$

where k is the symbol index, T_s the symbol duration, u_k is the transmitted symbol at time k , $p(t)$ and $s(u_k)$ are respectively the assigned pulse and amplitude for symbol u_k , and

$z(t)$ is complex white Gaussian noise with power spectral density N_0 . $p(t)$ is a unit-energy pulse of duration T_p . This signaling model encompasses modulation schemes such as on-off signaling, m -ary PPM, multi-level m -ary PPM, amplitude, and differential modulation. Note that ideally the pulse $p(t)$ would be equal to $\theta_1(t)$ and any other choice will induce a suboptimality in terms of average received signal to noise ratio. A guard interval of length T_d is left at the end of each symbol (from our memoryless assumption) so that $T_s \geq T_p + T_d$. For UWB signaling $T_s \ll T_c$ so that the channel can be assumed to be invariant over each symbol.

For the rest of the chapter we will use the following equivalent discrete-time channel model. Through a Karhunen-Loève expansion (see for example [34]), we rewrite the channel model in (II-7), for each symbol k , as follows

$$\begin{aligned} r_{k,i} &= h_{k,i} \sqrt{E_s \lambda_i} s(u_k) + z_{k,i}, i = 1, \dots, \infty \\ \underline{r}_k &= \{r_{k,1}, r_{k,2}, \dots\} \end{aligned} \quad (\text{II-8})$$

where $z_{k,i}$ is $\mathcal{N}_j(0, N_0)$ and $\{h_{k,i}\}$ are unit variance zero mean independent circularly symmetric complex Gaussian variables (i.e. non line-of-sight communications). The $\{\lambda_i\}$ are the solutions to

$$\lambda_i \phi_i(t) = \int_0^{T_d+T_p} R_o(t, u) \phi_i(u) du. \quad (\text{II-9})$$

where $\phi_i(t)$ and $R_o(t, u)$ are the eigenfunctions and the autocorrelation function of the composite channel $h_k(t) * p(t)$, respectively.

$$h_{k,i} = \int_0^{T_d+T_p} h_k(t) \phi_i(t) dt \quad (\text{II-10})$$

Because of the bandlimiting nature of the channels in this study, the channel will be characterized by a finite number, D , of significant eigenvalues in the sense that a certain proportion of the total channel energy will be contained in these D components. For rich environments D will be close to $1 + WT_d$.

Based on measurement campaigns [19] the number of significant eigenvalues can be large but significantly less than the approximate dimension of the signal-space $1 + WT_d$ [32, Chapter 8]. For a typical UWB channel, even though D is less than $1 + WT_d$ it is still relatively large. As a consequence the total channel received energy $\sum_{i=1}^D \lambda_i |h_i|^2$ is a

quasi-constant quantity irrespective of channel realization $\{h_1, h_2, \dots, h_D\}$. This property of UWB channels has been confirmed through measurements, in the frequency domain, conducted at Eurecom [19], as well as in other laboratories [25].

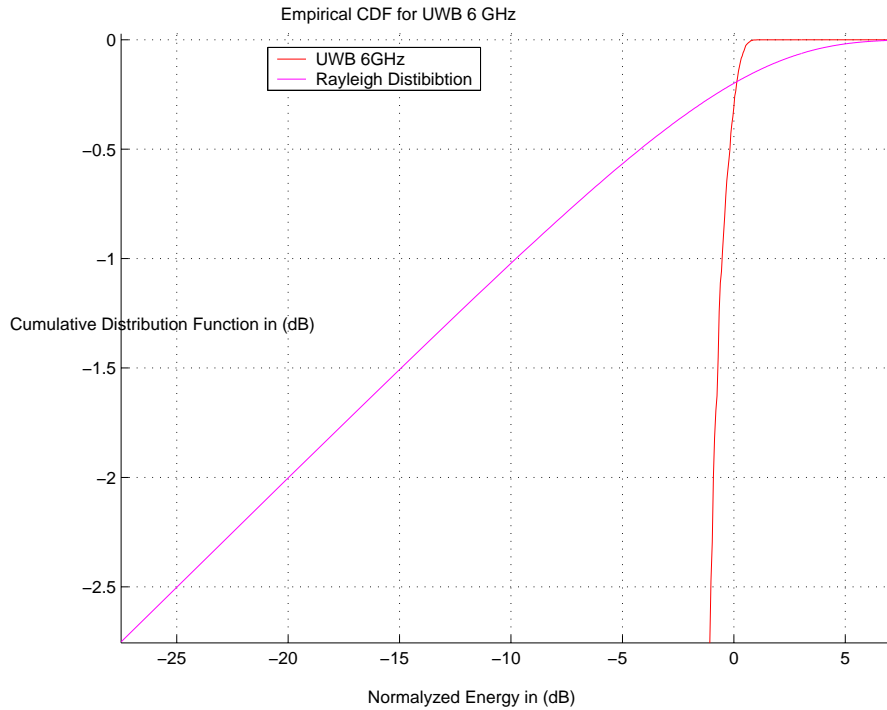


Fig. II-1. CDF of total channel received energy

Figure (II-1) shows the cumulative distribution function of the total received energy over a UWB channel of $2GHz$ bandwidth in comparison to a flat fading Rayleigh channel with the same average received energy. The measurements were conducted in a typical office environment. The CDF corresponding to the UWB channel is very close to a step function, which proves that the received energy is effectively constant irrespective of channel realization. The physical explanation for this behavior comes from the fact that the large bandwidths considered here ($>1GHz$) provide a high temporal resolution and enable the receiver to resolve a large number of paths of the impinging wavefront. Providing that the channel has a high diversity order (i.e. in rich multipath environments), the total channel gain is slowly varying compared to its constituent components. It has been shown [25, 26, 27] through measurements that in indoor environments, the UWB channel can con-

tain several hundreds of paths of significant strength. We may assume, therefore, that for all practical purposes, the total received energy should remain almost constant at its average path strength, irrespective of the particular channel realization. Variations in the received signal power will typically be caused by shadowing rather than fast fading. We will exploit this property of UWB channels in some later developments and, without loss of generality, will assume total channel gain constant and equal to 1. This assumption essentially says that the received signal energy is not impaired by signal fading due to the rich scattering environment. For notational convenience, we will assume that the eigenvalues are ordered by decreasing amplitude. An example of an eigenvalue distribution is shown in Fig. II-2. This corresponds to an exponentially decaying multipath intensity profile with delay-spread 50ns filtered by a window function of width 1ns, corresponding to a system bandwidth of 1 GHz.

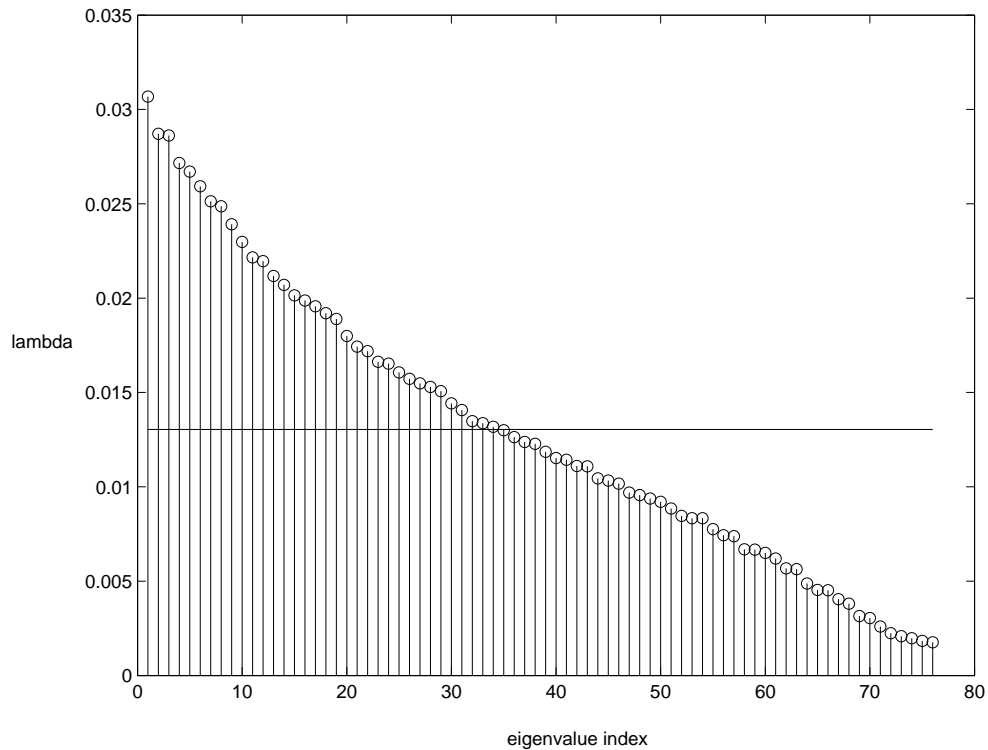


Fig. II-2. Example Eigenvalue Distribution: $T_d=50$ ns, $W=1$ GHz. Mean value indicated by a horizontal bar

D ERGODIC ACHIEVABLE RATES

In this chapter we are interested in characterizing the performance of pure non coherent detection, in the sense of considering the case where the piecewise constant³ nature of the channel is not exploited in order to implicitly perform channel estimation. We assume that the channel realization in every block is independent and identically distributed, so that $E[h_k(t)h_l^*(u)] = R_h(t, u)\delta_{k,l}$, where $R_h(t, u)$ is the auto-correlation function of the channel response in a particular interval. In practice, this implies that a sufficiently large number of channel realizations span the codeword length. This can be achieved by first interleaving the transmitted symbols, using an infinite depth interleaver, before sending them over the channel. Thus, we can assume that the deinterleaved symbols at the receiver face independent channel realizations. Generally speaking, this channel model is useful only as a first approximation for short range communications.

Nevertheless, for UWB signaling with non-coherent detection, this channel model is adequate thanks to the high diversity order D of UWB channels. As stated in the previous section, the overall received energy over a typical UWB channel is constant (fig II-1) irrespective of particular channel realizations. Thus, in a sense, the channel almost does not suffer any fading⁴. Therefore, ergodic mutual information is a significant measure of the achievable data rates for practical systems due to the fact that the probability of the information outage event is vanishing. The information outage event is defined as the probability of having the instantaneous mutual information, between the transmitted symbol and the received signal, less than the coding rate. This reasoning will be further strengthened later in the chapter (see section (E.1)) when the ML detection metric, for the considered channel model and signaling scheme, is shown to break down to exactly the received energy within each symbol time.

In the rest of this section we derive and numerically evaluate the ergodic mutual information. The latter is then used to analyze the impact of the most important channel and design parameters, on the system performance. We also, a posteriori, motivate the use of the considered channel model by showing that non-coherent UWB signaling achieves exactly the same data rate as over a non-ergodic UWB channel whose gain⁵ is assumed to be strictly constant. The later channel model will be described in more detail further in this section.

For the rest of this section we drop the time index k for a better clarity of mathematical expressions. Recalling the notations from the signaling model (II-7), we have that $s(0) = 0$, $s(1) = \sqrt{\frac{E_s}{\eta}}$, and $T_s = T_d + T_p$. Then \underline{R} is a zero-mean Gaussian vector with covariance

³From our block fading channel model

⁴From the perspective of a non-coherent detector which captures the received energy over the channel.

⁵i.e. total received energy over the channel

matrix $E[\underline{R}\underline{R}^T] = \text{diag}(s(u_k)E_s\lambda_i + N_0)$. It is shown in (Appendix II.0.1) that

$$\begin{aligned}
I(u; \underline{r}) = & \\
& - \frac{1}{T_s} E_{\underline{Y}} \left[\eta \log \left(\eta + (1 - \eta) \sqrt{\prod_{i=1}^D \left(1 + \frac{E_s \lambda_i}{\eta N_0} \right)} \exp \left(-\underline{Y}^\dagger (\text{diag}(\frac{N_0 \eta}{E_s \lambda_i}))^{-1} \underline{Y} \right) \right) \right. \\
& \left. + (1 - \eta) \log \left((1 - \eta) + \frac{\eta}{\sqrt{\prod_{i=1}^D \left(1 + \frac{E_s \lambda_i}{\eta N_0} \right)}} \exp \left(\underline{Y}^\dagger (\text{diag}(\frac{N_0 \eta}{E_s \lambda_i} + 1))^{-1} \underline{Y} \right) \right) \right] \text{ bits/s}
\end{aligned} \tag{II-11}$$

where \underline{Y} is a zero-mean complex Gaussian vector with covariance matrix \mathbf{I} and \dagger stands for complex conjugate transpose. This is easily computed numerically using the Monte Carlo method. The transmit probability η is optimized as function of system parameters and average signal to noise ratio (SNR).

Figure (II-3) shows the achieved capacity versus the average SNR for 2 scattering environment examples. The system bandwidth is taken to be equal to 1GHz and channel delay spread $T_d = 25ns$. The latter value is obtained from measurements in a typical office environment using a carrier frequency of 5GHz [25]. The mutual information is computed for both a typical scattering environment and a very rich one⁶. In the first case the number of significant dimensions of the received signal D is equal to $1 + WT_d = 26$ while in the second case it is equal to 10. The achieved capacity in the low SNR regime is close to the wideband capacity C_∞ though saturates in the high SNR region due to the limited maximum transmission rate of the considered signaling scheme⁷ $R_{\max} = 1/T_s$. As we can see, unlike the case of a coherent receiver, increasing the number of dimensions of the received signal (i.e. diversity) decreases the system performance.

Figure (II-4) shows the achieved capacity versus the average signal to noise ratio SNR for system bandwidths ranging from 500MHz to 7.5GHz. A typical scattering environment is considered and $T_d = 25ns$. Again, we see that increasing diversity, through an increase of system bandwidth, degrades the achieved capacity. This behavior can be explained by a signal *over-spreading phenomena*; if we note T_p the transmitted pulse duration and T_d the channel delay spread, then the received signal occupies a signal-space of dimension of the order of $(T_d + T_p)/T_p$, which means that for increasing bandwidth (i.e. decreasing T_p) the number of dimensions increases because $T_d + T_p \simeq T_d$. This confirms previous results on the so-called bandwidth-scaled signals, that showed that using spread spectrum

⁶The eigenvalues profile is assumed to be exponentially decaying, with a smaller decaying factor in the case of rich scattering environment. $\lambda_i = \beta e^{-\alpha i}$ where α is the decaying factor and β a normalization factor. For the very rich scattering environment, we considered here the limiting case where the eigenvalue profile is flat (i.e. $\alpha = 0$)

⁷due to the use of a guard interval at the end of each symbol

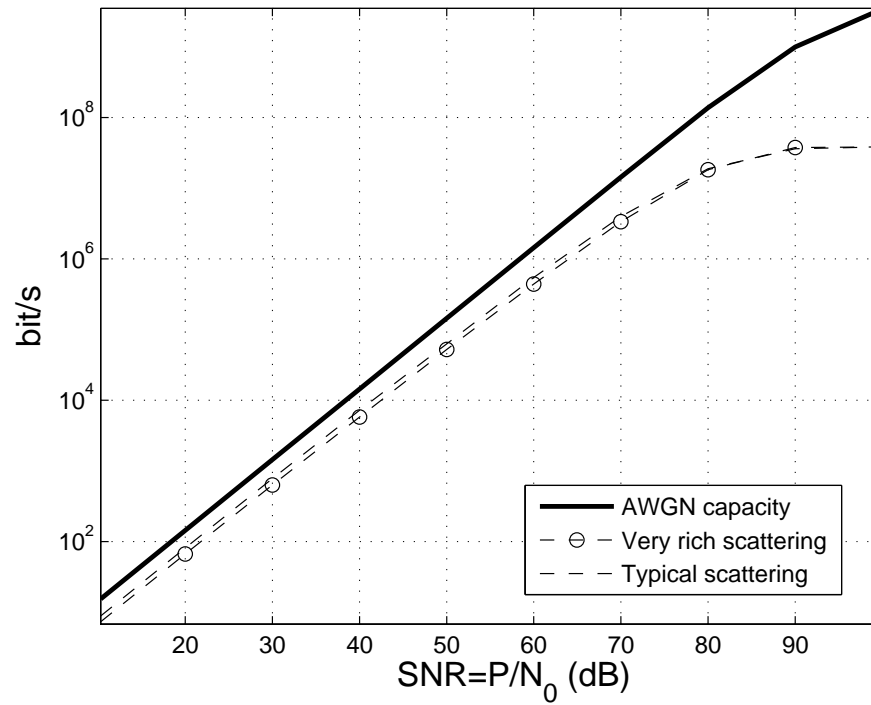


Fig. II-3. Capacity versus SNR: different scattering environments. $T_d=25\text{ns}$, $W=1\text{GHz}$. The AWGN capacity is equal to $W \log \left(1 + \frac{P}{WN_0} \right)$

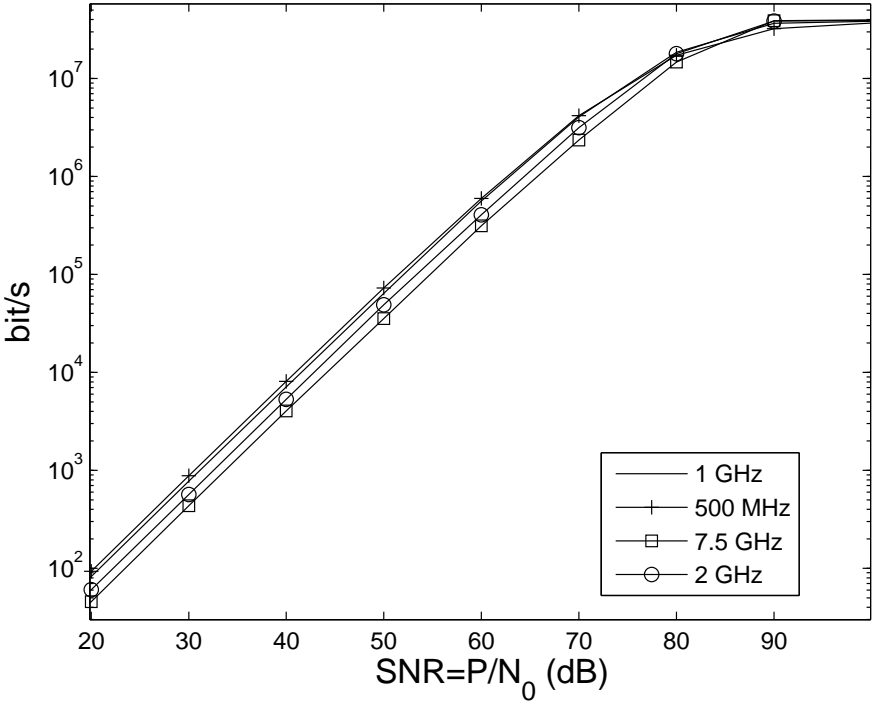


Fig. II-4. Capacity versus SNR:different bandwidths. Td=25ns

signaling, such as direct sequence CDMA, leads to a vanishing systems capacity in the limit of infinite bandwidth ([22], [23], [37]).

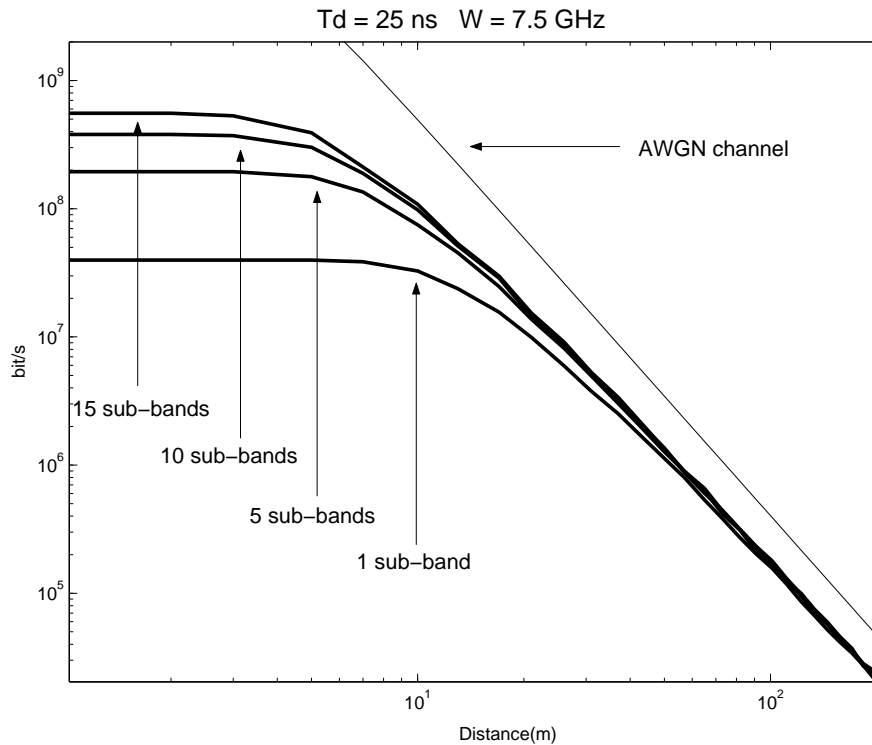


Fig. II-5. Multiband signaling: Capacity versus distance, different bandwidths. $T_d=25\text{ns}$

The current regulation on UWB signaling [13] imposes that the bandwidth occupied by a UWB signal has to be no less than 500MHz. Therefore, the discussion above suggests that the optimal bandwidth for a typical non-coherent UWB system should be 500MHz. Nevertheless, the regulation also imposes a limit on the power spectral density of allowed UWB signaling which implies that the total allowed transmit power is proportional to the signaling bandwidth. Combining the two arguments leads to the use of multiband signaling over bandwidths of 500MHz each. The generalization to the multi-band setting is straight forward; independent data streams are transmitted on each band. Adjacent bands are assumed to not interfere with each other through the use of band-limiting filtering (see figure II-6). Figure (II-5) shows the achievable data rates for systems with different numbers of multi-bands. The results are plotted versus distance⁸ between the transmitted (*On-off* signaling)

⁸rather than versus SNR as done so far

and the receiver. We assume that the transmitter transmits at the maximum allowed power $P_{max} = W * P_d$, where W is the signaling bandwidth in MHz and P_d the limit on the allowed transmitted power spectral density $P_d = -41.3\text{dBm/Mhz}$. The transmitted power is split equally over all the used sub-bands. We use the indoor pathloss model proposed in [18] where the transmitted signal attenuation as function of d the distance between the transmitter and the receiver is given by $1 / (10^{5.49} d^{3.1})$. We can see, on the figure, that multi-band signaling allows to achieve higher data rates in the short range region (high SNR) while not bringing any improvement in the long range region (low SNR).

In chapter IV, we will further push the concept of multiband (carrier) signaling by considering multi-carrier *On-off* signaling.

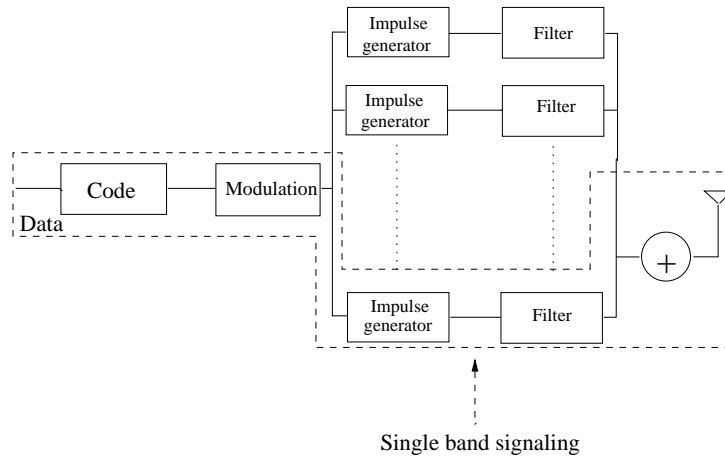


Fig. II-6. Multiband signaling

Figure (II-7) shows the minimum SNR per bit $E_b/N_0 = P/(N_0R)$, required for reliable communications, versus system's target data rate. System's bandwidth W is respectively taken to be equal to 500MHz, 1GHz, and 2GHz. $T_d = 25ns$. We can see that when operating in the low data rate region the penalty due to unknown channel, in terms of minimum E_b/N_0 for reliable communications, between non-coherent *On-off* signaling and the AWGN channel with the same bandwidth is on the order of 1.2dB.

$$\left(\frac{E_b}{N_0}\right)_{\min} = \lim_{W \rightarrow +\infty} \frac{P}{N_0 W \log\left(1 + \frac{P}{W N_0}\right)} = \frac{1}{\ln(2)} \quad (\text{II-12})$$

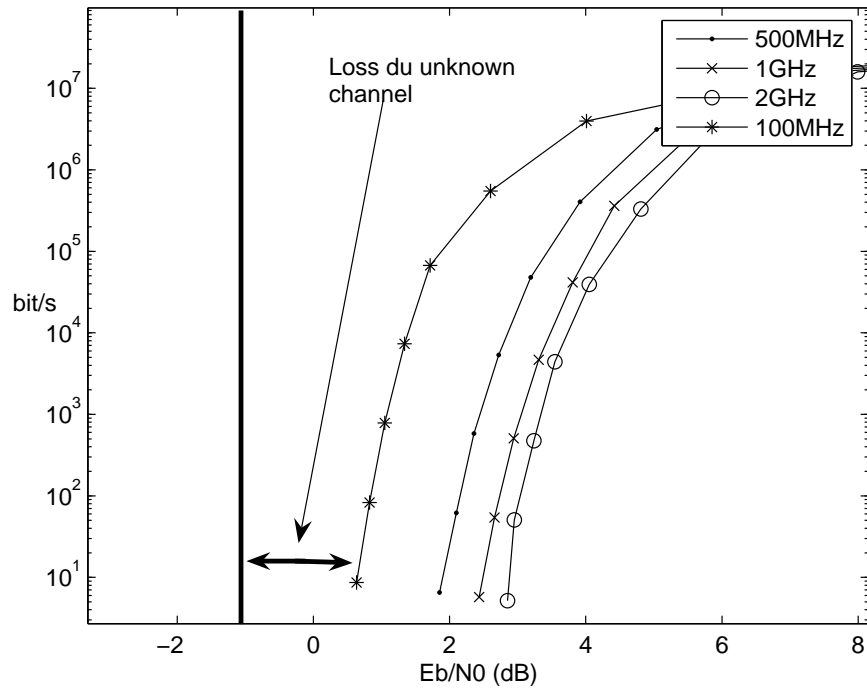


Fig. II-7. Data rates versus E_b/N_0 . $T_d=25\text{ns}$, $W=500\text{ MHz}$

D.1 Constant received energy UWB channel

In order to further test the assumptions of the adopted channel model, in particular the ergodicity of the channel process, we consider here a non-coherent non-ergodic channel model assuming that the total received energy, over the channel, is strictly constant irrespective of channel realization, or equivalently.

$$\sum_{i=1}^D |h_{k,i}|^2 = 1 \quad (\text{II-13})$$

By non-coherent channel we designate the channel that for each input symbol u_k outputs the received energy during a symbol period T_s .

$$\begin{aligned} y_k &= \sum_{i=1}^D |r_{k,i}|^2 \\ &= \sum_{i=1}^D \left| \sqrt{\frac{E_s \lambda_i}{\eta N_0}} h_{k,i} u_k + n_{k,i} \right|^2 \\ &= \mu_k \end{aligned} \quad (\text{II-14})$$

where μ_k is a random variable distributed according to a non-central chi-square distribution with $2D$ degrees of freedom and non-centrality parameter $\sum_{i=1}^D \frac{E_s \lambda_i}{\eta N_0} |h_{k,i}|^2 u_k = \frac{E_s}{\eta N_0} u_k$ (from our no fading-channel assumption). This model assumes that, before capturing the received energy, the received signal is first projected over a signal subspace in order to limit the amount of collected noise. We choose the latter subspace to be the one spanned by the eigen-functions corresponding to the D most significant eigen-values $\lambda_1, \dots, \lambda_D$.

Computing the average mutual information between u_k and y_k , in the case of flat channel eigenvalues profile, we see that it is exactly equal (numerically) to the one achieved over the ergodic channel model⁹. This suggests that the ergodic channel model is capable of correctly describing the behavior of a UWB channel when using non-coherent type of detection. This is explained by the fact that dominant contribution in the overall average mutual information is due to the richness of the scattering rather than the time-variation of the channel process. In the case of non-flat eigenvalues profile, the achievable data rates over the constant energy channel are slightly lower. This suboptimality is due to a non-channel matched energy detection at the receiver. In the following section we analyze more detail the performance of both matched and non channel-matched energy receivers.

⁹The obtained curves are not shown here because they perfectly overlap and thus are not convenient to draw.

E PRACTICAL NON-COHERENT DETECTION RECEIVERS

In this section we consider practical non-coherent type of receivers for UWB systems using m -ary pulse position modulation (PPM). m -ary PPM can be seen as a specially-designed channel code for *On-off* signaling, this link will be further detailed further in this section. The motivation for this interest is two-fold : first, as we saw in the previous section, non-coherent detection is capable of approaching the performance of coherent detection. The second motivation comes from system's complexity considerations. In fact, as seen in the previous section a UWB channel contains a large number of propagation paths of significant strength. This property has two implications on the complexity of a coherent Detector. i) it makes channel estimation very complex due to the large number of parameters to be estimated. ii) The Rake structure of a typical coherent detector will contain a large number of fingers. Both those aspects combined to the fact that the received signal needs to be sampled at a rate of several GHz, prior to entering the receiver, make an optimal coherent detector very complex and induces that in practice only suboptimal versions of it can be implemented. In Chapter 2, we will consider practical coherent detectors, in the sense those which only have access to an imperfect channel estimate. Therefore, we will address the question of how good this channel estimate needs to be in order to significantly outperform a non-coherent detector.

The aim of the analysis performed in this section is to derive alternative receivers, to the coherent receiver, that are more attractive from complexity point of view. We are, in particular, interested in solutions that can be implemented with analog frontends, and that can still perform close to the optimal performance. Two different receivers are considered in the sequel. The first one (see figure (II-9)) is the maximum likelihood non-coherent receiver, while the second (see figure (II-10)) corresponds to a suboptimal solution.

As stated earlier in this section, m -ary PPM can be seen as a particular implementation of *On-off*. Each m -PPM symbol corresponds to choosing one out of m symbol times, constituting a PPM frame, in which to emit the transmit pulse $p(t)$, which is a special case of *On-off* with $\eta = 1/m$ and exactly one pulse transmitted per frame. In the following we term w as the transmitted symbol and define \underline{R} as the set of observation vectors over all the slots constituting an m -PPM frame,

$$\underline{R} = \{\underline{r}_1, \underline{r}_2, \dots, \underline{r}_m\} \quad (\text{II-15})$$

In this case groups of m symbols $u_k, u_{k+1}, \dots, u_{k+m-1}$ will be constrained to the form $(0, 0, \dots, 0, 1, 0, \dots, 0)$. Similarly to (II-11) we compute the ergodic mutual information between the transmitted symbol w and the observation \underline{R} . Figure (II-8) compares the achievable data rates of both signaling strategies. As can be seen m -ary PPM, which is the practical implementation of asymmetric *On-off*, does not suffer any suboptimality a

part from a saturation in the very high data rate region. This is overcome by using *On-off* signaling, with on probability equal to 1/2, in the high SNR region.

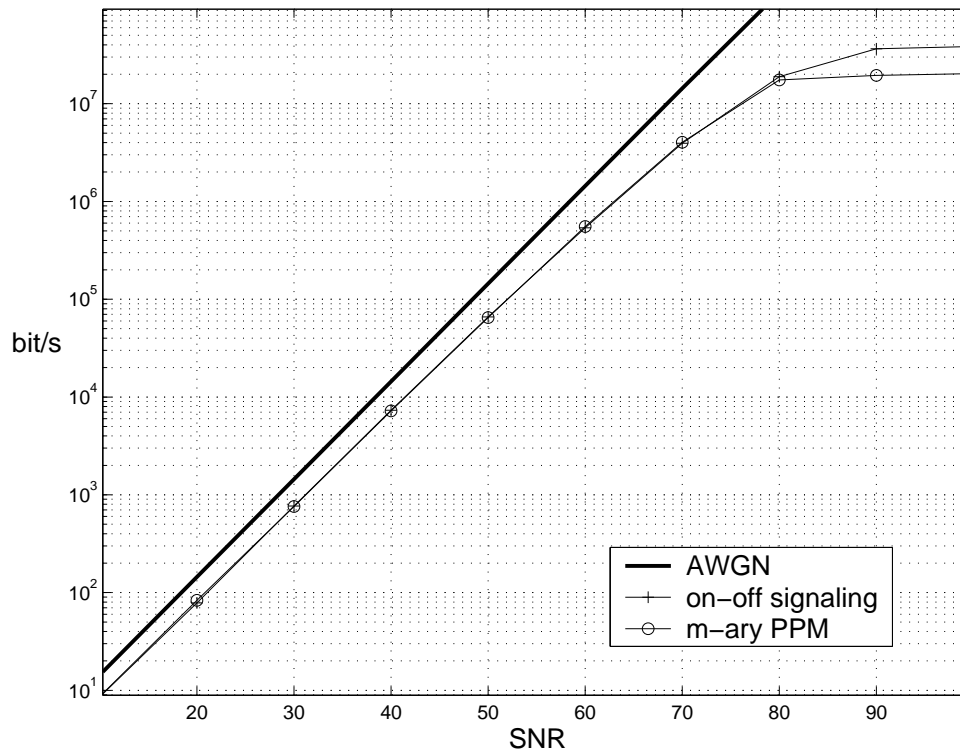


Fig. II-8. Achievable data rates of *On-off* signaling versus *m*-ary PPM. $T_d=25\text{ns}$, $W=1\text{GHz}$

In the following we use *m*-ary PPM as signaling scheme. We obtain sufficient detection statistics, for each of the considered detection settings, through the derivation of the maximum-likelihood detection rule for each of them. Given the statistical independence of channel realizations faced by any two different *m*-PPM symbols¹⁰ the ML detection metric of a sequence of *m*-PPM symbols (i.e. codeword) is additive over the set symbols constituting the sequence. Therefore, in the following we concentrate on the derivation of the symbol ML detection. Throughout this section, we denote q_k the output of the receiver (i.e. the decision metric that is fed to the decoder).

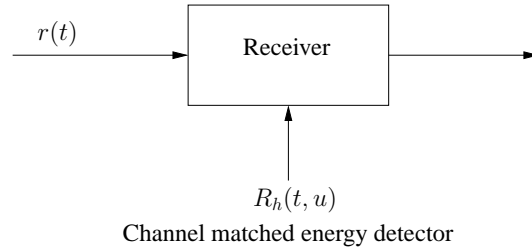


Fig. II-9. Channel matched non-coherent receiver

E.1 Channel-Matched Non-Coherent Receiver

By definition, the ML detection rule can be written as follows

$$\hat{k} = \underset{k=1, \dots, m}{\operatorname{argmax}} \Pr(\underline{r}|w = k) \quad (\text{II-16})$$

The conditional probability in (II-16) is developed as follows

$$\begin{aligned} \Pr(\underline{r}|w = k) &\stackrel{(a)}{=} \prod_{j=1}^m \prod_{i=1}^D \Pr(r_{j,i}|w = k) \\ &= \prod_{j \neq k} \left(\prod_{i=1}^D \left(\frac{1}{\pi N_0} e^{-\frac{|r_{j,i}|^2}{N_0}} \right) \right) \\ &\quad \prod_{i=1}^D \left(\frac{1}{\pi (E_s \lambda_i + N_0)} e^{-\frac{|r_{k,i}|^2}{E_s \lambda_i + N_0}} \right) \end{aligned} \quad (\text{II-17})$$

in (a) we use the fact that, conditioned on the transmitted codeword, the observation vector components $r_{j,i}$ $j = 1, \dots, m$ $i = 1, \dots, D$ are statistically independent. The maximum likelihood detection rule can thus be written equivalently as follows

¹⁰from our ergodic channel model

$$\begin{aligned}
\hat{k} &= \operatorname{argmin}_{k=1,\dots,m} \left(\sum_{\substack{j=1 \\ j \neq k}}^m \sum_{i=1}^D \frac{|r_{j,i}|^2}{N_0} + \sum_{i=1}^D \frac{|r_{k,i}|^2}{E_s \lambda_i + N_0} \right) \\
&= \operatorname{argmin}_{k=1,\dots,m} \sum_{i=1}^D \frac{|r_{k,i}|^2}{E_s \lambda_i + N_0} - \sum_{i=1}^D \frac{|r_{k,i}|^2}{N_0} \\
&= \operatorname{argmax}_{k=1,\dots,m} \mathbf{r}_k Q^{-1} \mathbf{r}_k^\dagger
\end{aligned} \tag{II-18}$$

with $Q = \mathbf{diag}(N_0 (1 + \frac{N_0}{E_s \lambda_i}))$ ¹¹.

Thus the ML detection rule breaks down to a weighted energy detection

$$\operatorname{argmax}_{k=1,\dots,m} \sum_{i=1}^D \frac{|r_{k,i}|^2}{N_0 (1 + \frac{N_0}{E_s \lambda_i})} \tag{II-19}$$

This detector can be implemented using a time-varying filter. This representation is likely not of practical interest but serves to upper-bound the performance of suboptimal schemes.

E.2 Mismatched Non-Coherent Receiver

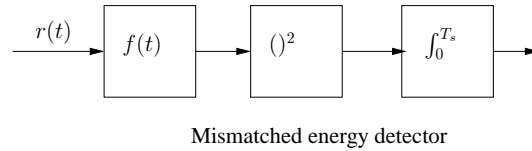


Fig. II-10. Mismatched non-coherent receiver

We now consider a suboptimal non-coherent receiver that would be of interest either in the case where the receiver does not have access to channel statistics¹² and/or is constrained to the use of single frontend filter for the sake of lower implementation complexity. The received signal is first filtered by the time-limited unit-energy filter $f(t)$ of duration T_f .

¹¹this detector is equivalent to the classical estimator-correlator [34]

¹²For instance, in case the channel is not second order stationary

This filtering operation aims to reduce the amount of receiver noise while capturing the majority of its information bearing part

$$\begin{aligned} r_f(t) = (r * f)(t) &= ((s + z) * f)(t) \\ &= s_f(t) + z_f(t) \end{aligned} \quad (\text{II-20})$$

Then, its energy is successively captured over the slots, of duration $T_d + T_p$ each, of the m -PPM frame.

$$\begin{cases} q_k = \int_{(k-1)(T_d+T_p)}^{k(T_d+T_p)} r_f^2(t) dt \\ k = 1, \dots, m \end{cases} \quad (\text{II-21})$$

In the following analysis we will represent $r_f(t)$ with its equivalent discrete-time representation

$$q_k = \begin{cases} \sum_{i=1}^D \lambda_i r_{f,i}^2 & k = w \\ \sum_{i=1}^D \mu_i r_{f,i}^2 & k \neq w \end{cases} \quad (\text{II-22})$$

with λ_i and μ_i being the solutions to

$$\lambda_i \phi_i(t) = \int_0^{T_d+T_p} \mathbf{R}_{s_f+z_f}(t, u) \phi_i(u) du \quad (\text{II-23})$$

$$\mu_i \theta_i(t) = \int_0^{T_d+T_p} \mathbf{R}_{z_f}(t, u) \theta_i(u) du \quad (\text{II-24})$$

where $\mathbf{R}_{s_f+z_f}(t, u)$ and $\mathbf{R}_{z_f}(t, u)$ are the autocorrelation functions of the filtered received signal respectively with and without the presence of a transmitted pulse and $\{\phi_{n,1}, \dots, \phi_{n,D}\}$ and $\{\theta_{n,1}, \dots, \theta_{n,D}\}$ are the resulting basis functions in the Karhunen-Loève decompositions. The $r_{f,i}$ are zero mean unit variance random variables resulting from the projection of r_f on the basis functions. This representation is not computed by the receiver, it serves only to derive the performance of the energy detector.

E.3 Achievable data rates

At present we turn to the computation of the achievable data rates of *on-off* signaling when using the non-coherent receivers previously presented. We compute their corresponding ergodic mutual information. From (E.1) and (E.2) we can write the decision variable for each of the considered receivers as a quadratic form of a zero-mean unit-variance complex

Gaussian random vector U of dimension D . Moreover, the matrix of the quadratic form is diagonal.

$$q_k = U \mathbf{A} U^T \quad (\text{II-25})$$

such that

- Channel matched detector

$$\mathbf{A} = \begin{cases} \mathbf{diag} \left(\frac{E_s \lambda_i}{N_0} \right) & \text{for } k = w \\ \mathbf{diag} \left(\frac{E_s \lambda_i}{E_s \lambda_i + N_0} \right) & \text{for } k \neq w \end{cases} \quad (\text{II-26})$$

- Mismatched detector

$$\mathbf{A} = \begin{cases} \mathbf{diag} (\lambda_i) & \text{for } k = w \\ \mathbf{diag} (\mu_i) & \text{for } k \neq w \end{cases} \quad (\text{II-27})$$

Hence for the two considered receivers, the computation of the average mutual information, breaks down to the computation of the mutual information between an m -ary PPM u and an observation vector $\underline{q} = \{q_1, \dots, q_m\}$ each of its entries is a quadratic form of zero-mean unit-variance random Gaussian vector \underline{v} of dimension D

$$\begin{cases} \text{for } k = w & q_k = \underline{v}_k \mathbf{A}_1 \underline{v}_k^T \\ \text{for } k \neq w & q_k = \underline{v}_k \mathbf{A}_2 \underline{v}_k^T \end{cases} \quad (\text{II-28})$$

where \mathbf{A}_1 and \mathbf{A}_2 are diagonal matrices with strictly positive entries. In the following we assume that the entries of \mathbf{A}_1 (respectively \mathbf{A}_2) are distinct.

In the following, we drop the time index k . Conditioned on the transmitted symbol u , the probability density function of q_s , for $s = 1, \dots, m$, is then written as follows ([35],[36])

$$P_{q_s}(z|u) = \Pr(q_s = z|u) = \sum_{i=1}^D \frac{1}{\lambda_i} \left(\prod_{\substack{j=1 \\ j \neq i}}^D \frac{\lambda_i}{\lambda_i - \lambda_j} \right) \exp\left(-\frac{z}{\lambda_i}\right) \quad (\text{II-29})$$

Where $\{\lambda_1, \dots, \lambda_D\}$ are the eigenvalues of \mathbf{A}_1 (resp. \mathbf{A}_2) if $u = w$ (resp. $u \neq w$). Thus the probability density function of q_s is a weighted sum of exponential distributions. Given that conditioned on u , the variables $\{q_s, s = 1, \dots, m\}$ are independent, we can write the

ergodic mutual information between the transmitted symbol and received signal as follows

$$\begin{aligned}
I(u; q_1, \dots, q_m) &= -\frac{1}{m} \sum_{s=1}^m \int_{q_1, \dots, q_m} \log \left(\frac{1}{m} \left(1 + \frac{\sum_{j \neq s} \prod_{k=1}^m P_q(q_k | u = j)}{\prod_{t=1}^m P_q(q_t | u = s)} \right) \right) P_q(q_1) \dots P_q(q_m) dq_1 \dots dq_m. \quad (\text{II-30})
\end{aligned}$$

The integration operation in equation (II-30) is numerically performed through Monte Carlo averaging.

E.4 Numerical results

Figure (II-11) shows the achievable data rates of the two considered non-coherent receivers. The comparison is performed in the case of a typical UWB indoor scattering environment (i.e. non-flat eigenvalues profile). We can see that the channel matched receiver achieves the same achievable rates as the non-receiver constrained non coherent *On-off* signaling. This behavior is to be expected since the channel-matched receiver uses the ML detection metric which is known to be a sufficient statistic. The non-matched receiver suffers a performance degradation on the order of 2dB. In the case of a flat eigenvalue profile, both receivers perform identically, since the channel is *isotropic* and thus no channel matching is required.

F APPENDIX

II.0.1 on-off: mutual Information computation

$$\begin{aligned}
I(u; \underline{r}) &= \eta \int_{\underline{r}} \Pr(\underline{r} | u = 1) \log \left(\frac{\Pr(\underline{r} | u = 1)}{\eta \Pr(\underline{r} | u = 1) + (1 - \eta) \Pr(\underline{r} | u = 0)} \right) \\
&+ (1 - \eta) \int_{\underline{r}} \Pr(\underline{r} | u = 0) \log \left(\frac{\Pr(\underline{r} | u = 0)}{\eta \Pr(\underline{r} | u = 1) + (1 - \eta) \Pr(\underline{r} | u = 0)} \right) \quad (\text{II-31})
\end{aligned}$$

where

$$\begin{aligned}
\Pr(\underline{r} | u = 0) &= \frac{1}{(\pi N_0)^D} \exp \left(-\underline{r} (N_0 \mathbf{I})^{-1} \underline{r}^\dagger \right) \\
\Pr(\underline{r} | u = 1) &= \frac{1}{(\pi)^D \prod_{i=1}^D \left(N_0 + \frac{\lambda_i E_s}{\eta} \right)} \exp \left(-\underline{r} \left(\text{diag} \left(N_0 + \frac{\lambda_i E_s}{\eta} \right) \right)^{-1} \underline{r}^\dagger \right) \quad (\text{II-32})
\end{aligned}$$

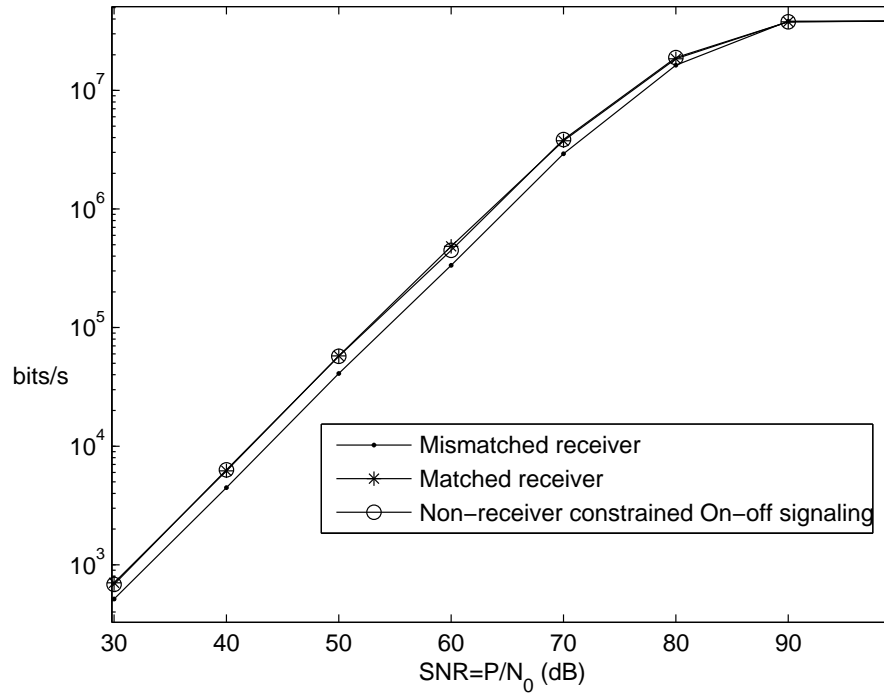


Fig. II-11. Comparison of the achievable data rates of the considered practical non-coherent receivers. A typical (i.e. $\alpha = 0.1$) scattering environment is considered. $T_d=25\text{ns}$, $W=1\text{GHz}$.

Performing respectively variable changes $\underline{y} = \sqrt{\frac{1}{N_0}} \underline{r}$ and $\underline{s} = \underline{r} \text{diag} \left(\sqrt{N_0 + \frac{\lambda_i E_s}{\eta}} \right)^{-1}$ in the first and second integral of the right-hand side of equation II-31 we obtain the desired result.

UWB *On-off* Signaling With Imperfect Channel Estimation

In the previous chapter we analyzed the achievable data rates of non-coherent UWB channels when using *On-off* signaling. We showed that this scheme approaches, without reaching, the AWGN capacity in the low data rate region. The observed suboptimality is compliant with, the previously cited, result by Verdu on the slope at the origin of the growth of spectral efficiency versus $(E_b/N_0)_{\min}$. Nevertheless, the suboptimality of non-coherent detection versus coherent detection, shown by verdu in the non-null spectral efficiency regime, do not consider the cost of channel estimation required to perform coherent detection.

In this chapter we try to bring a better insight onto the question of characterizing the suboptimality of non-coherent detection, with respect to coherent detection, for UWB systems. The analysis is restricted to the case where *On-off* signaling is used. The results of the previous chapter suggest this signaling strategy is a *good* one, even though not proved to be best, in the low spectral efficiency region. We address the considered problem, by looking at the case where the receiver have access to an imperfect channel state information (CSI). Indeed, we analyze how good the latter needs to be in order to significantly improve the achievable data rates with respect to those of a fully non-coherent receiver. This analysis will allow to assess both the performance of practical coherent receivers, since in practice only imperfect CSI is available to the receiver, and the suboptimality of non-coherent detection.

The effect of channel estimation imperfections on system performance, have been studied

for some particular channels and settings. In [39],[41], [42] finite-state channels with imperfect CSI at the receiver are considered and the effect of the later on mutual information analyzed. In [40], Caire and Shamai looked at the impact of some configurations of CSI at both the transmitter and the receiver on the optimal coding strategies. They consider both channels with and without state memory, in particular finite-state Markov and Rayleigh fading channels. Lapidoth and Shamai[38] considered flat fading channels and analyzed the robustness of the optimality of Gaussian codebooks when channel estimation is subject to imperfections (i.e. partially known channels). Unlike previous works they considered practical decoding rules rather than implicitly assume the use of the optimal one. Lately UWB channels were considered [43] and [44]. In [43], uncoded PPM modulation, over a discrete frequency selective channel, is analyzed in the case where the receiver has access to an imperfect genie-aided channel estimation. The authors derived the system's performance, in terms of error probability and achievable data rates under ML decoding. They also have drawn the implications of the quality of the channel estimate on the optimal number of channel taps to be estimated when using RAKE type of receivers. In [44], the impact of imperfect paths amplitudes estimation on the performance of antipodal modulation is analyzed. The results were obtained for a diversity combining receiver.

In the previous chapter we compared the performance of non-coherent detection (i.e. channel always unknown) and coherent detection (genie-aided). The first one was shown to perform very close to the second in low spectral efficiency regime but still suffer a significant suboptimality in higher spectral efficiency regime. Here we explore the effect of channel stationarity, which allows for channel estimation, on closing the gap from the performance of the genie-aided coherent receiver. In our work we consider a realistic setting, in the sense that the channel estimate available to the receiver is obtained through the use of training sequences. A longer training sequence results in both a better channel estimate and a higher cost in terms of reduction of the useful transmitted symbols. Hence, the considered problem brakes down to answering the question of how much effort should be put into channel estimation in order to minimize the detection error probability for a given effective (i.e. useful) achievable transmission data rate. The analysis is achieved through the derivation of bounds on the decoding error probability assuming that the systems uses finite length codes and either an ML receiver or a suboptimal version of it.

A MODELS

We use the signaling scheme and block fading channel model introduced in chapter (II). The transmitted *On-off* symbols are gathered into codewords of length BN before being transmitted over the channel. The symbols constituting a same codeword are transmitted in a sequential fashion over the channel. N is being choosed such that NT_s is equal to

the channel coherence time T_c ¹. Therefore, each consecutive block of N symbols, face the same channel realization². B is the number of blocks.

Recalling the notations from the previous chapter, we write the received signal during the k th symbol duration of the b th symbol block, as follows

$$r_{i,k,b} = \sqrt{\frac{E_s \lambda_i}{\eta}} h_{i,b} u_{k,b} + z_{i,k,b} \quad (\text{III-1})$$

where again $\underline{h}_b = [h_{1,b}, \dots, h_{D,b}]$ is a zero-mean complex random vector with identity covariance matrix and $u_{k,b}$ is the k th transmitted symbol within the b th block. In the following we term \underline{u}_b the vector of transmitted symbols within the b th block. From our model, the channel random process contains BD degrees (DoF) of freedom over the BN -long block of symbols. In [50], Verdú and Han show that if, as the codeword length goes to infinity, the number of degrees of freedom of the channel random process stays finite³ then its capacity converges to the one of an AWGN channel with the same bandwidth.

B SEQUENCE ML DETECTION RULE

In this section we derive the maximum likelihood sequence detection rule for the considered setting.

$$\underset{\underline{u}_b; b=1,\dots,B}{\operatorname{argmax}} \Pr(\{r_{k,b}; k=1,\dots,N; b=1,\dots,B\} | \underline{u}_b; b=1,\dots,B) \quad (\text{III-2})$$

In the following developments we replace the set of received signal vectors $\{r_{k,b}; k=1,\dots,N; b=1,\dots,B\}$ with the equivalent set of vectors $\{\underline{y}_{i,b}; i=1,\dots,D; b=1,\dots,B\}$ for convenience, where $\underline{y}_{i,b}$ is defined as follows

$$\underline{y}_{i,b}^T = \begin{bmatrix} \sqrt{\frac{E_s \lambda_i}{\eta}} h_{i,b} u_{1,b} + z_{i,1,b} \\ \sqrt{\frac{E_s \lambda_i}{\eta}} h_{i,b} u_{2,b} + z_{i,2,b} \\ \dots \\ \sqrt{\frac{E_s \lambda_i}{\eta}} h_{i,b} u_{N,b} + z_{i,N,b} \end{bmatrix} = \sqrt{\frac{E_s \lambda_i}{\eta}} h_{i,b} \underline{u}_b + \underline{z}_{i,b} \quad (\text{III-3})$$

¹To be more precise N is chosen such that $NT_s \leq T_c < (N+1)T_s$

²From our block fading channel model

³From our model this would correspond to having an infinite channel coherence-time T_c

Conditioned on the transmitted codeword (i.e. symbol sequence), vectors $\underline{y}_{i,b}$ are zero mean complex Gaussian. Their cross-correlation is given by

$$\mathbf{K}_i(\underline{u}_b) = E \left[\underline{y}_{i,b}^H \underline{y}_{i,b} | \underline{u}_b \right] \quad (\text{III-4})$$

$$= \frac{E_s \lambda_i}{\eta} \underline{u}_b^T \underline{u}_b \quad (\text{III-5})$$

Note that vectors $\{\underline{y}_{i,b}\}$ are statistically independent for different values of block index b from our channel model. Moreover, for the same value of b we have that

$$E \left[\underline{y}_{i,b}^H \underline{y}_{j,b} | \underline{u}_b \right] = \mathbf{0} \quad \text{for } i \neq j \quad (\text{III-6})$$

Thus the probability distribution of the observation vectors conditioned on $\{\underline{u}_b\}$ is written as follows

$$\begin{aligned} & \Pr \left(\{ \underline{y}_{i,b}; i = 1, \dots, D; b = 1, \dots, B \} | \underline{u}_b; b = 1, \dots, B \right) \\ &= \prod_{b=1}^B \prod_{i=1}^D \Pr \left(\underline{y}_{i,b} | \underline{u}_b \right) \end{aligned} \quad (\text{III-7})$$

$$= \prod_{b=1}^B \prod_{i=1}^D \frac{1}{|\det(\mathbf{K}_i(\underline{u}_b))|} e^{-\underline{y}_{i,b}^H \mathbf{K}_i^{-1}(\underline{u}_b) \underline{y}_{i,b}} \quad (\text{III-8})$$

The matrix $\frac{E_s \lambda_i}{\eta N_0} \underline{u}_b^T \underline{u}_b + \mathbf{I}$ has two distinct eigenvalues. The first one is $1 + \frac{E_s \lambda_i}{\eta N_0} \underline{u}_b^T \underline{u}_b$, with multiplicity 1, associated to the eigenvector $\frac{1}{\|\underline{u}_b\|} \underline{u}_b$. The second eigenvalue is 1 with multiplicity $N - 1$. Through an eigenvalue decomposition we rewrite $\mathbf{K}_i(\underline{u}_b)$ as follows

$$\mathbf{K}_i(\underline{u}_b) = N_0 \mathbf{A}_i^H(\underline{u}_b) \mathbf{\Lambda}_i \mathbf{A}_i(\underline{u}_b) \quad (\text{III-9})$$

where $\mathbf{\Lambda}_i = \mathbf{diag} \left(1 + \frac{E_s \lambda_i}{\eta N_0} \underline{u}_b^T \underline{u}_b, 1, \dots, 1 \right)$ and $\mathbf{A}_i(\underline{u}_b)$ a unitary matrix whose first vector is \underline{u}_b . For $i = 1, \dots, D$ let $\underline{v}_{i,b} = \mathbf{A}_i^H(\underline{u}_b) \underline{u}_b$.

$$\det(\mathbf{K}_i(\underline{u}_b)) = N_0^N \left(1 + \frac{E_s \lambda_i}{\eta N_0} \underline{u}_b^T \underline{u}_b \right) \quad (\text{III-10})$$

Considering blockwise constant weight codebooks (i.e. all codewords containing the same number of *ones* within each block⁴) $\underline{u}_b \underline{u}_b^T$ is independent of \underline{u}_b . Throughout the rest of

⁴of size N

the chapter we assume the use of blockwise constant weight codebooks⁵ so that the terms $|\det(\mathbf{K}_i(\underline{u}_b))|$ are independent of codeword block \underline{u}_b .

$$\begin{aligned}
& \underset{\underline{u}_b}{\operatorname{argmax}}_{b=1,\dots,B} \Pr(\{\underline{r}_{k,b} \mid k=1,\dots,N \quad b=1,\dots,B\} | \underline{u}_b, b=1,\dots,B) \\
&= \underset{\underline{u}}{\operatorname{argmin}}_{b=1,\dots,B} \sum_{b=1}^B \sum_{i=1}^D y_{i,b} \mathbf{K}_i^{-1}(\underline{u}_b) y_{i,b}^H \\
&= \underset{\underline{u}}{\operatorname{argmin}}_{b=1,\dots,B} \sum_{b=1}^B \sum_{i=1}^D v_{i,b} \mathbf{\Lambda}_i^{-1}(\underline{u}_b) v_{i,b}^H \tag{III-11}
\end{aligned}$$

Noting that $v_{i,b} v_{i,b}^H = \underline{y}_{i,b} \underline{y}_{i,b}^H$ is independent of \underline{u}_b , we rewrite (III-11) as follows

$$\begin{aligned}
& \underset{\underline{u}_b}{\operatorname{argmax}}_{b=1,\dots,B} \Pr(\{\underline{r}_{k,b} \mid k=1,\dots,N \quad b=1,\dots,B\} | \underline{u}_b, b=1,\dots,B) \\
&= \underset{\underline{u}_b}{\operatorname{argmin}}_{b=1,\dots,B} \sum_{b=1}^B \left(\sum_{i=1}^D v_{i,b} \mathbf{\Lambda}_i^{-1}(\underline{u}_b) v_{i,b}^H - \sum_{i=1}^D v_{i,b} v_{i,b}^H \right) \\
&= \underset{\underline{u}_b}{\operatorname{argmin}}_{b=1,\dots,B} \sum_{b=1}^B \sum_{i=1}^D v_{i,b} (\mathbf{\Lambda}_i^{-1} - \mathbf{I}) (\underline{u}_b) v_{i,b}^H \\
&\stackrel{(a)}{=} \underset{\underline{u}_b}{\operatorname{argmax}}_{b=1,\dots,B} \sum_{b=1}^B \sum_{i=1}^D \alpha_i \left| \underline{y}_{i,b} \underline{u}_b^T \right|^2 \tag{III-12}
\end{aligned}$$

Where $\alpha_i = \left(\frac{\frac{E_s \lambda_i}{\eta N_0} \underline{u}_b \underline{u}_b^T}{1 + \frac{E_s \lambda_i}{\eta N_0} \underline{u}_b \underline{u}_b^T} \right)$. In (a) we use the fact that $\mathbf{\Lambda}_i^{-1} - \mathbf{I} = \mathbf{diag} \left(-\frac{\frac{E_s \lambda_i}{\eta N_0} \underline{u}_b \underline{u}_b^T}{1 + \frac{E_s \lambda_i}{\eta N_0} \underline{u}_b \underline{u}_b^T}, 0, \dots, 0 \right)$ and that $\frac{1}{\|\underline{u}_b\|} \underline{u}_b$ is the first eigenvector of \mathbf{A} .

B.1 Training sequence

We consider now the particular case where a fraction of the transmitted symbols, within each block, is used as a training sequence (i.e. an all 1 sequence).

$$\underline{u}_b = \begin{bmatrix} (\underline{u}_b^t)^T \\ (\underline{u}_b^d)^T \end{bmatrix}^T \tag{III-13}$$

⁵ m -PPM modulation is a particular case of such channel coding strategy

We similarly decompose $\underline{y}_{i,b}$ as follows

$$\underline{y}_{i,b} = \begin{bmatrix} \left(\underline{y}_{i,b}^t \right)^T \\ \left(\underline{y}_{i,b}^d \right)^T \end{bmatrix}^T \quad (\text{III-14})$$

Thus

$$\begin{aligned} \left| \underline{y}_{i,b} \underline{u}_b^T \right|^2 &= \left| \sum_{j=1}^T y_{i,j,b} + \sum_{j=T+1}^N u_{j,b} y_{i,j,b} \right|^2 \\ &= \left| \sum_{j=1}^T y_{i,j,b} \right|^2 + \left| \sum_{j=T+1}^N u_{j,b} y_{i,j,b} \right|^2 \\ &\quad + 2\mathcal{R}e \left(\left(\sum_{j=1}^T y_{i,j,b} \right) \left(\sum_{j=T+1}^N u_{j,b} y_{i,j,b}^* \right) \right) \end{aligned} \quad (\text{III-15})$$

$\left| \sum_{j=1}^T y_{i,j,b} \right|^2$ is independent of \underline{u}_b thus

$$\begin{aligned} &\underset{\underline{u}_b; b=1,\dots,B}{\operatorname{argmax}} \Pr \left(\{r_{k,b}; k=1,\dots,N; b=1,\dots,B\} | \underline{u}_b; b=1,\dots,B \right) \\ &= \underset{(\underline{u}_b)^d; b=1,\dots,B}{\operatorname{argmax}} \sum_{b=1}^B \sum_{i=1}^D \alpha_i \left(\left| \underline{y}_{i,b}^d (\underline{u}_b^d)^T \right|^2 + 2T\mathcal{R}e \left(\hat{h}_{i,b}^* \left(\underline{y}_{i,b}^d (\underline{u}_b^d)^T \right) \right) \right) \end{aligned} \quad (\text{III-16})$$

where $\hat{h}_{i,b} = \frac{1}{T} \sum_{j=1}^T y_{i,j,b}$. $\hat{h}_{i,b}$ is the channel estimate obtained by the receiver from the transmitted training sequence. We note that the ML decision rule when using a training sequence (III-16) is the sum of the decision metric of the fully non-coherent case (III-12) and a *correction* term corresponding to a coherent detection⁶.

The obtained detection rule (III-16) is different (i.e. contains an additional term) from the commonly used detection metric for coherent receivers (i.e. RAKE receivers).

$$\begin{aligned} &\underset{\underline{u}_b; b=1,\dots,B}{\operatorname{argmax}} \Pr \left(\{r_{k,b}; k=1,\dots,N; b=1,\dots,B\} | \underline{u}_b; b=1,\dots,B \right) \\ &= \underset{(\underline{u}_b)^d; b=1,\dots,B}{\operatorname{argmax}} \sum_{b=1}^B \sum_{i=1}^D \alpha_i \mathcal{R}e \left(\hat{h}_{i,b}^* \left(\underline{y}_{i,b}^d (\underline{u}_b^d)^T \right) \right) \end{aligned} \quad (\text{III-17})$$

⁶To be more rigorous, it corresponds to a quasi-coherent detection, since the receiver uses an imperfect channel estimate

This means that the latter is suboptimal. Nevertheless one should note that the non-coherent detection term is non additive unlike the coherent detection one. This means that in practice the use of the complete ML detection rule will significantly increase the complexity of trellis-based decoding algorithms, such as the Viterbi [46] and Forward-backward algorithms [47]. In the following we will characterize the performance degradation induced by not considering the non-coherent energy detection term in (III-16).

C ERROR PROBABILITY UPPER-BOUND

In this section we derive upper bounds on the decoding error probability of the considered system. The derivation follows standard arguments used to derive random coding bounds [45],[32]. First a Chernoff bound on the pairwise error probability is computed then a union bound is used. The latter, is averaged over all random codebook realizations.

The data is encoded using a randomly generated codebook $\mathcal{U} = \{\underline{u}^{(1)}, \underline{u}^{(2)}, \dots, \underline{u}^{(M)}\}$ of cardinality M and codeword length BN . Each codeword $\underline{u}^{(l)}$ is constituted by B symbol blocks. We note, $\underline{u}_b^{(l)}$, the b th symbol block of codeword $\underline{u}^{(l)}$. As stated in the previous section, we restrict the transmitter to the use of blockwise constant-weight codebooks. Thus, all codewords blocks $\underline{u}_b^{(l)}$ contain the same number ηN of *ones*. The system has the possibility to use a fraction of those *ones* (i.e. transmitted pulses) as a training sequence. Let $\eta_t N$ be the length of the training sequence⁷, $0 \leq \eta_t < \eta$. For given transmit probability η , training sequence proportion η_t and codebook length BN we can construct orthogonal codebooks with as many codewords as $M = \left(\binom{(1 - \eta_t)N}{(\eta - \eta_t)N} \right)^B$. Later, the length of the training sequence will be optimized to minimize the error probability. Note that when using the exact ML detection rule, one should expect the optimal training sequence length to be equal to zero since the random coding scheme includes codebooks with arbitrary training sequence lengths. Of course the latter statement holds only assuming that random coding is capable of achieving (asymptotically in codeword length) the capacity of the considered channel constrained to the use of *On-off* signaling. Nevertheless, the optimization of $\eta_t N$, is definitely of interest when considering the suboptimal ML detection rule (III-17).

The decoder forms the decision variables $q(l)$ for all candidate codewords $\{\underline{u}^{(l)} \quad l = 1, \dots, M\}$ and uses the following threshold decoding rule to decide on a message: if $q(l)$ exceeds a certain threshold ρ for exactly one value of l , say \hat{l} , then it will declare that \hat{l} was transmitted. Otherwise, it will declare a decoding error. This is the same sub-optimal decoding scheme considered in [31]. In the following $q(l)$ will be chosen to be either exact

⁷We assume that η and η_t are chosen such that ηN and $\eta_t N$ are integers.

ML decoding metric (III-16) or the suboptimal ML detection metric (III-17). The threshold detection is commonly used in similar settings to prove coding theorems.

$$P_e = E_{\mathcal{U}} \left[P_{e|\mathcal{U}} \right] \quad (\text{III-18})$$

We term c the index of the actually transmitted codeword. Due to the problem symmetry, c can be arbitrarily chosen without loss of generality. Using a union bound we upper bound the probability of error

$$P_{e|\mathcal{U}} \leq \sum_{\substack{l=1 \\ l \neq c}}^M \Pr(q(l) \geq \rho|\mathcal{U}) + \Pr(q(c) \leq \rho|\mathcal{U}) \quad (\text{III-19})$$

We upper bound error probability terms using Chernoff bound. Codewords are independent and identically distributed, from our random coding assumption. Therefore (III-19) is developed as

$$\begin{aligned} P_e &\leq \sum_{\substack{l=1 \\ l \neq c}}^M E_{\mathcal{U}} [\Pr(q(l) \geq \rho|\mathcal{U})] + \Pr(q(c) \leq \rho) \\ &= (M-1) E_{\mathcal{U}} [\Pr(q(l) \geq \rho|\mathcal{U})] + \Pr(q(c) \leq \rho) \\ &= (M-1) E_{\mathcal{U}} \left[\min_{s>0} e^{-s\rho} E \left[e^{sq(l)} | \mathcal{U} \right] \right] + \min_{t>0} e^{t\rho} E \left[e^{-tq(c)} \right] \end{aligned} \quad (\text{III-20})$$

C.1 ML detection metric

$q(l)$ is defined as in (III-16). Nevertheless, for the sake of higher clarity in the mathematical developments, we will rather use the following equivalent metric

$$q(l) = \sum_{b=1}^B \sum_{i=1}^D \frac{\alpha_i}{(\eta N)^2} \left| y_{i,b} \left(\underline{u}_b^{(l)} \right)^T \right|^2 \quad (\text{III-21})$$

Note that the later metric is equal to the one in (III-16) up to an additive constant (i.e. independent of $\underline{u}_b^{(l)}$).

Let k_b be the number of *collisions* between codewords $\underline{u}_b^{(l)}$ and $\underline{u}_b^{(c)}$ defined as follows

$$k_b = \left(\underline{u}_b^{(l)} \right)^d \left(\left(\underline{u}_b^{(c)} \right)^d \right)^T \quad (\text{III-22})$$

k_b take values between 0 and $(\eta - \eta_t)N$. Let $\sigma_{l,b}(\cdot)$ be a permutation of the ordered ensemble $\{\eta_t N + 1, \dots, N\}$ such that the indices of the transmitted pulses within codeword $\underline{u}_b^{(l)}$, are $\{\sigma_{l,b}(\eta_t N + 1), \dots, \sigma_{l,b}(\eta_t N + k)\}$. We rewrite $q(l)$ as follows

$$\begin{aligned} q(l) &= \sum_{b=1}^B \sum_{i=1}^D \alpha_i \left| \left(\frac{\eta_t}{\eta} + \frac{k}{\eta N} \right) \sqrt{\frac{E_s \lambda_i}{\eta}} h_{i,b} + \frac{1}{\eta N} \left(\sum_{j=1}^{\eta_t N} n_{i,j,b} + \sum_{j=1}^{(\eta - \eta_t)N} n_{i,\sigma_{l,b}(j),b} \right) \right|^2 \\ &= \sum_{b=1}^B \sum_{i=1}^D \alpha_i |a_{i,k,b}|^2 \end{aligned} \quad (\text{III-23})$$

where $a_{i,l,b}$ is a zero-mean complex Gaussian random variable with variance $\left(\frac{\eta_t}{\eta} + \frac{k}{\eta N} \right) \frac{E_s \lambda_i}{\eta} + \frac{N_0}{\eta N}$.

$$\begin{aligned} E \left[e^{sq(l)} | \mathcal{U} \right] &= \prod_{b=1}^B \prod_{i=1}^D E \left[e^{s\alpha_i |a_{i,k,b}|^2} | \mathcal{U} \right] \\ &= \prod_{b=1}^B \prod_{i=1}^D \frac{1}{1 - s\alpha_i \left(\left(\frac{\eta_t}{\eta} + \frac{k_b}{\eta N} \right) \frac{E_s \lambda_i}{\eta} + \frac{N_0}{\eta N} \right)} \end{aligned} \quad (\text{III-24})$$

For the sake of feasibility of the analytical minimization of equation (III-37) as function of s we assume that the channel has a flat eigenvalues profile $\lambda_i = \lambda = 1/D$ $i = 1, \dots, D$. Thus, α_i , $i = 1, \dots, D$ maybe set to 1 without modifying the problem. Throughout the rest of this section we take $\alpha_i = 1$, $i = 1, \dots, D$.

$$\begin{aligned} E \left[e^{sq(l)} | \mathcal{U} \right] &= \prod_{b=1}^B \left(\frac{1}{1 - s \left(\left(\frac{\eta_t}{\eta} + \frac{k_b}{\eta N} \right) \frac{E_s \lambda}{\eta} + \frac{N_0}{\eta N} \right)} \right)^D \\ &= \prod_{k=0}^{(\eta - \eta_t)N} \left(\frac{1}{1 - s \left(\left(\frac{\eta_t}{\eta} + \frac{k}{\eta N} \right) \frac{E_s \lambda}{\eta} + \frac{N_0}{\eta N} \right)} \right)^{Dm_k} \end{aligned} \quad (\text{III-25})$$

where m_k is the multiplicity k in the sequence $\{k_1, \dots, k_B\}$. Similarly we compute $e^{t\rho} E \left[e^{-tq(c)} | \mathcal{U} \right]$

and show that

$$\begin{aligned}
e^{t\rho} E \left[e^{-tq(c)} | \mathcal{U} \right] &= e^{t\rho} \left(\frac{1}{1 + t \left(\frac{E_s \lambda}{\eta} + \frac{N_0}{\eta N} \right)} \right)^{DB} \\
&= e^{t\rho - DB \log \left(1 + t \left(\frac{E_s \lambda}{\eta} + \frac{N_0}{\eta N} \right) \right)} \\
&= e^{f(s)}
\end{aligned} \tag{III-26}$$

minimizing $e^{t\rho} E \left[e^{-tq(c)} | \mathcal{U} \right]$ as function of t is equivalent to minimizing, as function of t , $f(t)$. Where $f(t)$ is defined as follows

$$f(t) = t\rho - DB \log \left(1 + t \left(\frac{E_s \lambda}{\eta} + \frac{N_0}{\eta N} \right) \right) \tag{III-27}$$

The later minimization yields

$$\min_{t>0} e^{t\rho} E \left[e^{-tq(c)} \right] = e^{DB - \frac{\rho}{\frac{E_s \lambda}{\eta} + \frac{N_0}{\eta N}} - DB \log \left(\frac{DB}{\rho} \left(\frac{E_s \lambda}{\eta} + \frac{N_0}{\eta N} \right) \right)} \tag{III-28}$$

Decoding threshold

We choose the decoding threshold ρ to be equal to $(1 - \epsilon)DB (E_s \lambda / \eta + N_0 / \eta N)$. Such that $0 \leq \epsilon < 1$. The reasoning behind this choice is that as B goes to infinity, $q(c)$ converges to $DB (E_s \lambda / \eta + N_0 / \eta N)$. Therefore, as B goes to infinity $q(c)$ can be made larger than ρ for arbitrarily small values of ϵ . In our finite block length analysis, we will optimize ϵ as function of the codeword length BN and other system parameters.

Random coding

As shown earlier in this section $E \left[e^{s(q(l) - \rho)} | \mathcal{U} \right]$ does not depend on the particular choice of codewords \underline{u}_l and \underline{u}_c but only on the sequence $\{m_0, \dots, m_B\}$. Indeed, in equation (III-20) the expectation over the set of codebooks breaks down to an expectation over $\{m_0, \dots, m_B\}$. Given that the codebooks are generated randomly, $\{m_0, \dots, m_B\}$ is distributed according to a multinomial distribution for $\eta N \leq \lfloor \frac{N}{2} \rfloor$. Performing a looser minimization over s we obtain

$$E_{\mathcal{U}} \left[\min_{s>0} e^{-s\rho} E \left[e^{sq(l)} | \mathcal{U} \right] \right] \leq \min_{s>0} E_{\mathcal{U}} \left[e^{-s\rho} E \left[e^{sq(l)} | \mathcal{U} \right] \right] \tag{III-29}$$

Indeed, equation (III-20) can be rewritten as follows

$$\begin{aligned}
P_e \leq & (M-1) \min_{s>0} \sum_{m_0, \dots, m_B} \binom{B}{m_0, \dots, m_B} \\
& \prod_{k=0}^{(\eta-\eta_t)N} \left(\left(\frac{\eta-\eta_t}{1-\eta_t} \right)^k \left(1 - \left(\frac{\eta-\eta_t}{1-\eta_t} \right) \right)^{(\eta-\eta_t)N-k} \right)^{m_k} \\
& \left(\frac{1}{1-s \left(\left(\frac{\eta_t}{\eta} + \frac{k}{\eta N} \right) \frac{E_s \lambda}{\eta} + \frac{N_0}{\eta N} \right)} \right)^{Dm_k} \\
& + \min_{t>0} e^{t\rho} E \left[e^{-tq(c)} \right]
\end{aligned} \tag{III-30}$$

Let R be the transmitted data rate. R is written as function of the codebook size M as follows

$$R = \frac{1}{NT_s} \log_2(M) \tag{III-31}$$

Thus, (III-30) can be rewritten as follows

$$\begin{aligned}
P_e \leq & (2^{BNRT_s-1}) \\
& \left[\sum_{k=0}^{(\eta-\eta_t)N} \left(\left(\frac{\eta-\eta_t}{1-\eta_t} \right)^k \left(1 - \left(\frac{\eta-\eta_t}{1-\eta_t} \right) \right)^{(\eta-\eta_t)N-k} \right) \right. \\
& \left. \left(\frac{1}{1-s \left(\left(\frac{\eta_t}{\eta} + \frac{k}{\eta N} \right) \frac{E_s \lambda}{\eta} + \frac{N_0}{\eta N} \right)} \right)^{D} \right]^B \\
& + e^{DB - \frac{\rho}{\frac{E_s \lambda}{\eta} + \frac{N_0}{\eta N}} - DB \log \left(\frac{DB}{\rho} \left(\frac{E_s \lambda}{\eta} + \frac{N_0}{\eta N} \right) \right)}
\end{aligned} \tag{III-32}$$

The minimization over s will be performed numerically.

Orthogonal codes

Rather than using codebooks generated at random as in section () , in this section we consider orthogonal codebooks. By orthogonal codebook, we term a codebook whose any pair of codewords has a null number of collisions $m_k = 0$ for $k > 0$. For given transmit probability η , training sequence proportion η_t and codebook length BN we can construct

orthogonal codebooks with as many codewords as $M = \left(\frac{1-\eta_t}{\eta-\eta_t}\right)^B$. For orthogonal codebooks the pairwise error probability is uniform and can be obtained directly from (C.1) taking $m_k = 0$ for $k > 0$. Thus, the average error probability achieved by orthogonal codebooks is

$$\begin{aligned}
P_e &\leq (M-1) \min_{s>0} e^{-s\rho} \left(\frac{1}{1-s \left(\left(\frac{\eta_t}{\eta}\right) \frac{E_s\lambda}{\eta} + \frac{N_0}{\eta N} \right)} \right)^{DB} \\
&= (2^{BNRT_s}-1) e^{DB - \frac{\rho}{\frac{\eta_t}{\eta} \frac{E_s\lambda}{\eta} + \frac{N_0}{\eta N}} - DB \log \left(\frac{DB \left(\frac{\eta_t}{\eta} \frac{E_s\lambda}{\eta} + \frac{N_0}{\eta N} \right)}{\rho} \right)} \\
&+ e^{DB - \frac{\rho}{\frac{E_s\lambda}{\eta} + \frac{N_0}{\eta N}} - DB \log \left(\frac{DB}{\rho} \left(\frac{E_s\lambda}{\eta} + \frac{N_0}{\eta N} \right) \right)} \tag{III-33}
\end{aligned}$$

One can expect orthogonal codes to be optimal in the low data rate region (i.e. low SNR region) since they achieve the lowest average pairwise error probability among the set of all possible codebooks and at the same time allow for large enough codebooks to target the data rates of interest in the considered SNR region.

C.2 Suboptimal ML detection metric

$q(l)$ is defined as in (III-17). We recall the definition of k_b from the previous section (C.1) and again assume that the channel eigenvalue profile is flat.

$$\begin{aligned}
q(l) &= \sum_{b=1}^B 2\mathcal{R}e \left[\left(\sqrt{\frac{E_s\lambda}{\eta}} h_{i,b} + \frac{1}{\eta_t N} \sum_{j=1}^{\eta_t N} n_{i,j,b} \right)^* \right. \\
&\quad \left. \left(\frac{k_b}{(\eta-\eta_t)N} \sqrt{\frac{E_s\lambda}{\eta}} h_{i,b} + \frac{1}{(\eta-\eta_t)N} \sum_{j=\eta_t N+1}^{\eta N} n_{i,j,b} \right) \right] \tag{III-34}
\end{aligned}$$

In the following we note respectively $e_{1,i,b} = \frac{1}{\eta_t N} \sum_{j=1}^{\eta_t N} n_{i,j,b}$, $e_{2,i,b} = \frac{1}{(\eta-\eta_t)N} \sum_{j=\eta_t N+1}^{\eta N} n_{i,\sigma_{1,b}(j),b}$, and $e_{3,i,b} = \sqrt{\frac{E_s\lambda}{\eta}} h_{i,b}$. $e_{1,i,b}$, $e_{2,i,b}$, and $e_{3,i,b}$ are independent complex Gaussian variables.

In order to compute $E[e^{sq(l)}|\mathcal{U}]$, we rewrite $q(l)$ as a sum of independent Hermitian quadratic forms of complex Gaussian vectors which allows us to use Turin's result on the character-

istic functions of Hermitian quadratic forms in complex normal variables [48]. Indeed, we reformulate $q(l)$ as follows

$$q(l) = \sum_{b=1}^B \sum_{i=1}^d \underline{g}_{i,b} \mathbf{M}_{i,b} \underline{g}_{i,b}^H \quad (\text{III-35})$$

where $\underline{g}_{i,b} = [e_{1,i,b} e_{2,i,b} e_{3,i,b}]$ is a size 3 complex Gaussian vector of zero mean and covariance matrix $\mathbf{R}_i = \mathbf{diag} \left(\frac{N_0}{\eta_t N}, \frac{N_0}{(\eta - \eta_t) N}, \frac{E_s \lambda}{\eta} \right)$. While $\mathbf{M}_{i,b}$ is the matrix with real entries defined as follows

$$\mathbf{M}_{i,b} = \begin{pmatrix} 0 & 1 & \nu(k_b) \\ 1 & 0 & 1 \\ \nu(k_b) & 1 & 2\nu(k_b) \end{pmatrix} \quad (\text{III-36})$$

where $\nu(k_b) = k_b / ((\eta - \eta_t) N)$. Applying Turin's result [48] we obtain

$$\begin{aligned} E \left[e^{sq(l)} | \mathcal{U} \right] &= \prod_{b=1}^B \prod_{i=1}^D E \left[e^{s \underline{g}_{i,b} \mathbf{M}_{i,b} \underline{g}_{i,b}^H} | \mathcal{U} \right] \\ &= \prod_{b=1}^B \prod_{i=1}^D \left(\frac{1}{|\mathbf{I} - s \mathbf{R}_i \mathbf{M}_{i,b}|} \right) \\ &= \prod_{b=1}^B \left(\frac{1}{|\mathbf{I} - s \mathbf{R}_i \mathbf{M}_{i,b}|} \right)^D \end{aligned} \quad (\text{III-37})$$

$$|\mathbf{I} - s \mathbf{R}_i \mathbf{M}_{i,b}| = 1 - 2\nu(k_b) \frac{E_s \lambda}{\eta} s - \left(\frac{N_0}{(\eta - \eta_t) N} \left(\frac{E_s \lambda}{\eta} + \frac{N_0}{\eta_t N} \right) + \nu^2(k_b) \frac{E_s \lambda}{\eta} \frac{N_0}{\eta_t N} \right) s^2 \quad (\text{III-38})$$

Decoding threshold

Following the same reasoning as in section () we take the decoding threshold to be equal to $(1 - \epsilon) B \frac{E_s}{\eta}$.

$$\begin{aligned} \rho &= (1 - \epsilon) \quad 0 \leq \epsilon \leq 1 \\ &= (1 - \epsilon) \frac{E_s}{\eta} \end{aligned} \quad (\text{III-39})$$

Orthogonal codes

For the sake of feasibility of mathematical developments, we restrict the system to the use of orthogonal codebooks defined as in section (). Therefore

$$\begin{aligned} E \left[e^{sq(l)} \right] &= \left(1 - 2\nu(0) \frac{E_s \lambda}{\eta} s - \left(\frac{N_0}{(\eta - \eta_t)N} \left(\frac{E_s \lambda}{\eta} + \frac{N_0}{\eta_t N} \right) + \nu^2(0) \frac{E_s \lambda}{\eta} \frac{N_0}{\eta_t N} \right) s^2 \right)^{DB} \\ &= e^{-DB \log(f(s))} \end{aligned} \quad (\text{III-40})$$

Thus

$$\begin{aligned} \min_{s>0} e^{-s\rho} E \left[e^{sq(l)} \right] &= \min_{s>0} e^{-s\rho - DB \log(f(s))} \\ &= e^{\min_{s>0} g(s)} \end{aligned} \quad (\text{III-41})$$

Minimizing $g(s)$ as function of s yields the following expression

$$\begin{aligned} \underset{s>0}{\text{argmin}} g(s) &= -\frac{D}{\rho} - \frac{\nu_0 \left(\frac{E_s \lambda}{\eta} \right)}{\frac{N_0}{(\eta - \eta_t)N} \left(\frac{E_s \lambda}{\eta} + \frac{N_0}{\eta_t N} \right) + \nu^2(0) \frac{E_s \lambda}{\eta} \frac{N_0}{\eta_t N}} \\ &+ \sqrt{\frac{D^2}{\rho^2} + \frac{\nu^2(0) \left(\frac{E_s \lambda}{\eta} \right)^2}{\left(\frac{N_0}{(\eta - \eta_t)N} \left(\frac{E_s \lambda}{\eta} + \frac{N_0}{\eta_t N} \right) + \nu^2(0) \frac{E_s \lambda}{\eta} \frac{N_0}{\eta_t N} \right)^2} + \frac{1}{\frac{N_0}{(\eta - \eta_t)N} \left(\frac{E_s \lambda}{\eta} + \frac{N_0}{\eta_t N} \right) + \nu^2(0) \frac{E_s \lambda}{\eta} \frac{N_0}{\eta_t N}}} \end{aligned} \quad (\text{III-42})$$

Similarly we compute $E \left[e^{-tq(c)} \right]$. The numerical optimization of the decoding error probability as function of design parameters (i.e. η , η_t , ϵ) is still in progress and will be presented later on.

C.3 Pure non-coherent receiver

In this section we look at the performance of the non-coherent receiver introduced in chapter II. The latter is an energy receiver which does not exploit channel stationarity in order to implicitly perform a channel estimation. The motivation for analyzing the performance of this receiver is twofold. i), as seen in the previous chapter, this receiver allows for a low complexity implementation. ii) We are interested in characterizing the penalty, in terms of minimum achieved codeword error probability for a given transmission rate, endured by the non-coherent receiver when not exploiting channel stationarity.

The decision metric of the considered receiver is written as follows

$$q(l) = \sum_{b=1}^B \sum_{k=1}^N \frac{1}{\eta N} \|r_{k,b}\|^2 u_{k,b}^{(l)} \quad (\text{III-43})$$

Note that since the performance comparison with the previously introduced receivers will be performed in the case of flat channel eigenvalues profile, we considered here the non-matched energy detector that was shown, in the previous chapter, to perform as good as the channel-matched receiver in these conditions.

Decoding threshold

Again, following the same reasoning as in section () we take the decoding threshold to be equal to $\rho = (1 - \epsilon)BD \left(\frac{E_s \lambda}{\eta} + N_0 \right)$.

Orthogonal codebooks

We restrict our analysis to the case of orthogonal codebooks

$$\begin{aligned} E \left[e^{sq(l)} \right] &= \prod_{b=1}^B \prod_{k=1}^N E \left[e^{s \frac{1}{\eta N} \|r_{k,b}\|^2 u_{k,b}^{(l)}} \right] \\ &= \left(\frac{1}{1 - s \frac{N_0}{\eta N}} \right)^{B\eta N D} \end{aligned} \quad (\text{III-44})$$

Thus

$$\min_{s>0} e^{-s\rho} E \left[e^{sq(l)} \right] = e^{BD\eta N - \frac{\rho\eta N}{N_0} - BD\eta N \log\left(\frac{BDN_0}{\rho}\right)} \quad (\text{III-45})$$

$$\begin{aligned}
E \left[e^{-tq(c)} \right] &= \prod_{b=1}^B E_{\mathbf{h}_b} \left[\prod_{k=1}^N E \left[e^{-t \frac{1}{\eta N} \|\mathbf{r}_{k,b}\|^2 u_{k,b}^{(t)} | \mathbf{h}_b} \right] \right] \\
&= \prod_{b=1}^B \frac{E_{\mathbf{h}_b} \left[\prod_{i=1}^D e^{\frac{-t\eta N |h_{i,b}|^2}{1+t \frac{N_0}{\eta N}}} \right]}{\left(1+t \frac{N_0}{\eta N}\right)^{D\eta N}} \\
&= \left(\frac{1}{1+t \frac{N_0}{\eta N}} \right)^{BD\eta N} \left(\frac{1}{1+\frac{t}{1+t \frac{N_0}{\eta N}} \frac{E_s \lambda}{\eta}} \right)^{BD} \tag{III-46}
\end{aligned}$$

Therefore the codeword probability of error is upper-bounded as follows

$$\begin{aligned}
P_e &\leq (M-1) e^{BD\eta N - \frac{\rho \eta N}{N_0} - BD\eta N \log\left(\frac{BDN_0}{\rho}\right)} \\
&\quad + \min_{t>0} e^{t\rho} \left(\frac{1}{1+t \frac{N_0}{\eta N}} \right)^{BD\eta N} \left(\frac{1}{1+\frac{t}{1+t \frac{N_0}{\eta N}} \frac{E_s \lambda}{\eta}} \right)^{BD} \tag{III-47}
\end{aligned}$$

D ERROR PROBABILITY LOWER-BOUND

In this section we derive a lower bound on the codeword error probability. Combined to the upper bounds derived in the previous section, this will allow to better assess the performance of the considered signaling and detection scheme. The bound is based on a result due to Poor and Verdu [49]. In [49] they derive a lower bound on the probability of error in generic multi-hypothesis testing problems. The bound holds for finite number of equiprobable hypotheses as well as countably many hypotheses with an arbitrary prior distribution. The bound is summarized in the following result

Theorem 1: Suppose X and Y are random variables, with X taking on a finite (or countably infinite) number of values. The minimum probability of error ϵ in estimating X from Y satisfies the inequality

$$\epsilon \geq (1-\alpha) \Pr(P(X|Y) \leq \alpha) \tag{III-48}$$

for each $\alpha \in [0, 1]$, where $P(X|Y)$ denotes the posterior probability of X given Y .

The bound was shown to be always tighter than both Shannon [51] and Verdu-Han bounds [50] and shares their advantage over the Fano's inequality [30] of providing general converses in channel coding. Note that the Shannon bound [51] is a special case of the Verdu-Poor bound corresponding to the case where α is forced to the value $1/2$.

We use theorem (1) to derive a lower bound on the decoding error probability for the signaling scheme and channel used in the previous section.

$$P_e \geq \max_{\alpha \in [0,1]} (1 - \alpha) \Pr \left(P(\underline{u} | \{\underline{y}_i, i = 1, \dots, D\}) \leq \alpha \right) \quad (\text{III-49})$$

where $P(\underline{u} | \{\underline{y}_i, i = 1, \dots, D\})$ denotes the posterior probability of \underline{u} given $\{\underline{y}_i, i = 1, \dots, D\}$. We term $\mathbf{1}(\cdot)$ the identity function.

$$\Pr \left(P(\underline{u} | \{\underline{y}_i, i = 1, \dots, D\}) \leq \alpha \right) = E_{\underline{u} | \{\underline{y}_i, i=1, \dots, D\} | \underline{u}} \left[\mathbf{1} \left(P(\underline{u} | \{\underline{y}_i, i = 1, \dots, D\}) \leq \alpha \right) \right] \quad (\text{III-50})$$

Given the problem symmetry⁸ $E_{\{\underline{y}_i, i=1, \dots, D\} | \underline{u}} \left[\mathbf{1} \left(P(\underline{u} | \{\underline{y}_i, i = 1, \dots, D\}) \leq \alpha \right) \right]$ is independent of a particular realization of the transmitted codeword \underline{u} . Thus, without loss of generality we rewrite (III-50) as follows

$$\Pr \left(P(\underline{u} | \{\underline{y}_i, i = 1, \dots, D\}) \leq \alpha \right) = E_{\{\underline{y}_i, i=1, \dots, D\} | \underline{u} = \underline{u}_1} \left[\mathbf{1} \left(P(\underline{u}_1 | \{\underline{y}_i, i = 1, \dots, D\}) \leq \alpha \right) \right] \quad (\text{III-51})$$

The posterior probability of the transmitted symbol sequence given the received signal is related to the channel transition probability as follows

$$P(\underline{u}_1 | \{\underline{y}_i, i = 1, \dots, D\}) = \frac{P(\{\underline{y}_i, i = 1, \dots, D\} | \underline{u} = \underline{u}_1) P(\underline{u}_1)}{P(\{\underline{y}_i, i = 1, \dots, D\})} \quad (\text{III-52})$$

Expanding the unconditional probability of observing $\{\underline{y}_i, i = 1, \dots, D\}$ as follows

$$P_Y(\{\underline{y}_i, i = 1, \dots, D\}) = \sum_{j=1}^M P_u(\underline{u}_j) P_Y(\{\underline{y}_i, i = 1, \dots, D\} | \underline{u} = \underline{u}_j) \quad (\text{III-53})$$

we obtain the following expression for the lower bound on P_e

$$P_e \geq \max_{\alpha \in [0,1]} (1 - \alpha) E_{\{\underline{y}_i, i=1, \dots, D\} | \underline{u} = \underline{u}_1} \left[\mathbf{1} \left(\sum_{j=1}^M \frac{P_y(\{\underline{y}_i, i = 1, \dots, D\} | \underline{u} = \underline{u}_j)}{P_y(\{\underline{y}_i, i = 1, \dots, D\} | \underline{u} = \underline{u}_1)} \geq \frac{1}{\alpha} \right) \right] \quad (\text{III-54})$$

⁸From our codewords constant-energy and equal probability assumptions introduced in the previous section.

E RESULTS

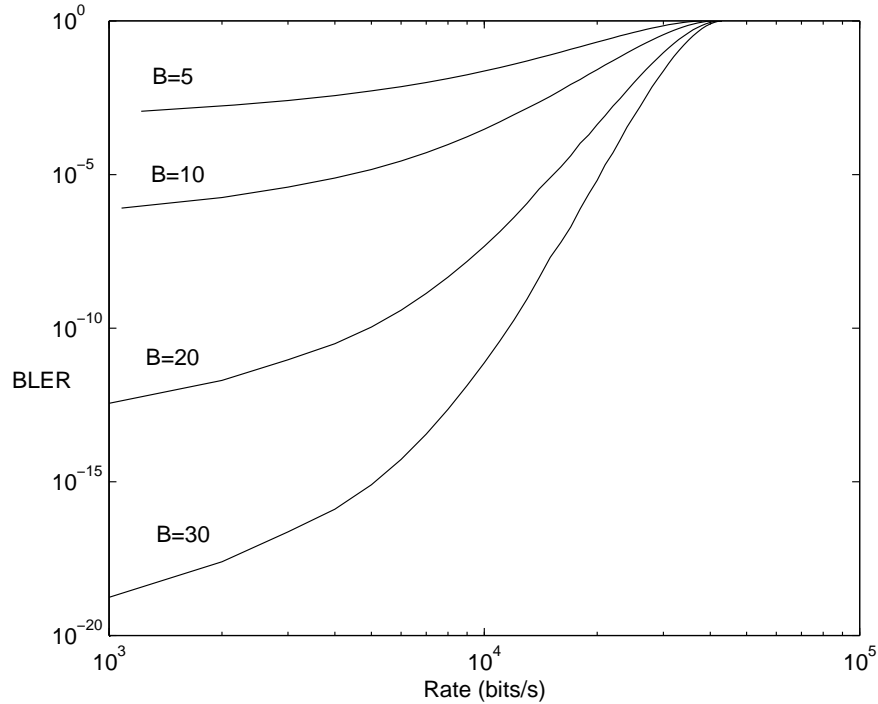


Fig. III-1. ML detection rule with orthogonal codebooks: upper bound on BLER versus the transmission data rate for a fixed block size $N = 10000$ and different number of blocks per codeword B . SNR=50dB, $T_d=25\text{ns}$, $T_p=1\text{ns}$.

In this section we numerically evaluate the error probability expressions derived in the current chapter and then analyze the impact of system and design parameters on the behavior of decoding error probability. In all considered settings η the asymmetric transmission probability of *On-off* signaling is optimized numerically as function of system parameters. We first consider the case where orthogonal codebooks are used with the full ML metric. Figure III-1 shows the minimum codeword error probability versus the transmission data rate. The block size (i.e. coherence time) is kept constant and equal to $N = 10000$ which corresponds to a channel coherence-time on the order of $T_c = 10000 * T_s = 250\mu\text{s}$. Increasing the number blocks, constituting a codeword, increases the slope of error probability decrease, as function of the transmission rate, while not impacting the waterfall point. On

the other hand, as can be seen on figure III-2, increasing the block size N while keeping the codeword length BN increases both the slope of decrease of the error probability and the waterfall point. Increasing B augments channel stationarity, and thus help better estimating the channel, and at the same time reduces the channel time diversity. Therefore, the observed behavior of the error probability, confirms that a UWB channel contains large enough number of degrees of freedom, and thus is not sensible to channel time-diversity degree.

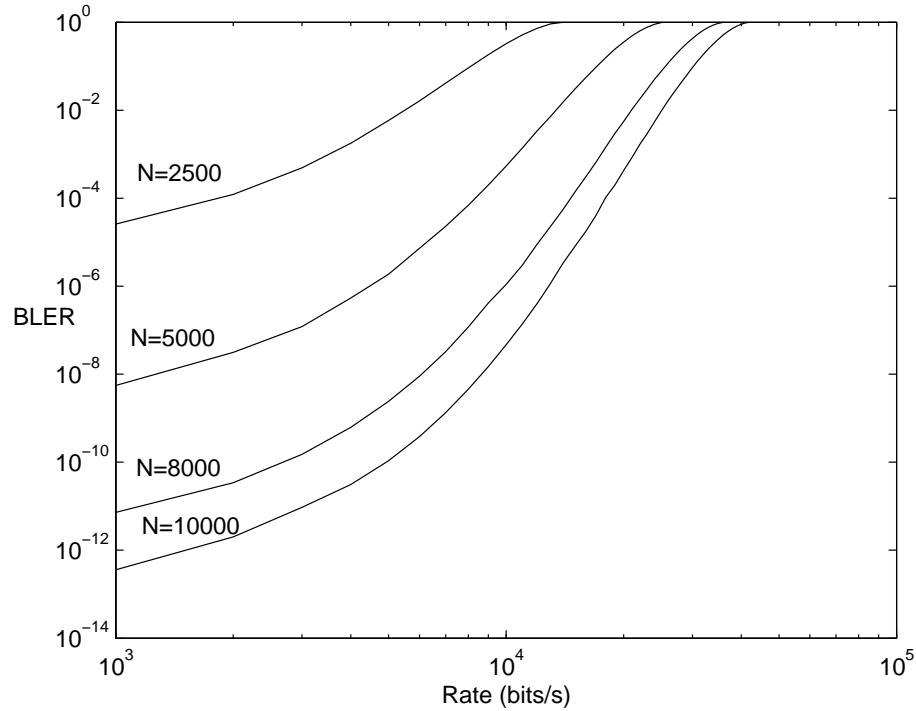


Fig. III-2. ML detection rule with orthogonal codebooks: upper bound on BLER versus the transmission data rate for fixed codeword length $BN = 200000$ and different block size values N . SNR=50dB, $T_d=25$ ns, $T_p=1$ ns.

Figure III-3 shows the effect of SNR level on the slope of the error probability curve. A higher SNR increases the slope for a fixed block size N . This may be explained by the fact that a higher SNR helps better estimate the channel and thus takes a bigger advantage of channel stationarity. Using randomly generated codebooks instead of orthogonal codebooks. Figure III-4 shows that randomly generated codebooks slightly outperforms orthog-

onal codebooks. This behavior may not hold for higher SNR levels. Note that when using the ML detection metric, the error probability term (C.1) turns out to be a strictly decreasing function of η_t . Therefore the optimal transmission strategy consists of not transmitting any pilot symbols, this is to be expected.

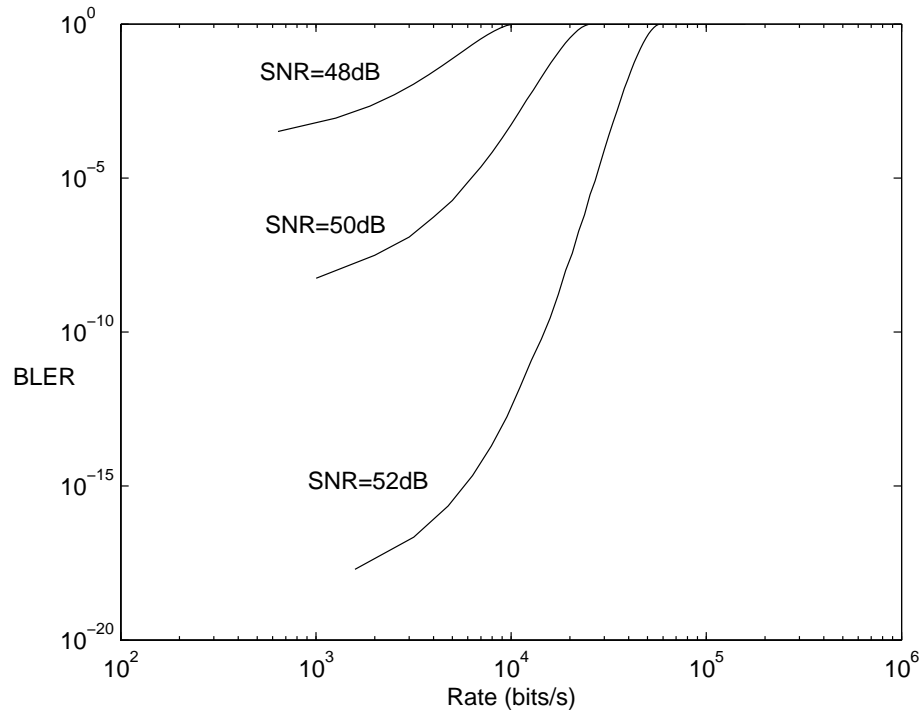


Fig. III-3. ML detection rule with orthogonal codebooks: upper bound on BLER versus the transmission data rate for fixed block size $N = 5000$ and number of blocks per codeword $B = 40$ and different SNR values. $T_d=25\text{ns}$, $T_p=1\text{ns}$.

We again consider orthogonal codebooks. Figure III-5 shows the lower and upper bounds previously computed on the codeword error probability of ML non-coherent receiver. The obtained upper bound is not tight but still give a good idea of the actual error probability of real system. The figure also shows the comparison between the error probability performance of both the ML non-coherent receiver and the pure non-coherent receiver. The comparison was drawn in the case of block size N equal to 5000 and number pf blocks per codeword equal to 40. As expected, the ML receiver significantly outperforms the pure non-coherent receiver given the large coherence time of the channel which allow for channel

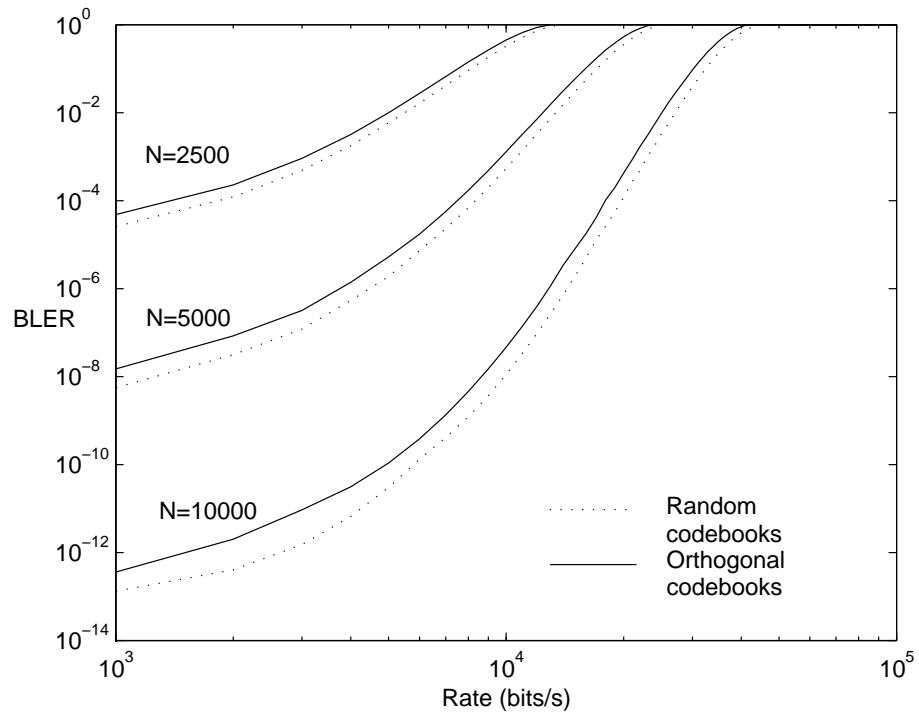


Fig. III-4. ML detection rule: orthogonal codebooks versus random codebooks. upper bound on BLER versus the transmission data rate for fixed block size $N = 5000$ and number of blocks per codeword $B = 40$ and different SNR values. $T_d=25\text{ns}$, $T_p=1\text{ns}$.

estimation. Note that the error probability of the pure non-coherent receiver has a slower convergence as function of the codeword size BN .

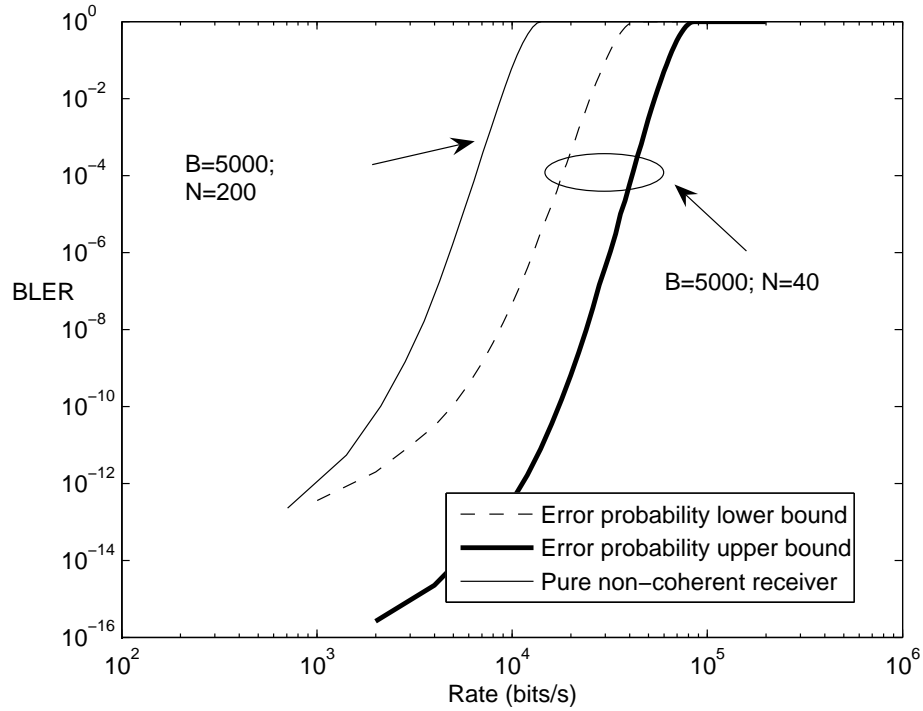


Fig. III-5. ML detection rule with orthogonal codebooks: upper and lower bounds on the BLER versus the transmission data rate for fixed block size $N = 5000$ and number of blocks per codeword $B = 40$. The figure also shows the lower bound on the error probability of the pure non-coherent receiver. $T_d=25\text{ns}$, $T_p=1\text{ns}$.

Multi-carrier *On-off* signaling

In chapter (II) the performance of non-coherent *On-off* signaling, with short impulses, was analyzed in the ultrawideband regime. The scheme was shown to perform very close to the wideband capacity, in the low data rate regime, for typical parameter values of UWB systems. Nevertheless this signaling scheme suffers performance degradation for increasing bandwidth and in the high data rate regime. This behavior can be explained by a signal *over-spreading phenomena*; Terming T_p the transmitted pulse duration and T_d the channel delay spread, the received signal occupies a signal-space of dimension of the order of $(T_d + T_p)/T_p$, which means that for increasing bandwidth (i.e. decreasing T_p) the number of dimensions increases because $T_d + T_p \simeq T_d$. This confirms previous results on the so-called bandwidth-scaled signals, that showed that using spread spectrum signaling, such as direct sequence CDMA, leads to a vanishing systems capacity in the limit of infinite bandwidth ([22], [23], [37]). From the above discussion, it arises that suitable signaling strategies for ultrawideband systems, in the high data rates region, need to use relatively narrow band signals (i.e. long duration signals: T_p on the order of T_d) to avoid over-spreading. Therefore, the previous reasoning suggests the use of multi-carrier signaling.

Lately multi-carrier UWB signaling has gained an increase of interest. It is mainly being explored in the form of classical OFDM signaling over UWB bandwidth associated to coherent receivers[57],[59],[61]. The capacity of this scheme as well as the achievable rates with some practical coding schemes were studied [60],[62],[55]. Other works concentrated on design and implementation issues such as channel estimation [52], transmit symbols opti-

mization [53],[58], power allocation [54], and receiver structures [56]. The main motivation behind the use of OFDM as a signaling scheme for UWB, is to benefit from the receiver complexity reduction¹ it allows. Multiband OFDM is one of the two last contenders for the IEEE 802.15.3a physical layer standard[63]. An other multi-carrier signaling scheme for UWB that has been investigated is impulsive FSK[29],[31]. This strategy was used to prove that in the limit of infinite bandwidth, channel knowledge at the receiver does not increase the capacity. In [64], Luo and Medard analyze the performance of impulsive single-tone and two-tone FSK for bandwidths in-line with those of *Ultrawideband* systems and show both schemes to achieve data rates of the order of capacity of AWGN channel with a better performance for two-tone FSK for small bandwidths.

In the following we introduce a family of signaling schemes (figure IV-1) we term OFDM *On-off* signaling. The latter corresponds to the most general way of using time-frequency dimensions. Information is coded simultaneously along time and frequency axes. Using a grid representation of the time-frequency signal space, each box of the grid is used in an on-off manner with a vanishing *on* probability as the total bandwidth goes to infinity. This scheme encompasses signaling schemes such as impulsive one-tone and multi-tone FSK; Using appropriate channel codes it can be down-casted into any of these signaling schemes (see section II for an example). This memoryless transmission strategy resembles OFDM signaling. Within each sub-band, however, impulsive signaling is still used. We should emphasize here the difference between the notions of *impulsive transmission*, used in [37]-[64], and *on-off* signaling along time dimension used in the proposed scheme in this work. In the first case it corresponds to the system switching between active and idle status, the active periods being known to both the transmitter and receiver. While in the second case it corresponds to encoding transmitted information along the time-dimension, and thus the receiver does not know a priori the location, in time, of transmitter active periods.

The remainder of this chapter is organized as follows. We first introduce channel and signaling models. Then upper and lower bounds on the average mutual information of introduced signaling scheme are derived. Finally the achieved data rates are compared to those of impulsive multi-tone FSK and discussed.

A SYSTEM DESCRIPTION

A general finite-gain continuous-time multipath block-fading channel model is considered. We again note T_d and T_c respectively it's delay spread and coherence time. Throughout the chapter we will assume the symbol duration T_s to be smaller than channel coherence-time, so that the latter can be assumed to be constant over each symbol. When $x(t)$ is transmitted,

¹In particular regarding channel estimation

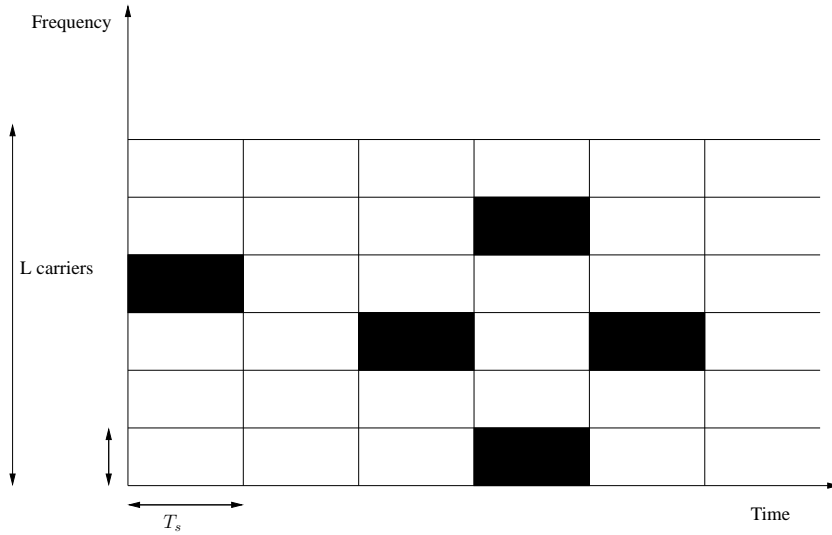


Fig. IV-1. OFDM-on-off signaling

the received signal during time interval $[nT_s + T_d, (n + 1)T_s[$ is given by

$$y(t) = \int_0^{T_d} h_n(u)x_n(t - u)du \tag{IV-1}$$

where $h_n(u)$ is the channel impulse response during the n th symbol time. Parallel independent memoryless signal streams are transmitted on L sub-carriers. We denote ΔF the spacing between two adjacent carriers such that the total system bandwidth W is related to the number of sub-carriers, L as follows $L = \lfloor W/\Delta F \rfloor$. Each subcarrier is modulated with a data symbol $x_{l,n}$, where l represents the subcarrier index number and n the time slot number. Binary data is encoded using a randomly generated codebook $\mathcal{U} = \{\mathbf{U}_1, \mathbf{U}_2, \dots, \mathbf{U}_M\}$ of cardinality M and codeword length N . Each codeword \mathbf{U}_m is a sequence of N vectors $\mathbf{U}_m = \{\underline{u}_{m,1}, \underline{u}_{m,2}, \dots, \underline{u}_{m,N}\}$ each of them corresponding to the transmitted symbols on each of the L sub-carriers during the n th symbol-time (i.e. a box in the time-frequency grid (IV-1)). $\underline{u}_{m,n} = (u_{m,n,1}, \dots, u_{m,n,L})$ with

$$u_{m,n,l} = \begin{cases} 1 & \text{with probability } \eta \\ 0 & \text{with probability } (1 - \eta) \end{cases} \tag{IV-2}$$

As code length N goes to infinity, all the used codewords have the same energy. To satisfy the power constraint for any finite code length N we impose that for any codeword m

$$\sum_{n=1}^N \sum_{l=1}^L u_{m,n,l} = \eta NL \tag{IV-3}$$

which means that each codeword uses exactly ηNl boxes of the *time-frequency grid*. Impulsive FSK signaling can be obtained from the previous scheme by constraining the codewords U_m to be of the following form (see figure (IV-2))

$$\sum_{l=1}^L u_{m,n,l} = \begin{cases} 1 & \text{if } \text{mod}(n, k) = 0 \\ 0 & \text{otherwise} \end{cases} \quad (\text{IV-4})$$

Recalling the terminology of impulsive FSK [64], $1/k$ corresponds to the duty cycle.

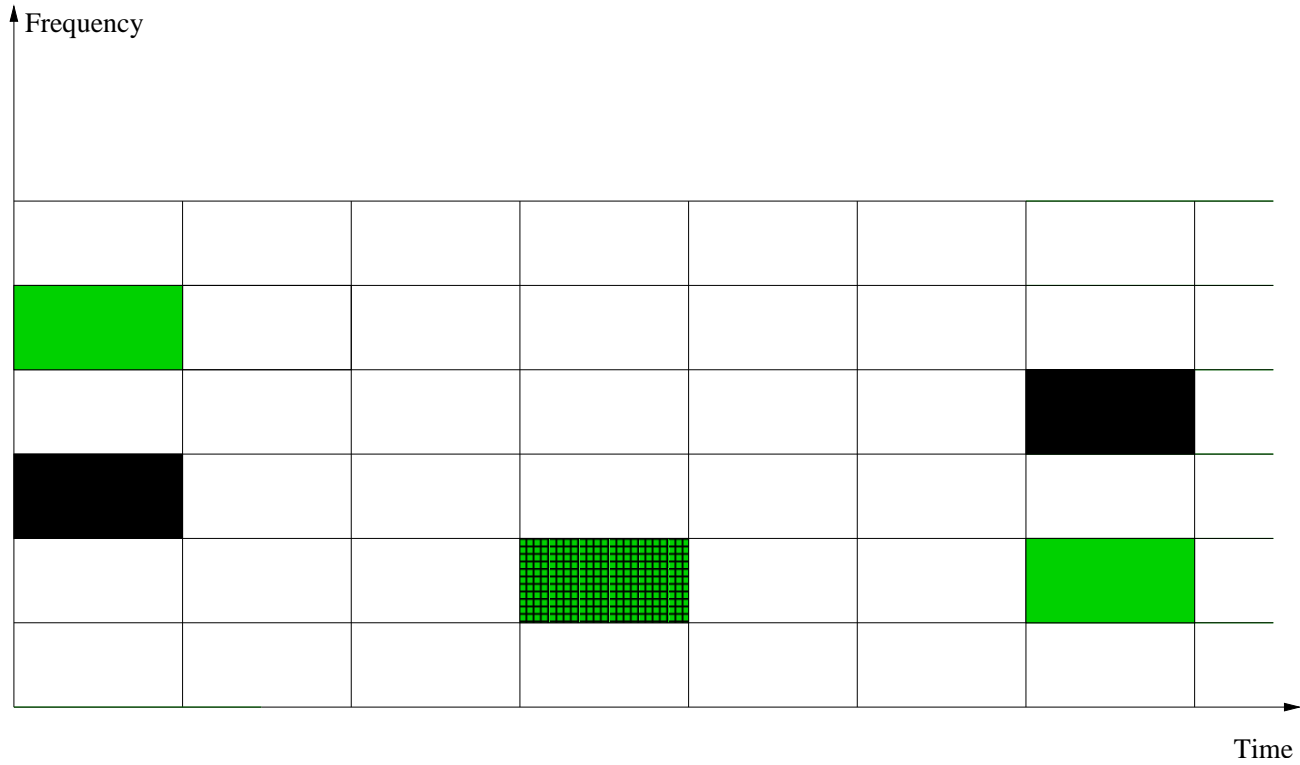


Fig. IV-2. Impulsive FSK

In the following we note v the index of the actually transmitted codeword. Its corresponding transmitted signal is written as follows

$$\begin{aligned} x(t) &= \sum_{n=1}^N x_n(t) \\ &= \sum_{n=0}^{N-1} \left(\sum_{l=1}^L u_{v,n,l} \sqrt{\frac{E_s}{\eta L}} \Phi_l(t - nT_s) \right) \end{aligned} \quad (\text{IV-5})$$

where the transmitted pulse $\Phi()$ is given by

$$\Phi_l(t) = \begin{cases} \frac{1}{\sqrt{T_s}} e^{j2\pi f_l t} & \text{for } t \in [0, T_s] \\ 0 & \text{elsewhere} \end{cases} \quad (\text{IV-6})$$

The average symbol transmitted energy E_s is given by (the detailed derivation is given in Appendix A)

$$\frac{PT_s}{1 + \left(\frac{2\eta}{L}\right) \sum_{l=1}^{L-1} \sum_{k=l+1}^L \text{sinc}\left(2\pi(k-l)\frac{T_s}{T_s-T_d}\right)} \quad (\text{IV-7})$$

Note that for practical system parameters values, the second term of the denominator of expression IV-7 is negligible with respect to the first term irrespective of the value of the transmission probability η . For example consider $T_s = 27ns$, $T_d = 25ns$, and $W = 7.5\text{GHz}$. Then

$$\left(\frac{2}{L}\right) \sum_{l=1}^{L-1} \sum_{k=l+1}^L \text{sinc}\left(2\pi(k-l)\frac{T_s}{T_s-T_d}\right) = 3.4 \times 10^{-16} \ll 1 \quad (\text{IV-8})$$

Substituting the transmitted signal $x(t)$ with its expression (IV-5) in (IV-1) we rewrite the received signal during time-interval $[nT_s + T_d, (n+1)T_s]$ as follows

$$y(t) = \sum_{l=1}^L u_{v,n,l} \sqrt{\frac{E_s}{\eta L T_s}} e^{j2\pi f_l t} \left(\int_0^{T_d} h_n(s) e^{-j2\pi f_l s} ds \right) \quad (\text{IV-9})$$

where

$$h_{n,l} = \left(\int_0^{T_d} h_n(s) e^{-j2\pi f_l s} ds \right) \quad (\text{IV-10})$$

is the complex phasor representing the amplitude gain and phase shift on the l th carrier, during the interval $[nT_s + T_d, (n+1)T_s]$. In the following $h_{n,l}$ will be assumed to be a complex circularly symmetric Gaussian zero mean variable, and without loss of generality of unit variance. At the receiver a guard interval is left at the beginning of each symbol, from our memoryless assumption². To guarantee orthogonality of the sub-carriers at reception we choose the carrier frequencies to be $f_l = f_0 + \frac{l}{T_s - T_d}$ (i.e $\Delta F = \frac{1}{T_s - T_d}$). Thus the received signal on the l th Carrier during the n th time-slot is

$$\begin{aligned} y_{n,l} &= \frac{1}{\sqrt{T_s - T_d}} \int_{nT_s + T_d}^{(n+1)T_s} y(t) e^{-j2\pi f_l t} dt \\ &= \sqrt{\frac{T_s - T_d}{T_s}} h_{l,n} \sqrt{\frac{E_s}{\eta L}} u_{v,n,l} + z_{n,l} \end{aligned} \quad (\text{IV-11})$$

where $h_{.,l}$, $z_{.,l}$ are sequences of complex independent Gaussian variables with zero-mean and unit-variance.

²The guard-interval plays the role of the cyclic prefix in classical OFDM.

B BOUNDS ON MUTUAL INFORMATION

In this section we compute the ergodic mutual information of the considered channel model when the input distribution is restricted to the previously introduced OFDM-*on-off* signaling, and then compare it the capacity of impulsive 2-tone *FSK* input distribution. We assume that no channel side information is available to the receiver nor the transmitter.

We compute the average mutual information between the transmitted information symbols over the L carriers, during a single symbol time, and the corresponding received signal. In the rest of this section time and codeword indexes are dropped in the notation introduced in the previous section for a better clarity of mathematical developments. We denote $\underline{u} = (u_1, \dots, u_L)$ the vector of transmitted symbols (instead of $\underline{u}_{t,n} = (u_{t,n,1}, \dots, u_{t,n,L})$ in the previous notation), and $\underline{y} = (y_1, \dots, y_L)$ the vector of received signals on the L carriers. Though the transmitted symbols u_l are uncorrelated, the received signal vector Y has correlated components, because of the correlation of channel frequency samples h_1, h_2, \dots, h_L . A correlation channel model is needed for the computation of the exact mutual information. In the following we do not consider any particular correlation model but upper and lower bound the actual value of mutual information by its value in the two limiting cases : no correlation and full correlation (i.e. the channel is frequency flat). The average mutual information is given by

$$I(\underline{u}; \underline{y}) = H(\underline{u}) - H(\underline{u}/\underline{y}) \quad (\text{IV-12})$$

where

$$\begin{aligned} H(\underline{u}) &= \sum_{l=1}^L H(u_l | u_{l-1}, \dots, u_1) \\ &\stackrel{(a)}{=} \sum_{l=1}^L H(u_l) \end{aligned} \quad (\text{IV-13})$$

(a) follows from the independence of u_l $l = 1, \dots, L$.

$$\begin{aligned} H(\underline{u}/\underline{y}) &= \sum_{l=1}^L H(u_l | \underline{y}, u_{l-1}, \dots, u_1) \\ &\stackrel{(b)}{\leq} \sum_{l=1}^L H(u_l | y_l) \end{aligned} \quad (\text{IV-14})$$

in (b) we use that conditioning reduces entropy. Thus

$$\begin{aligned}
 I(\underline{u}; \underline{y}) &\geq \sum_{l=1}^L (H(u_l) - H(u_l | y_l)) \\
 &= L(H(u_1) - H(u_1 | y_1)) \\
 &= L(H(y_1) - H(y_1 | u_1))
 \end{aligned} \tag{IV-15}$$

$H(y_1 | u_1)$ is derived in Appendix B. We now turn to the derivation of the upper bound

$$I(\underline{u}; \underline{y}) = H(\underline{y}) - H(\underline{y} | \underline{u}) \tag{IV-16}$$

where

$$\begin{aligned}
 H(\underline{y} | \underline{u}) &= \sum_{\underline{x}} Pr(\underline{u} = \underline{x}) H(\underline{y} | \underline{u} = \underline{x}) \\
 &= \sum_{\underline{u} \in \{0,1\}^L} Pr(\underline{u}) \left(\ln((2\pi e)^L) \left| \mathbf{R}_{\underline{y} | \underline{u}} \right| \right)
 \end{aligned} \tag{IV-17}$$

where $\mathbf{R}_{\underline{y} | \underline{u}}$ is the autocorrelation matrix of the received vector conditioned on the realization of codeword \underline{u} .

$$\underline{y} | \underline{u} = \sqrt{\frac{(T_s - T_d) E_s}{T_s \eta L}} [h_1 u_1, \dots, h_L u_L]^T + \underline{z} \tag{IV-18}$$

$|\cdot|$ stands for the determinant operator. Let l_u be the number of non-zero elements of \underline{u} . Since the determinant is invariant to permutations of rows and columns we hence have that

$$\left| \mathbf{R}_{\underline{y} | \underline{u}} \right| = \left| \mathbf{R}_{\underline{y}' | \underline{u}} \right| \tag{IV-19}$$

where $\underline{y}' | \underline{u} = [\underline{y}_1, \underline{y}_2]^T$ is a reordered version of $\underline{y} | \underline{u}$ where we have put in \underline{y}_1 the entries corresponding to the non-zero entries of \underline{u} , while \underline{y}_2 contains the remaining elements of $\underline{y}' | \underline{u}$. Thus

$$\mathbf{R}_{\underline{y}' | \underline{u}} = \begin{bmatrix} \mathbf{R}_{\underline{y}_1} & 0 \\ 0 & N_0 \mathbf{I}_{L-l_u} \end{bmatrix} \tag{IV-20}$$

where \mathbf{I}_l stands for the identity matrix of size l . Thus

$$\left| \mathbf{R}_{\underline{y} | \underline{u}} \right| = \left| \mathbf{R}_{\underline{y}_1} \right| N_0^{L-l_u} \tag{IV-21}$$

with $\mathbf{R}_{\underline{y}_1} = \frac{(T_s - T_d) E_s}{T_s \eta L} \mathbf{R}_{h_1} + N_0 \mathbf{I}_{l_u}$. Note that \mathbf{R}_{h_1} is a Hermitian positive semi-definite matrix whose entries are of modulus less than or equal to one.

Lemma 2: Let \underline{y} be a size l vector of i.i.d complex Gaussian correlated random variables corrupted by additive white Gaussian noise $\underline{y} = \underline{h} + \underline{z}$. Where $\mathbf{R}_{\underline{z}} = \alpha \mathbf{I}_l$ and \underline{h} has zero-mean unit-variance entries. Then $|\mathbf{R}_{\underline{y}}|$ is minimized for $\underline{h} = h\phi$ where h is a zero mean unit variance complex Gaussian variable and ϕ is any complex deterministic vector with unit modulus entries.

Note that minimizing the determinant of the autocorrelation function of a Gaussian random vector is equivalent to minimizing its differential entropy³. Thus the result of lemma 2 is intuitive in the sense that it says that the uncertainty about a Gaussian random vector is minimized when the correlation of its entries is maximized. Proof of lemma (2) is given in Appendix C.

Applying the result of lemma 2 to the right side term of equation (IV-21) we obtain the following inequality

$$|\mathbf{R}_{\underline{y}_{|\underline{u}}}| \geq |\mathbf{R}_{\underline{y}'_1}| N_0^{L-l_u}$$

where $\underline{y}'_1 = \sqrt{\frac{(T_s - T_d)E_s}{T_s \eta L}} h\phi + \underline{z}$. Taking vector ϕ to be the all one vector $\phi = \mathbb{1}^L$ and again using the invariance of the determinant operator to permutations of rows and columns inequality (IV-22) becomes

$$|\mathbf{R}_{\underline{y}_{|\underline{u}}}| \geq |\mathbf{R}_{\underline{y}_{|\underline{u}, \underline{h}=h\mathbb{1}^L}}| \quad (\text{IV-22})$$

injecting the obtained inequality in equation (IV-17) we obtain an upper bound on the mutual information between the transmitted symbols and received signal

$$I(\underline{u}; \underline{y}) \leq H(\underline{y}) - H\left(\underline{y}_{|\underline{u}, \underline{h}=h\mathbb{1}^L}\right) \quad (\text{IV-23})$$

Note that the obtained bounds both the upper and lower one are tight since they are reached when channel taps correlation corresponds to the two limiting cases of full correlation and no correlation.

C DISCUSSION

In this section we compare the mutual information of the proposed signaling scheme to the capacity of impulsive multi-tone FSK ([64]). In particular, the average transmitted power spectral density is limited and set to be at the same level as the power spectral density of thermal noise ([13]). Thus the average transmitted power is a linearly increasing function of

³Differential entropy of a random Gaussian vector is a strictly increasing function of the determinant of its autocorrelation function

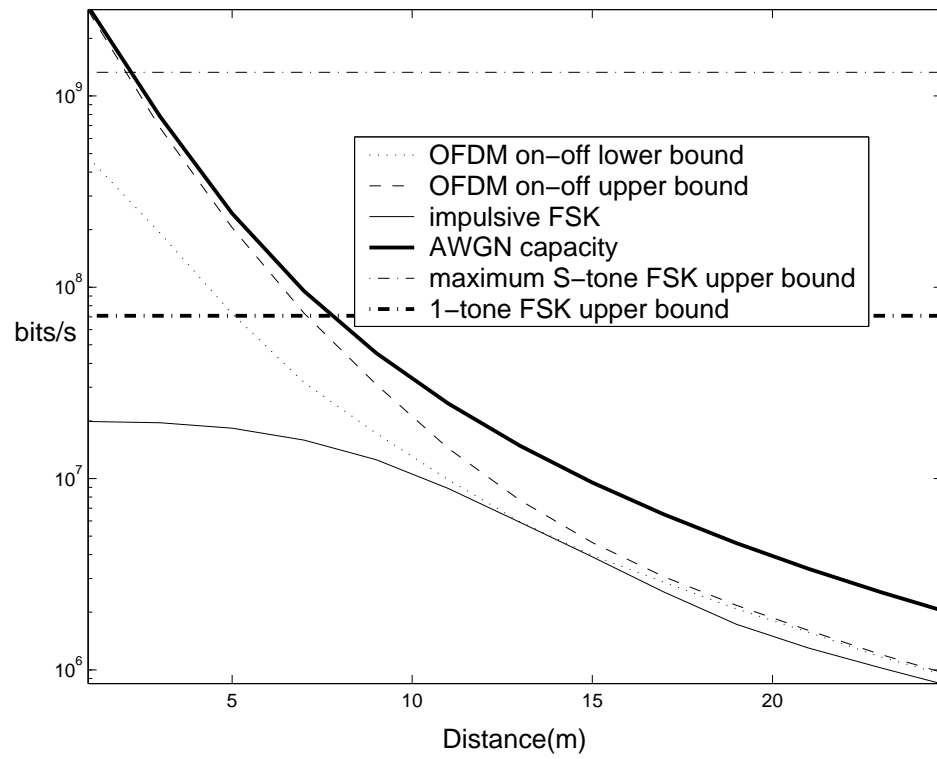


Fig. IV-3. Achievable rates versus distance: $T_s = 0.5\mu s, T_d = 30ns, W = 1GHz$

system bandwidth. We numerically evaluate the derived bounds on the capacity of OFDM-on-off signaling and compare them to the capacity of impulsive FSK([64], [37]). Both the on-probability η of OFDM-*on-off* signaling and the activity duty cycle of the impulsive FSK are optimized as function of system bandwidth and SNR. Note that we restrict our comparison to 1-tone FSK because, apart from the very high SNR region, it has sensibly the same capacity as higher order multi-tone FSK. Note that the capacity of S-tone FSK is

upper bounded by $\frac{\log_2 \left(\binom{S}{L} \right)}{T_s}$ bits/s. This bound expresses the fact that the size of the modulation is finite. We denote this bound as the bandwidth limited bound. This bound is tight in the region of very high SNR and takes its maximum value for $S = \lfloor L/2 \rfloor$. Moreover, for numerical stability considerations, we considered a looser upper bound on capacity of OFDM-*on-off*, where in (IV-23) we upper bound the term $H(\underline{y})$ by $\sum_{i=1}^L H(y_i)$.

C.1 S-tone impulsive FSK

In figure B we look at the behavior of the achievable rates, of the two considered systems, as function of the distance between the transmitter and the receiver. Here we again use the pathloss model and transmission power(compliant with FCC regulation) introduced in section (D). We have also plotted on this figure the bandwidth-limited upper bound for 1-tone FSK and S-tone FSK with $S = \lfloor L/2 \rfloor$. The bandwidth is kept constant. OFDM-*on-off* outperforms 1-tone FSK in particular for short range communications ($< 10m$). The gap between the two schemes ranges from 3dB to more than 10dB. Note that at a distance of about 13m between the transmitter and the receiver, the two schemes perform almost the same which means that for this particular SNR and bandwidth values 1-tone FSK is optimal and that the codebook that achieves the capacity of OFDM-on-off is the one than that downcast it to 1-tone FSK.

In the long range communications region (i.e. large values of distance D) the upper and lower bound merge. This behavior is due to the fact that channel is difficult to estimate even with full correlation of channel frequency tones because of the low signal to noise ratio of the received signal. On the other hand, in the short range communications region (i.e. high SNR) channel is easy to estimate and benefits from the high correlation of channel frequency tones. Performance of a true channel will lie in between as a function of its number of degrees of freedom.

In figure C.1, we draw the mutual information versus the bandwidth for a fixed SNR. As can be seen the growth of capacity versus bandwidth is very slow for both compared schemes. Both curves have sensibly the same slope for bandwidths larger than 1GHz. This behavior is consistent with the analysis of Verdu in [28] where he showed that the slope of spectral

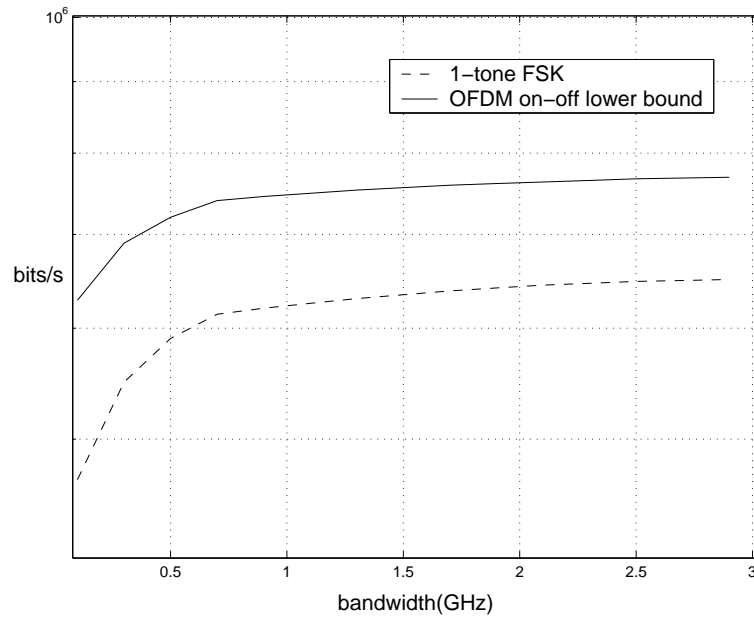


Fig. IV-4. Capacity versus bandwidth: $T_s = 0.5\mu s, T_d = 30ns, SNR = 60dB$

efficiency versus the minimum needed SNR per bit for reliable communications, is zero at the origin if no channel state information is available to the receiver.

D CONCLUSION

In the limit of infinite bandwidth and without any CSI at the receiver, impulsive frequency-shift keying (FSK) achieves the wideband capacity. We introduce a new generalized multi-carrier signaling scheme and compare it to impulsive single and multi-tone FSK in terms of achieved capacity with no CSI at the receiver. We derive tight upper and lower bounds on the capacity of the proposed signaling scheme over the set of all possible channel frequency correlation patterns. We show that the introduced scheme outperforms impulsive multi-tone FSK for bandwidths inline with those of Ultrawideband systems, and still achieves the wideband capacity in the limit of infinite bandwidth.

E APPENDIX

IV.0.1 Average transmitted power

Writing the average transmitted energy during symbol time $[nT_s, (n+1)T_s]$, we obtain

$$\begin{aligned}
E \left[\int_0^{T_s} |x(t)|^2 dt \right] &= E \left[\int_0^{T_s} \sum_{l=1}^L \sum_{k=1}^L u_{t,n,l} u_{t,n,k} \left(\frac{E_s}{\eta L} \right) \Phi_l(t) \Phi_k^*(t) dt \right] \\
&= \int_0^{T_s} \sum_{l=1}^L \sum_{k=1}^L E [u_{t,n,l} u_{t,n,k}] \left(\frac{E_s}{\eta L} \right) \Phi_l(t) \Phi_k^*(t) dt \\
&= \sum_{l=1}^L E [u_{t,n,l}^2] \left(\frac{E_s}{\eta L} \right) \int_0^{T_s} \Phi_l(t) \Phi_l^*(t) dt \\
&\quad + \sum_{l=1}^{L-1} \sum_{k=l+1}^L E [u_{t,n,l} u_{t,n,k}] \left(\frac{E_s}{\eta L} \right) \int_0^{T_s} 2 \operatorname{Re} (\Phi_l(t) \Phi_k^*(t)) dt \\
&= E_s + \sum_{l=1}^{L-1} \sum_{k=l+1}^L \left(\frac{\eta E_s}{L} \right) \int_{T_s - T_d}^{T_s} \frac{2}{T_s} \cos \left(2\pi \frac{k-l}{T_s - T_d} \right) dt \\
&= E_s + \left(\frac{2\eta E_s}{L} \right) \sum_{l=1}^{L-1} \sum_{k=l+1}^L \operatorname{sinc} \left(2\pi (k-l) \frac{T_s}{T_s - T_d} \right) \quad (\text{IV-24})
\end{aligned}$$

Next, relating the average transmitted energy to the average transmitted power P , we obtain the following expression for E_s

$$E_s = \frac{PT_s}{1 + \left(\frac{2\eta}{L} \right) \sum_{l=1}^{L-1} \sum_{k=l+1}^L \operatorname{sinc} \left(2\pi (k-l) \frac{T_s}{T_s - T_d} \right)} \quad (\text{IV-25})$$

IV.0.2 Bounds on the mutual information of OFDM on-off signaling

We first compute $H \left(\sqrt{\frac{(T_s - T_d) E_s}{T_s \eta L}} h \underline{u} + \underline{z} \mid \underline{u} \right)$

$$H \left(\sqrt{\frac{(T_s - T_d) E_s}{T_s \eta L}} h \underline{u} + Z \mid \underline{u} \right) = E_{\underline{u}} \left[H \left(\sqrt{\frac{(T_s - T_d) E_s}{T_s \eta L}} h \underline{u} + \underline{z} \mid \underline{u} \right) \right] \quad (\text{IV-26})$$

where

$$\underline{y}|\underline{u} = \sqrt{\frac{(T_s - T_d) E_s}{T_s \eta L}} h \underline{u} + \underline{z} \sim \mathcal{N}_c \left(\underline{0}; N_0 \mathbf{I} + \frac{(T_s - T_d) E_s}{T_s \eta L} \underline{u} \underline{u}^T \right) \quad (\text{IV-27})$$

thus

$$\begin{aligned} H \left(\sqrt{\frac{(T_s - T_d) E_s}{T_s \eta L}} h \underline{u} + \underline{z} | \underline{u} \right) &= \frac{E}{\underline{y}|\underline{u}} \left[\underline{y}^H \left(N_0 \mathbf{I} + \frac{(T_s - T_d) E_s}{T_s \eta L} \underline{u} \underline{u}^T \right)^{-1} \underline{y} \right. \\ &\quad \left. + \log \left(\det \left(\pi \left(N_0 \mathbf{I} + \frac{(T_s - T_d) E_s}{T_s \eta L} \underline{u} \underline{u}^T \right) \right) \right) \right] \end{aligned}$$

The matrix $\mathbf{I} + \frac{E_s}{\eta L N_0} \underline{u} \underline{u}^T$ has two different eigenvalues: 1 with multiplicity $L - 1$ and $1 + \frac{E_s}{\eta L N_0} \underline{u} \underline{u}^T$ with multiplicity one. Thus

$$\det \left(\mathbf{I} + \frac{(T_s - T_d) E_s}{T_s \eta L N_0} \underline{u} \underline{u}^T \right) = \log \left(1 + \frac{(T_s - T_d) E_s}{T_s \eta L N_0} \underline{u} \underline{u}^T \right) \quad (\text{IV-28})$$

Then using that

$$\frac{E}{\underline{y}|\underline{u}} \left[\underline{y} \left(N_0 \mathbf{I} + \frac{(T_s - T_d) E_s}{T_s \eta L} \underline{u} \underline{u}^T \right)^{-1} \underline{y}^H \right] = L \quad (\text{IV-29})$$

(see [30]) we end up with following expression

$$H \left(\sqrt{\frac{(T_s - T_d) E_s}{T_s \eta L}} h \underline{u} + \underline{z} | U = u \right) = L \log(\pi e N_0) + \log \left(1 + \frac{(T_s - T_d) E_s}{T_s \eta L N_0} \underline{u} \underline{u}^T \right) \quad (\text{IV-30})$$

and finally

$$\begin{aligned} H \left(\sqrt{\frac{(T_s - T_d) E_s}{T_s \eta L}} h \underline{u} + \underline{z} | \underline{u} \right) &= L \log(\pi e N_0) + \frac{E}{\underline{u}} \left[\log \left(1 + \frac{(T_s - T_d) E_s}{T_s \eta L N_0} \underline{u} \underline{u}^T \right) \right] \\ &\stackrel{(e)}{=} L \log(\pi e N_0) \\ &\quad + \sum_{k=0}^L \binom{L}{k} \eta^k (1 - \eta)^{L-k} \log \left(1 + \frac{k (T_s - T_d) E_s}{T_s \eta L N_0} \right) \end{aligned}$$

in (e) we use the equidistribution of u_i $i = 1, \dots, L$. Taking $L = 1$ in the previous equality we obtain the expression of $H(y_1 | u_1)$

$$H(y_1 | u_1) = \log(\pi e N_0) + \eta \log \left(1 + \frac{(T_s - T_d) E_s}{T_s \eta L N_0} \right) \quad (\text{IV-31})$$

IV.0.3 Proof of lemma 1

$$\mathbf{R}_y = \mathbf{R}_h + \alpha \mathbf{I}_1 \quad (\text{IV-32})$$

where \mathbf{R}_h is a Hermitian positive semi-definite matrix whose entries are of modulus less or equal to one. Let $\nu_l \geq \nu_{l-1} \cdots \geq \nu_1 \geq 0$ be its ordered eigenvalues. Thus

$$|\mathbf{R}_y| = \prod_{i=1}^l (\alpha + \nu_i) \quad (\text{IV-33})$$

Moreover the eigenvalues $\{\nu_i\}$ satisfy the following trace equation $\sum_{i=1}^l \nu_i = \text{trace}(\mathbf{R}_h) = l$. Thus minimizing $|\mathbf{R}_y|$ is equivalent to minimizing $\prod_{i=1}^l (\alpha + \nu_i)$ subject to the following constrains ⁴

$$\begin{cases} \nu_l \geq \nu_{l-1} \cdots \geq \nu_1 \geq 0 \\ \sum_{i=1}^l \nu_i = l \end{cases} \quad (\text{IV-34})$$

we reformulate the minimization problem as follows

$$\underset{\substack{(\nu_1, \dots, \nu_l) \\ \nu_i \geq 0, \sum_{i=1}^l \nu_i = l}}{\text{argmin}} \prod_{i=1}^l (\alpha + \nu_i) = \underset{\substack{(\nu_1, \dots, \nu_l) \\ \nu_i \geq 0, \sum_{i=1}^l \nu_i = l}}{\text{argmin}} \sum_{i=1}^l \log(\alpha + \nu_i) \quad (\text{IV-35})$$

Considering the following Lagrange multiplier

$$\mathcal{L}(\underline{\lambda}, \rho, \underline{\beta}) = \sum_{i=1}^l \log(\alpha + \nu_i) + \rho \left(\sum_{i=1}^l \nu_i - l \right) + \sum_{i=1}^l \beta_i \nu_i \quad (\text{IV-36})$$

we show that (see Appendix IV.0.4)

$$\underset{\substack{(\nu_1, \dots, \nu_l) \\ \nu_i \geq 0, \sum_{i=1}^l \nu_i = l}}{\text{argmin}} \sum_{i=1}^l \log(\alpha + \nu_i) = (l, 0, \dots, 0) \quad (\text{IV-37})$$

⁴The considered constrains on the eigenvalues $\{\nu_i\}$ are necessary and sufficient in the sense they are equivalent to the constrains that channel taps $\{h_i\}$ are subject to.

let \underline{h}_m be the channel vector associated with the solution to the minimization problem. Then $\mathbf{R}_{\underline{h}_m}$ is a rank one matrix and thus

$$\mathbf{R}_{\underline{h}_m} = \underline{v}_1 \underline{v}_2^H \quad (\text{IV-38})$$

since $\mathbf{R}_{\underline{h}_m}$ is a hermitian matrix then $\underline{v}_2^* = \underline{v}_1$. Moreover $\text{diag}(\mathbf{R}_{\underline{h}_m}) = \mathbb{1}_l$. Thus \underline{V}_1 has unit modulus entries.

IV.0.4 Solution of the constrained minimization problem

Deriving the Khun-Tucker conditions we obtain

$$\begin{cases} \frac{\partial \mathcal{L}}{\partial \nu_i} = \frac{1}{\alpha + \nu_i} + \rho + \beta_i \\ \nu_i \geq 0, \beta_i \geq 0 \\ \beta_i \nu_i = 0, \sum_{i=1}^l \nu_i = l \end{cases} \quad (\text{IV-39})$$

We first prove that if one eigenvalue ν_i is equal to zero then there is exactly $l-1$ eigenvalues equal to zero. Assume that $\nu_1 = 0$, thus $\frac{1}{\alpha} + \rho + \beta_1 = 0$. If we assume that for all $i \geq 2$, $\nu_i > 0$ we obtain that

$$\nu_i = -\alpha - \frac{1}{\rho} \quad \forall i \geq 2 \quad (\text{IV-40})$$

Injecting the obtained equalities in the equation $\sum_{i=1}^l \nu_i = l$ we obtain that $\rho = -\frac{l-1}{(l-1)\alpha+l}$ for any $l \geq 2$. Injecting the latest equality in the equation $\frac{1}{\alpha} + \rho + \beta_1 = 0$ we obtain that $\beta_1 = -\frac{l}{\alpha((l-1)\alpha+l)} < 0$ which is a contradiction with the fact that β_1 is greater or equal to zero. Thus $\nu_2 = 0$. Similarly we recursively prove that $\nu_1 = \nu_2 = \dots = \nu_{l-1} = 0$ and that $(\nu_1, \dots, \nu_l) = (0, \dots, 0, l)$ is the only solution that has at least a zero value and satisfies all the conditions.

Now we see if there is any solution to the problem such that $\nu_i > 0$ for $i = 1, \dots, l$. Assume that $\nu_i > 0$ for $i = 1, \dots, l$. This implies that $\beta_i = 0$ for $i = 1, \dots, l$. Thus $\frac{1}{\alpha + \nu_i} + \rho = 0$ for $i = 1, \dots, l$. Using the equality $\sum_{i=1}^l \nu_i = l$ we finally obtain that $\nu_1 = \nu_2 = \dots = \nu_l = 1$. In conclusion the considered function, subject to the constrains, admits extremums at exactly 2 points $(1, \dots, 1)$ and $(0, \dots, 0, l)$. Nothing that the function $f(x)$ defined as

$$f(x) = x \log\left(1 + \frac{x}{\alpha}\right) \quad x \geq 0 \quad (\text{IV-41})$$

is monotonically increasing we prove that the point $(\nu_1, \dots, \nu_l) = (0, \dots, 0, l)$ corresponds to the minimum of the considered function and thus solution to the constrained minimization problem.

Non-Coherent UWB Peer-to-Peer Networks

The networks which will likely employ UWB signaling, for example *Wireless Personal Area Networks (WPAN)* and *sensor networks*, are characterized by direct links between nodes in the network without the need for a central access-point. Therefore, those networks are characterized not only by a rich scattering propagation environment but also by requirements for adhoc and peer-to-peer (P2P) communications. This latter requirement has a significant impact on systems design, since the signaling schemes must be robust to strong impulsive interference (from nearby interferers) as shown in Fig. V. Here we show a small network consisting of 2 transmitter-receiver pairs. The receiving nodes are both far from their respective transmitters and suffer from strong interference. In contrast to CDMA networks with a basestation/mobile topology, UWB adhoc networks will likely not benefit significantly from centralized or distributed power control resulting in extreme near-far interference.

Here we show a small network consisting of 2 transmitter-receiver pairs. The receiving nodes are both far from their respective transmitters and suffer from strong interference. In contrast to CDMA networks with a basestation/mobile topology, UWB adhoc networks will likely not benefit significantly from centralized or distributed power control resulting in extreme near-far interference. The purpose of this study is to investigate the suitability of UWB signaling techniques for such networks, and to determine the achievable rates as a function of the density of the network, channel bandwidth and propagation characteristics, and SNR.

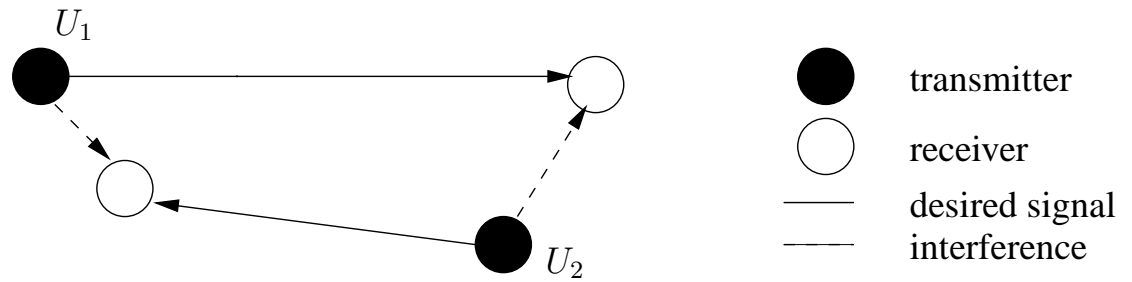


Fig. V-1. Peer-to-peer Network

The use of m -ary PPM can be extended to the case of multiple-access networks. Similar to direct-sequence spread-spectrum, the data modulation positions are further modulated by an n -ary sequence (known as a *time-hopping sequence*) for mitigating inter-user interference in a multiuser setting [17].

In the literature, the impact of multiple access interference on UWB signaling has been studied for systems using coherent receivers. Modeling the contribution of the aggregate interference¹ to the received signal as a Gaussian process, the performance of multiple access(MA) UWB systems, in terms of bit error probability, has been studied for different multiple access and modulation schemes [17], [76], [67], [68], [69]. Other works, [71], [72], [78], [77], [74], considered the performance of MA UWB systems, in terms of achievable data rates, for various multi-user synchronization scenarios. The effect of multiple-access interference on the spectrum of the received signal has been investigated in [66] and [75]. Lately, the validity of the Gaussian approximation of the interference process was questioned [79] and more precise evaluation of the probability of error was performed [65], [70], [73]. Numerous papers tackled the problem of designing multiuser detection schemes for UWB multiple access systems.

In our work we consider decentralized networks which we assume to be time-synchronized for simplicity of the analysis. *On-off* signaling is used as a combined channel coding and multiple-access scheme. The impulsive nature of *On-off* signaling has several advantages. First, it overcomes the near-far effect in the same manner frequency-hopping radio does. It also allows, each node, when not transmitting, to sense the channel and receive data from other nodes. Given the low transmission duty-cycle, of *On-off* signaling, each node can correctly receive the data addressed to it with high probability without the need for assigning dedicated slots for reception. Therefore, this signaling scheme allows for a more efficient duplexing of transmitted and received data which render it adequate for adhoc, sensor and mesh networks.

¹From all the interferers

Here we characterize the achievable data rates in interference networks. We concentrate on systems using non-coherent type of receivers. We derive upper and lower bounds on the achievable data rates. We first consider a genie-aided receiver whose performance stands for the upper bound. Then we introduce a, threshold based, practical receiver whose performance, as well as the one of a quantized version of it, is analyzed and stand for a lower bound.

A MULTIPLE ACCESS CHANNEL MODEL

We consider a general wireless peer-to-peer network using UWB signaling in a multipath fading environment. We assume that the network contains permanently Q transmitters. Let 1 be the index of the desired transmitter². The considered channel model is a generalization, to the multiple-access case, of the block fading channel model used in chapter (II). We again consider *On-off* signaling as introduced in II-1. The received signal during the k th symbol duration, is written as follows

$$r(t) = \sum_{q=1}^Q u_k^{(q)} \sqrt{\frac{E_s^{(q)}}{\eta}} p(t - kT_s - \tau_{q,k}) * h_k^{(q)}(t) + z(t), \quad t \in [(k-1)T_s, kT_s]. \quad (\text{V-1})$$

where $u_k^{(q)}$ is the transmitted symbol by user q , $h_k^{(q)}(t)$ its corresponding channel impulse response³, τ_q (resp. $E_s^{(q)} = P_q T_s$) its corresponding asynchronous transmission time (resp. received energy), and $z(t)$ is a complex additive white Gaussian noise with power spectral density N_0 . It is assumed that the different users signals are loosely synchronized in the network, at least so that the duration of a typical channel impulse response (T_d) includes their asynchronism.

Again, through a karhunen-Loeve expansion we rewrite the channel model in (V-1), for each symbol time k as the equivalent set of parallel independent channels

$$r_{k,i} = \sqrt{\frac{E_s^{(1)} \lambda_i}{\eta}} u_k^{(1)} h_{k,i}^{(1)} + \sum_{q=2}^Q \sqrt{\frac{E_s^{(q)} \lambda_i}{\eta}} u_k^{(q)} h_{k,i}^{(q)} + z_{k,i}, \quad i = 1, \dots, D \quad (\text{V-2})$$

when performing the expansion in (V-2), we assume that the channels from all the transmitters to the receiver, have the same output signal-space eigenvalue profile $\{\lambda_1, \dots, \lambda_D\}$.

²users $q = 2 \dots Q$ are interferers

³ $h_k^{(q)}(t)$ is the impulse response of the wireless channel linking transmitter q to the receiver

For $k = 1, \dots, N$, let $\underline{r}_k = \{r_{k,1}, \dots, r_{k,D}\}$. $\{h_{k,i}^{(q)}, i = 1, \dots, D; q = 1, \dots, Q\}$ and $\{z_{k,i}, i = 1, \dots, D; q = 1, \dots, Q\}$ are independent zero-mean complex Gaussian random variables, of variance respectively 1 and N_0 .

B GENIE-AIDED RECEIVER - UPPER BOUND

In order to have a first intuition on the impact of the multiuser interference on the achievable data rates of the pair of user of interest we first look at the simpler configuration depicted in (V). We constrain the users to the use of *On-off* signaling transmission strategy. Ignoring the constraints on data rate from the point-of-view of the receiver 2, we can show that a decoder using knowledge of codebooks of both the desired signal and the interferer is governed by the following rate region

$$\begin{aligned} R^{(1)} &\leq \frac{1}{T_s} I(u_k^{(1)}; \underline{r}_k^{(1)}, u_k^{(2)}) \\ R^{(1)} + R^{(2)} &\leq \frac{1}{T_s} I(u_k^{(1)}, u_k^{(2)}; \underline{r}_k^{(1)}) \end{aligned} \quad (\text{V-3})$$

$R^{(1)}$ (resp. $R^{(2)}$) is the transmission data rate between transmitter 1 (resp. transmitter 2) and receiver 1 (resp. receiver 2). This region reflects the influence of the data rate of user 2 on the achievable rate of user 1, when it is considered as “decodable” interference. It is most meaningful in the case of very strong interference, where we first decode the interferer (provided $R^{(2)} \leq I(u_k^{(2)}; \underline{r}_k^{(1)})$), and then decode the desired signal. The rate of the desired user’s signal is

$$\begin{aligned} R^{(1)} &\leq I(u_k^{(1)}; \underline{r}_k^{(1)}, u_k^{(2)}) \\ &= I(u_k^{(1)}; \underline{r}_k^{(1)} | u_k^{(2)}) \\ &= (1 - \eta) I(u_k^{(1)}; \underline{r}_k^{(1)} | u_k^{(2)} = 0) + \eta I(u_k^{(1)}; \underline{r}_k^{(1)} | u_k^{(2)} = 1/\eta) \end{aligned} \quad (\text{V-4})$$

In the case of very strong interference, the second term of the mutual information in (V-4) will be negligible. We see therefore, that the influence of the interference is a reduction in throughput by a factor $1 - \eta$. To achieve this throughput, however, knowledge of the interfering positions is required.

We come back now to the general case (V-1). The achievable rates without complete channel side information at the receiver, of transmitter 1, is given by $I(u^1; \{\underline{r}\})$. This is difficult to compute numerically but is upper-bounded as

$$\begin{aligned} \frac{1}{T_s} I(u_k^{(1)}; \{\underline{r}_k\}) &\leq I(u_k^{(1)}; \{\underline{r}_k\}, \{u_k^{(q)}, q = 2, \dots, Q\}) \\ &= \frac{1}{T_s} I(u^{(1)}; \{\underline{r}_k\} | \{u_k^{(q)}, q = 2, \dots, Q\}) \end{aligned} \quad (\text{V-5})$$

This upper-bound is interpreted as a genie-aided receiver who has access to the symbols of the interference but not their channels. As a result it cannot strip out the interference but it knows where it occurs and thus can use this information in the decoding process. This is also an upper-bound on the achievable rate with *On-off* signaling for the non-coherent receiver which can decode the interferers with received signal strength stronger than the desired signal.

The achievable rates for the genie-aided receiver can be shown to be given by

$$\begin{aligned} \frac{1}{T_s} I(u_k^{(1)}; \{\underline{r}_k\} | \{u_k^{(q)}, q = 2, \dots, Q\}) &= -\frac{1}{T_s} E E_a \underline{y} \left[\eta \log \left(\eta + (1 - \eta) \prod_{i=1}^D \left(1 + \frac{E_s^1 \lambda_i}{\eta N_0 + k E_s' \lambda_i} \right) \right. \right. \\ &\quad \left. \left. e^{-\underline{y} \text{diag} \left(\frac{E_s^1 \lambda_i}{\eta N_0 + k E_s' \lambda_i} \right) \underline{y}^H} \right) \right. \\ &\quad \left. + (1 - \eta) \log \left((1 - \eta) + \frac{\eta}{\prod_{i=1}^D \left(1 + \frac{E_s^1 \lambda_i}{\eta N_0 + k E_s' \lambda_i} \right)} \right. \right. \\ &\quad \left. \left. e^{\underline{y} \left(\text{diag} \left(1 + \frac{\eta N_0 + k E_s' \lambda_i}{E_s^1 \lambda_i} \right) \right)^{-1} \underline{y}^H} \right) \right] \end{aligned} \quad (\text{V-6})$$

Where \underline{y} is a zero mean complex Gaussian vector with variance equal to the identity matrix. $a_k = \sum_{q=2}^Q u_k^{(q)}$ is a random variable that represents the number of active interferers (i.e. transmitting a pulse) during the k th symbol time. In (V-6), and throughout the rest of this chapter, we assume that all the interferers have the same received energy per symbol that we note $E_s' = E_s^2 = \dots = E_s^Q$; this corresponds to a situation where a perfect power control is performed. This average mutual information can be efficiently computed numerically.

In the noise-limited region this is achieved by numerical integration and in the interference-limited region by Monte-Carlo averaging.

C THRESHOLD DETECTION - LOWER BOUND

In the previous section, we upper-bounded the achievable data rate of $I(u_k^{(1)}; \underline{r}_k)$ by the one of the genie-aided receiver which has access to the transmitted symbols by all interferers. In practice this could be achieved using a threshold rule on the receiver output, which is chosen so that the probability of detecting the presence of strong interference (and thus declaring an erasure) is very close to 1 when an interferer is transmitting.

In order to obtain a lower bound on $I(u_k^{(1)}; \underline{r}_k)$ and at the same time evaluate achievable rates of simple receivers, we note that

$$I(u_k^{(1)}; \underline{r}_k) \geq I(u^{(1)}; d_k) \quad (\text{V-7})$$

where

$$\begin{aligned} d_k &= \left(\sum_{i=1}^D \frac{|r_{k,i}|^2}{N_0 \left(1 + \frac{\eta^* N_0}{E_s \lambda_i}\right)} \right) I \left(\sum_{i=1}^D \frac{|r_{k,i}|^2}{N_0 \left(1 + \frac{\eta^* N_0}{E_s \lambda_i}\right)} < \xi \right) \\ &= e_k I(e_k < \xi) \end{aligned} \quad (\text{V-8})$$

with $I(\cdot)$ being the indicator function and ξ a threshold to be optimized. The lower bound in (V-7) is guaranteed by the data-processing inequality [32]. Note that this receiver is equivalent to the ML receiver in absence of interference (II-19). It aims to approach the optimal performance when the interferers active positions are perfectly known to the receiver (V-6); The erasor behaves as an interference detector and produces an estimate of interference positions state information. This estimate is asymptotically optimal for increasing interference strength E'_s . If interference strength E'_s is smaller than/or on the same order of the strength of the signal of interest E_s , the erasure allows controlling interference jams (simultaneous interference from several interferers).

C.1 Quantized threshold receiver

In practice, and in order to reduce the receiver's complexity, the received energy, e_k , is quantized when no erasure is declared (see figure C.1). The g -bits quantizer contains $L = 2^g$

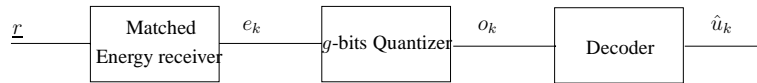


Fig. V-2. Quantized threshold receiver block diagramm

quantization levels $\{l_1, \dots, l_{L-1}\}$ in addition to the erasure status termed $E = l_L$. The quantizer output o_k is equal to l_i , $i = 1, \dots, L$ if the input e_k is within the range $[t_k, t_{k+1}]$. Where the quantization thresholds t_k are defined such that $t_1 = 0$ and $t_L = \xi$.

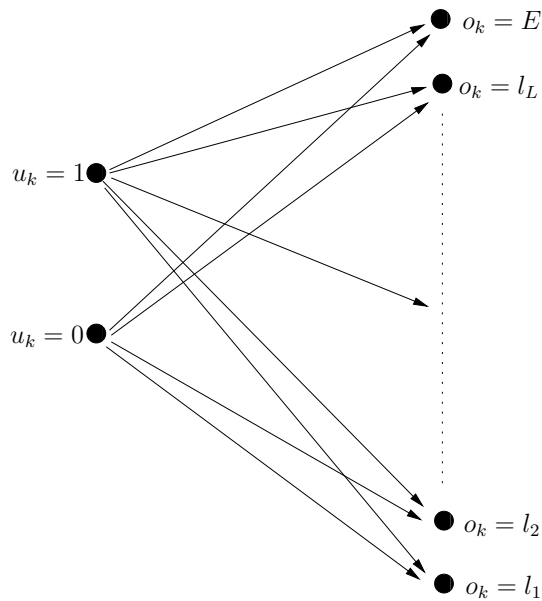


Fig. V-3. DMC equivalent channel model

From the perspective of the decoder, using the metrics at the output of the receiver described above, the communication channel relating the transmitted data symbols u_k to the quantizer's output variables o_k is a discrete memoryless channel(DMC) (see figure C.1).

Letting the number of quantization levels grow to infinity, the quantized threshold energy detector converges to the unquantized threshold receiver introduced in (V-8).

C.2 Extreme case: 2-level threshold receiver

The other extreme case consist of using a 1-bit quantizer

$$d_k = I \left(\sum_{i=1}^D \frac{|r_{k,i}|^2}{N_0 \left(1 + \frac{\eta^* N_0}{E_s \lambda_i} \right)} < \xi \right) \quad (\text{V-9})$$

This detector is a then a simple energy detector followed by hard-decision decoding and would model a minimalistic low-power UWB receiver which does not use an analog-to-digital converter. it would consist simply of filtering, amplification, and a square-law device such as a *Schottkey diode*. in addition, the decoding algorithm would also operate on a binary alphabet which could potentially reduce implementation complexity.

C.3 Ergodic achievable rates

The lower-bound is the capacity of a binary-input discrete-memoryless channel with transition probabilities depending on η and ξ . Conditioned on the interference level, the detected energy, e_k , is a quadratic form of complex Gaussian random variables

$$\begin{aligned} e_k &= \sum_{i=1}^D \frac{|r_{k,i}|^2}{N_0 \left(1 + \frac{\eta^* N_0}{E_s \lambda_i} \right)} \\ &= \underline{r}_k \mathbf{diag} \left(\frac{1}{N_0 \left(1 + \frac{\eta^* N_0}{E_s \lambda_i} \right)} \right) \underline{r}_k^H \\ &= \underline{t}_k \mathbf{\Gamma} \underline{t}_k^H \end{aligned} \quad (\text{V-10})$$

where $\mathbf{\Gamma} = \mathbf{diag} \left(\frac{N_0 + \frac{(a_k E_s' + u_k E_s) \lambda_i}{\eta}}{N_0 \left(1 + \frac{\eta^* N_0}{E_s \lambda_i} \right)} \right) = \mathbf{diag} (\nu_i(a_k, u_k))$ and \underline{t}_k a zero-mean random

Gaussian vector such that $E [\underline{t}_k^H \underline{t}_k] = \mathbf{I}$. Conditioned on the number of active interferers a_k and the transmitted symbol u_k , the probability density function of e_k is then written as follows ([35],[36])

$$P_{e_k}(t|a_k, u_k) = \Pr(e_k = t|a_k) = \sum_{i=1}^D \left(\frac{\nu_i^{D-2}(a_k, u_k)}{\prod_{\substack{j=1 \\ j \neq i}}^D (\nu_i(a_k, u_k) - \nu_j(a_k, u_k))} \right) \exp\left(-\frac{t}{\nu_i(a_k, u_k)}\right) \quad (\text{V-11})$$

Therefore, the transition probabilities of the considered DMC, conditioned on the number of active interferers, are as follows

$$\begin{aligned} P_{m|n}(a_k) &= \Pr(o_k = l_m | u_k = n, a_k) \quad n = 0, 1 ; m = 1, \dots, L-1 \\ &= \Pr(t_m \leq e_k \leq t_{m+1} | u_k = n, a_k) \\ &= \int_{t=t_m}^{t_{m+1}} P_{e_k}(t|a_k, n) dt \\ &= \sum_{i=1}^D \left(\frac{\nu_i^{D-1}(a_k, n)}{\prod_{\substack{j=1 \\ j \neq i}}^D (\nu_i(a_k, n) - \nu_j(a_k, n))} \right) \left[\exp\left(-\frac{t_m}{\nu_i(a_k, n)}\right) - \exp\left(-\frac{t_{m+1}}{\nu_i(a_k, n)}\right) \right] \\ P_{E|n}(a_k) &= \Pr(t_L \leq e_k | u_k = n, a_k) \quad n = 0, 1 \\ &= \int_{t=t_L}^{+\infty} P_{e_k}(t|a_k, n) dt \\ &= \sum_{i=1}^D \left(\frac{\nu_i^{D-1}(a_k, n)}{\prod_{\substack{j=1 \\ j \neq i}}^D (\nu_i(a_k, n) - \nu_j(a_k, n))} \right) \exp\left(-\frac{t_L}{\nu_i(a_k, n)}\right) \quad (\text{V-13}) \end{aligned}$$

The average mutual information between the transmitted symbol and decision variable is then given by

$$\begin{aligned} I(u_k; o_k) &= \frac{1}{T_s a_k} E \left[\eta \sum_{m=1}^L P_{m|1} \log_2 \left(\frac{P_{m|1}}{\eta P_{m|1} + (1-\eta) P_{m|0}} \right) \right. \\ &\quad \left. + (1-\eta) \sum_{m=1}^L P_{m|0} \log_2 \left(\frac{P_{m|0}}{\eta P_{m|1} + (1-\eta) P_{m|0}} \right) \right] \quad (\text{V-14}) \end{aligned}$$

a_k is distributed according to a binomial distribution. The optimization of η and the quantization levels, t_l $l = 1, \dots, L$ must be done numerically.

D RESULTS

We numerically evaluate the mutual information expressions derived earlier in this chapter. We again numerically optimize η . Figure V-4 shows the mutual information, versus the SNR, for different values of the number of active interferers. Two settings are considered: the first one correspond to the case where all the interference signals, received by the user of interest, have the same SNR level. This can be achieved with optimal power control. The second correspond to the case where interference signals have a 10 time higher SNR level. In both settings the achievable data rates are not affected by the presence of number of interferers as high as 50, for SNR values lower than 70dB. This is explained by the fact that in this SNR region, the probability of transmission η in absence of interference is low enough so that the probability of suffering any interference is almost null.

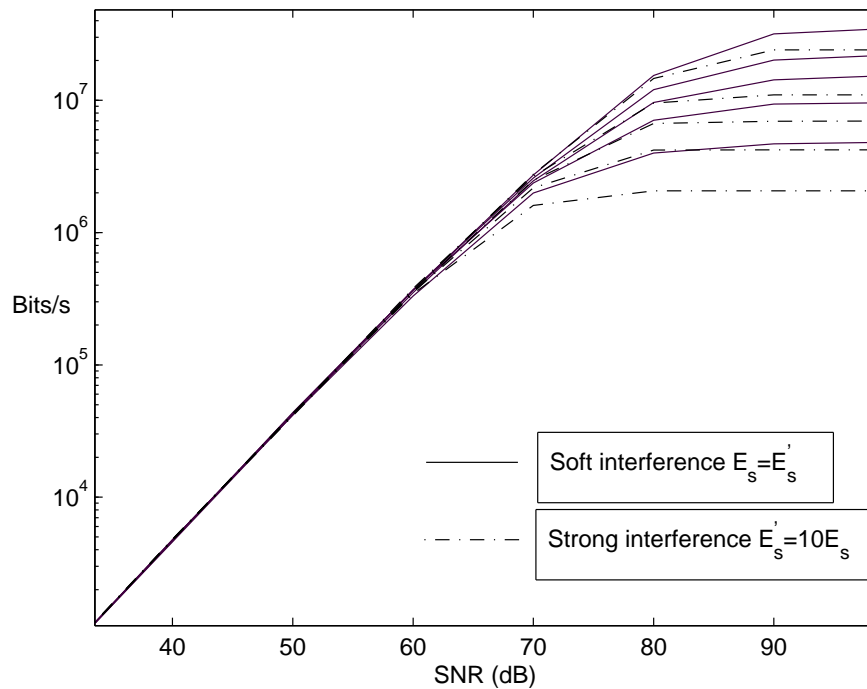


Fig. V-4. Achievable data rates of genie-aided receiver. $T_d=50$ ns, $W=1$ GHz. Number of interferers, from top to bottom: 1,5,10,20,50.

Figure V-5 shows the performance of the proposed practical threshold receiver. The figure

shows the impact of the number of quantization levels on the performance gap between the quantized threshold receiver and the genie-aided receiver whose performance is an upper bound on the performance of any practical receiver. We can see that surprisingly the two-level receiver performs significantly close to the performance of the genie aided receiver. We can also see that adding an extra quantization level brings the performance of the proposed receiver very close to the optimal one which suggests that the later receivers are well adapted to the considered setting.

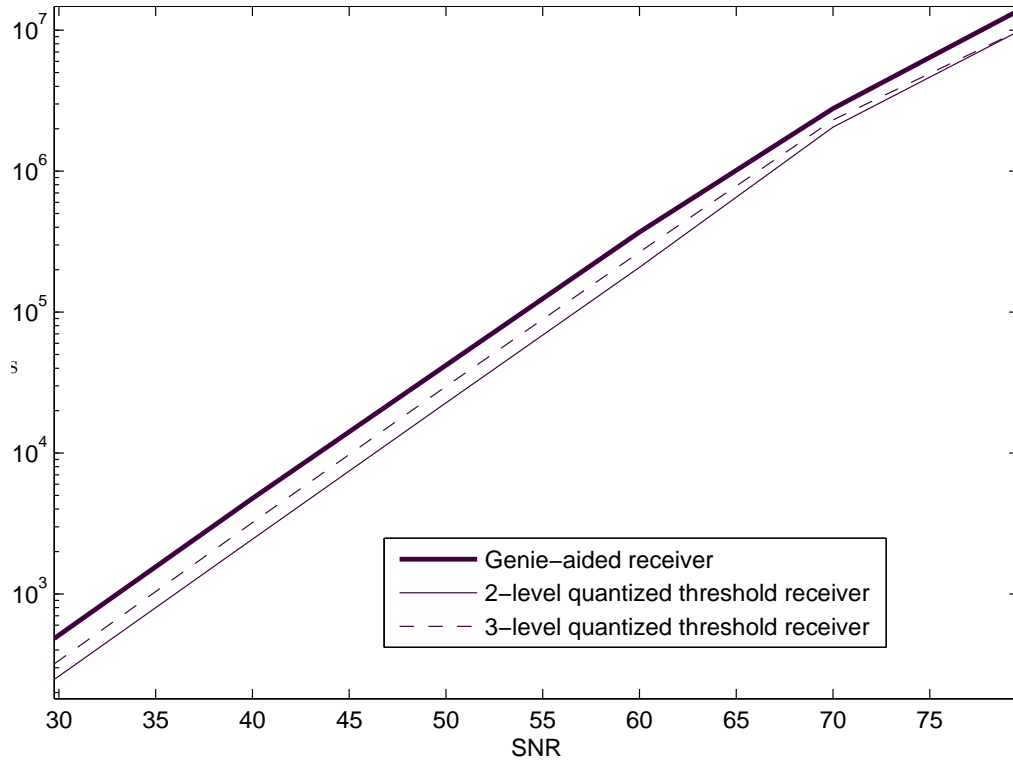


Fig. V-5. Achievable data rates of genie-aided versus quantized threshold receiver. $T_d=50$ ns, $W=1$ GHz, 1 strong interferer $E_s^I = 10E_s$

Code Constructions for *On-off* Ultra-wideband Systems

In considering signaling strategies for Ultra-Wideband (UWB) systems, we evaluated, in chapters (II) and (III), the achievable rates for non-coherent¹ detection of UWB *On-off* signals. Although significant loss in information rates compared to AWGN channel can be expected due to the extreme bandwidth (even for the low spectral efficiency associated with proposed UWB regulatory constraints on bandwidth and power), losses with respect to coherent detection with incomplete side information (i.e. imperfect channel estimation) are small. The savings in terms of implementation complexity are thus justified from a practical standpoint.

One particular way of implementing *On-off* signaling is the concatenation of a channel code with m -PPM modulation (here $\eta = 1/m$). This was considered for memoryless (rapidly-varying) Rayleigh fading channels in [92]. In [93] the design of channel codes for non-uniform input distributions was considered for memoryless channels.

In this work we consider suitable coding schemes for *flash-signaling* with non-coherent detection over a UWB channel. Such a coding scheme needs be a symmetric-input, asymmetric-output distribution binary code in order to correctly match the optimal input distribution for a given SNR. In the following we make the choice of enforcing the considered code con-

¹in the sense that the receiver has no channel side information of the underlying wideband channel process

structions to be of the form of binary symmetric-output code concatenated with an m -ary Pulse Position Modulation (m -PPM). The motivation for such a design choice is that designing binary codes with an asymmetric-output distribution is not a simple task. Furthermore, the use of binary symmetric-output distribution codes allows us to employ powerful optimization methods already developed in different contexts. The remainder of the chapter is organized as follows. The main goal of this work is to present code constructions for m -PPM modulation and examine their ability to approach channel capacity over an UWB channel with no channel state information at receiver side. Section II deals with the underlying system model for transmission and reception as well as the channel model. In section III we derive and evaluate BICM constrained capacity over UWB channel. Section IV contains the description of the presented codes as well as their optimization methodology. Finally in section V we discuss the considered codes performance in terms of decoding convergence thresholds and bit error rates.

A CHANNEL MODEL

We consider Non-coherent m -PPM signaling for an Ultrawideband system as a special case of the previously introduced flash-signaling (VI-1). Each m -PPM symbol, x_k , corresponds to choosing one out of m symbol times, constituting a PPM frame, in which to emit the transmit pulse $p(t)$. $x \in \{1, \dots, m\}$ is simply the position within the PPM frame where the pulse is transmitted. We restrict our study to strictly time-limited memoryless real-valued signals, both at the transmitter and receiver. We consider a block fading channel model so that the channel impulse response is time-invariant in any interval of $[kT_c, (k+1)T_c)$, where T_c is the *coherence-time* of the channel. We denote the channel in any block by $h_k(t)$ which is assumed to be a zero-mean process. For simplicity in the analytical developments, we assume that the channel realization in every block is independent and identically distributed, so that $E[h_k(t)h_l(u)] = R_h(t, u)\delta_{kl}$, where $R_h(t, u)$ is the auto-correlation function of the channel response in a particular interval. The received signal is

$$r(t) = \sum_{k=0}^N \sqrt{mE_s} p(t - (k * m + x_k)T_s) * h_k(t) + z(t) \quad (\text{VI-1})$$

where k is the symbol index, T_s the symbol duration, $E_s = PT_s$ the transmitted symbol energy, x_k is the transmitted symbol at time k , $p(t)$ is a unit-energy pulse of duration T_p , and $z(t)$ is white Gaussian noise with power spectral density N_0 . A guard interval of length T_d is left at the end of each symbol (from our memoryless assumption) so that $T_s \geq T_p + T_d$, and the symbol interval $T_s \ll T_c$. The received signal bandwidth W is roughly $1/T_p$, in the

sense that the majority of the signal energy is contained in this finite bandwidth.

Through a Karhunen-Loève expansion we rewrite the channel model in (VI-1), for each slot n (of duration T_s), as the equivalent set of parallel channels

$$\begin{aligned} r_{n,i} &= \sqrt{mE_s\lambda_i} + z_i, i = 1, \dots, \infty \\ \underline{r}_n &= \{r_{n,1}, \dots, r_{n,D}\} \end{aligned} \quad (\text{VI-2})$$

where z_i is $\mathcal{N}(0, N_0)$ and $\{h_i\}$ are unit variance zero mean independent Gaussian variables. The $\{\lambda_i\}$ are the solution to

$$\lambda_i \phi_i(t) = \int_0^{T_d+T_p} R_o(t, u) \phi_i(u) du. \quad (\text{VI-3})$$

where ϕ_i and $R_o(t, u)$ are the eigenfunctions and the autocorrelation function of the composite channel $h_k(t)*p(t)$, respectively. Because of the band-limiting nature of the channels in this study, the channel will be characterized by a finite number, D , of significant eigenvalues which for rich environments will be close to $1 + WT_d$, in the sense that a certain proportion of the total channel energy will be contained in these D components. we will assume that the eigenvalues are ordered by decreasing amplitude.

We note \underline{R}_n the received signal corresponding to the k th transmitted PPM symbol

$$\underline{R}_k = \{r_{m(k-1)+1}, \dots, r_{mk}\} \quad (\text{VI-4})$$

B CODING SCHEMES

B.1 BICM

Our reference coding scheme, will be a standard convolutional code used in Bit Interleaved Coded Modulation (BICM) construction. The encoder is obtained by the serial concatenation of a convolutional code and m -ary PPM modulation, through a bit interleaver fig (VI-1) (the accumulator we can see on the figure will be added later). Here the interleaver is assumed to be an ideal one (i.e. of infinite depth). The incoming information bits are first encoded with the convolutional code and passed through a bit interleaver. The coded bits are then grouped into sequences of m bits each and finally mapped onto corresponding m -PPM symbols and transmitted over the channel. The bit interleaver can be seen as a one-to-one

correspondence $\pi : k \rightarrow (k', i)$, where k denotes the time ordering of the coded bits c_k , k' denotes the time ordering of the signals $x_{k'}$, and i indicates the position of the bit c_k in the label of $x_{k'}$.

Capacity

We compute the constrained² capacity of BICM construction over the considered channel A. Note that here the capacity by allowing the convolutional code in figure (VI-1) to be replaced by any possible binary code. In the following we drop the time index k in (VI-4) for a better clarity of mathematical developments. Letting $P(\underline{R}|z)$ denote the transition probability of the transmission channel, the capacity of the considered system, in bits per second, can be written as follows [96]

$$\hat{C} = \frac{1}{mT_s} \left(m - \sum_{i=1}^m E_{b, \underline{R}} \left[\log_2 \left(\frac{\sum_{z \in \mathcal{X}} P(\underline{R}|z)}{\sum_{z \in \mathcal{X}_b^i} P(\underline{R}|z)} \right) \right] \right) \quad (\text{VI-5})$$

where \mathcal{X}_b^i denotes the set of codewords x whose i th label position is equal to b . Due to the symmetry of m -PPM modulation, \hat{C} is not sensitive to particular choices of the labeling function (that maps bit sequences onto m -PPM symbols). Thus \hat{C} can be rewritten as follows

$$\begin{aligned} \hat{C} &= \frac{1}{T_s} \left(1 - E_{b, \underline{R}} \left[\log_2 \left(\frac{\sum_{z \in \mathcal{X}} P(\underline{R}|z)}{\sum_{z \in \mathcal{X}_b^1} P(\underline{R}|z)} \right) \right] \right) \\ &= \frac{1}{T_s} \left(1 - \frac{1}{2m} \sum_{x=1}^m E_{\underline{R}|x} \left[\log_2 \left(1 + \frac{\sum_{z \in \mathcal{X}_0^1} P(\underline{R}|z)}{\sum_{z \in \mathcal{X}_1^1} P(\underline{R}|z)} \right) \right] \right) \\ &\quad + \frac{E_{\underline{R}|x}}{E_{\underline{R}|x}} \left[\log_2 \left(1 + \frac{\sum_{z \in \mathcal{X}_1^1} P(\underline{R}|z)}{\sum_{z \in \mathcal{X}_0^1} P(\underline{R}|z)} \right) \right] \end{aligned} \quad (\text{VI-6})$$

²Constrained to the use of m -PPM modulation

the channel transition probability is given by

$$P(\underline{R}|z) = \prod_{i=1}^D \frac{1}{mE_s\lambda_i + N_0} e^{-\frac{|r_{z,i}|^2}{mE_s\lambda_i + N_0}} \prod_{\substack{j=1 \\ j \neq z}}^m \prod_{i=1}^D \frac{1}{N_0} e^{-\frac{|r_{j,i}|^2}{N_0}} \quad (\text{VI-7})$$

Thus, exploiting symmetry of the channel transition probability and making the assumption that m is an even number, we re-write \hat{C} as follows

$$\begin{aligned} \hat{C} &= \frac{1}{T_s} \left(1 - \frac{1}{2} \frac{E}{\underline{R}|x=1} \left[\log_2 \left(1 + \frac{\sum_{z=1}^{m/2} P(\underline{R}|z)}{\sum_{z=(m/2)+1}^m P(\underline{R}|z)} \right) \right] \right. \\ &\quad \left. + \frac{1}{2} \frac{E}{\underline{R}|x=1} \left[\log_2 \left(1 + \frac{\sum_{z=(m/2)+1}^m P(\underline{R}|z)}{\sum_{z=1}^{m/2} P(\underline{R}|z)} \right) \right] \right) \end{aligned} \quad (\text{VI-8})$$

Using (VI-8) and (VI-7) we can numerically evaluate \hat{C} . On the other hand the capacity of non-coherent UWB channel constrained to the use of m -PPM (Coded modulation capacity) is given by

$$I(x; \underline{R}) = \frac{1}{mT_s} \left(\log_2(m) - \frac{E}{\underline{R}|x=1} \left[1 + \sum_{j=2}^m \frac{P(\underline{R}|x=j)}{P(\underline{R}|x=1)} \right] \right) \quad (\text{VI-9})$$

B.2 Convolutional Code+Binary Accumulator

In order to obtain a more powerful coding scheme, we explore in this section a new construction figure (VI-1). The construction is obtained by serial concatenation of the previous encoder and a unit-memory binary accumulator followed by a bit interleaver. The accumulator sums the incoming bit $\pi(c_k)$ with the previous output bit, d_{k-1} , in order to produce the new output bit d_k . The accumulator is rate one code, thus the overall coding rate of the proposed scheme is equal to the coding rate of the convolutional code R_c .

Decoding

Decoding is performed in an iterative manner. At each iteration the two decoder blocks (VI-2) exchange extrinsic information and recompute soft outputs on the coded bits. The decoding schedule at each decoding iteration is a two-step process: i) first, the inner decoder

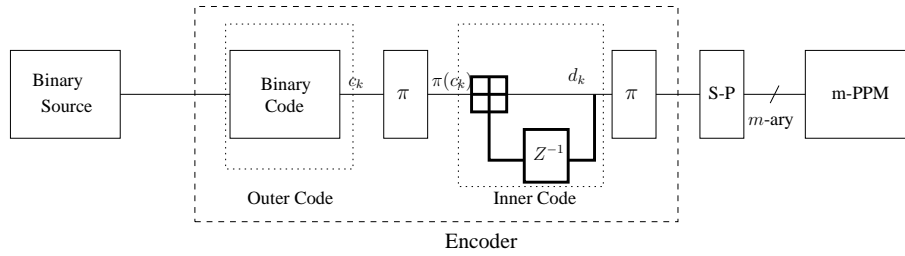


Fig. VI-1. Transmitter block diagram.

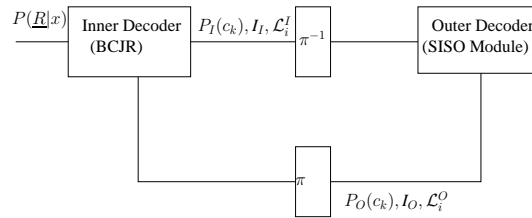


Fig. VI-2. Decoder block diagram.

uses the likelihoods $P_O(c_k)$, obtained from the outer decoder at the previous iteration, as a priori probabilities on the coded bits c_k in order to marginalize, using the BCJR algorithm, the likelihoods on the transmitted symbols $P_{CH}(\underline{R}_n|x_n)$; obtained through the transmission channel and compute new likelihoods on the coded bits c_k . ii) Second, the outer decoder uses the new likelihoods, $P_I(c_k)$, computed by the inner decoder in order to produce at its turn new likelihoods on the coded bits c_k . For the first iteration $P_O(c_k)$ are initialized with equiprobabilities. At the end of the decoding process, the outer code makes hard decisions on the information bits.

B.3 *m*-Ary Accumulator

We now replace the bit accumulator (and the bit interleaver following it) in the previous scheme by a weighted unit-memory symbol-level accumulator fig. (VI-3. The incoming symbol u_i is added to the previously transmitted symbol x_{i-1} multiplied by a factor f . Note that u_i, x_i, f , as well as the sum and product operations are defined over $GF(q)$. Throughout the paper q will be chosen to be equal to m . Again the overall coding rate is equal to the code rate of the convolutional code, since the symbol accumulator is a rate one code.

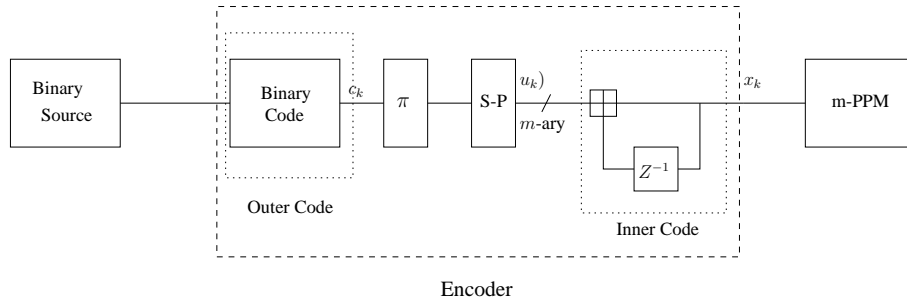


Fig. VI-3. Transmitter block diagram: m -ary Accumulator .

Exit Chart Analysis

Given the code construction, presented in this section, one can still optimize the performance of the code by making adequate choice of the convolutional code component. In order to perform this optimization over the set of all non-degenerated convolutional codes, we analyze the behavior of the concatenated code in the limit of infinite block lengths. The analysis is performed using exit charts of the code components taken separately. The exit chart of a block code is defined as transfer function T that gives, for a given extrinsic input mutual information I_{in} , the corresponding output mutual information I_{out} . I_{in} (respectively I_{out}) is the mutual information between the likelihood received (respectively emitted) through the extrinsic channel and its corresponding coded bit. In the following we note I_{In} (respectively I_O) such a quantity over the directional extrinsic channel from the inner decoder toward the outer decoder (respectively from the outer decoder toward the inner decoder)

$$I_{In} = I(c_i, \mathcal{L}_i^{In})$$

$$I_O = I(c_i, \mathcal{L}_i^O)$$

We associate to each decoding block an exit function as follows

$$\text{Inner decoder: } I_O = f(I_{In}, \mathcal{L}_{CH}) \tag{VI-10}$$

$$\text{Outer decoder: } I_{In} = g(I_O) \tag{VI-11}$$

Thus the iterative decoding process converges (i.e. achieves error free decoding) if and only if

$$x < g(f(x, L_{CH})) \quad \forall x \in [0, 1) \quad (\text{VI-12})$$

This condition prevents from having any fixed point, other than $x = 1$, for the function $x \mapsto f(g(x), L_{CH})$. Note that the existence for such a fixed point x_0 would mean that, if the decoder is initiated at a point lower than x_0 , the decoding will stick at this point and thus do not achieve $I_o = 1$ (i.e. do not achieve error free decoding). For the seek of feasibility of the estimation of functions $f(\cdot)$ and $g(\cdot)$, we make the assumption that the extrinsic channel is a Gaussian symmetric channel. Which implies that $P^O(c_i) = \frac{1}{2}(-1)^{c_i} \mathcal{L}_i^O$ and $P^{In}(c_i) = \frac{1}{2}(-1)^{c_i} \mathcal{L}_i^{In}$ where \mathcal{L}_i^O and \mathcal{L}_i^{In} are Gaussian distributed variables with mean respectively μ^O and μ^{In} , and variance respectively $2\mu^O$ and $2\mu^{In}$ (from the symmetry assumption).

I_O (respectively I_{In}) is linked to μ_O (respectively μ_{In}) through the following bijection relationship $I_O = \mathcal{J}(\mu_O)$ (respectively $I_{In} = \mathcal{J}(\mu_{In})$). Where \mathcal{J} is an invertible function defined as in [97]. We compute the exit functions through Monte Carlo simulation. For a given input mutual information I_{in} we generate iid input log-likelihood ratios \mathcal{L}_k^{int} according to its corresponding symmetric Gaussian distribution. Then for each of them we compute the output log-likelihood ratio \mathcal{L}_k^{out} using the BCJR algorithm and obtain the output mutual information as

$$\begin{aligned} I_{out} &= 1 - E_{\mathcal{L}^{out}} \left[h \left(\frac{1}{1 + e^{\mathcal{L}^{out}}} \right) \right] \\ &= 1 + \frac{1}{\log(2)} E_{\mathcal{L}^{out}} \left[\frac{\mathcal{L}^{out} e^{\mathcal{L}^{out}}}{1 + e^{\mathcal{L}^{out}}} - \log \left(1 + e^{\mathcal{L}^{out}} \right) \right] \end{aligned} \quad (\text{VI-13})$$

The code optimization procedure consist on picking, among all rate 1/2 convolutional code generators, the one that achieves, the lowest, necessary transmitted SNR per bit for error free decoding.

B.4 Extension:IRA Codes With a symbol Accumulator

In this section we introduce an extension to the previous scheme (B.3) through the replacement of the convolutional code by an irregular non-systematic repetition code. This modification aims to allow more degrees of freedom to the code optimization for a potentially better matching to the used modulation and channel statistics. The irregular repetition code is characterized, from its Tanner graph representation (VI-4), by its information bits edge degree distribution $\{\lambda_i\}$ and grouping factor a . Where λ_i is defined as the fraction of graph edges connected to a bit node of degree d_i equal to i . We denote d the maximum edge degree. Thus $\sum_{i=2}^d \lambda_i = 1$.

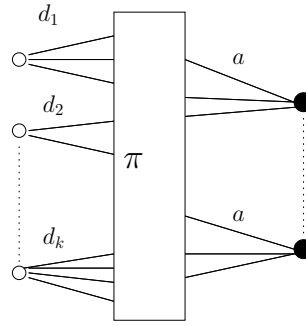


Fig. VI-4. Irregular repetition Tanner graph.

The overall coding rate, of the concatenated code, is equal to coding rate of the irregular repetition code and is given by

$$R_c = a \sum_{i=2}^d \lambda_i / i \tag{VI-14}$$

Code Optimization

The degrees of freedom of the considered coding scheme are the information bits degree distribution $\{\lambda_i\}$ and the grouping factor a . Thus, code optimization consist on finding the combination of $\{\lambda_i\}$ and a that maximizes the code rate for a given SNR under the condition that the iterative decoding converges and is error free. We use the code optimization methodology introduced in [94, 95]. The exit function of the accumulator $f(\cdot)$ is obtained using the same method and assumption as in (). Given the relative simplicity of the graph of a repetition code, $g(\cdot)$ can be analytically derived, using the same method as in [97], and shown to be written as follows

$$g(x) = \sum_{i=1}^d \lambda_i \mathcal{J} \left((i-1) \mathcal{J}^{-1} \left(1 - \mathcal{J} \left((a-1) \mathcal{J}^{-1} (1-x) \right) \right) \right) \tag{VI-15}$$

We solve the linear programming problem

$$\begin{cases} \text{maximize } R_c = a \sum_{i=2}^d \lambda_i / i & \text{subject to} \\ \sum_{i=2}^d \lambda_i = 1, \lambda_i \geq 0 \quad \forall i \\ x < g(f(x, L_{CH})) \quad \forall x \in [0, 1) \end{cases} \tag{VI-16}$$

C OPTIMIZATION RESULTS AND SIMULATIONS

All simulation and code optimization results were obtained for a pulse duration $T_p = 1e-9s$ and channel delay spread $T_d = 25e-9s$. Figure (C) shows code optimization results for the IRA type of codes with an m -ary accumulator for m -PPM modulation sizes equal to 4, 8, and 16. The maximum bit degree d was taken to be equal to 100. The optimized codes achieves convergence thresholds as close as 0.37 dB from the capacity limit. We note that the coding rates, corresponding to the distribution with lowest convergence threshold, have values around .5 which is in-line with the result, on optimal coding rate, from the capacity analysis of m-PPM. In figure (C) we see a comparison of convergence threshold of the considered coding schemes, for different modulation size values. We can see that the use of the m -ary accumulator, instead of the binary one, reduced the distance to the capacity limit by about 0.5 dB. Figure (C) contains bit error rates of the considered code constructions, obtained by simulations for block codes of 10000 bits and using randomly generated interleavers. We notice a gap, on the order of 1 dB, between the convergence thresholds obtained by the exit chart analysis and those obtained by simulation. This means that randomly generated interleavers are suboptimal (for this block size) and thus need to be optimized. Note also that the use of the Gaussian approximation of the extrinsic channel, usually lead to slightly too optimistic results [94].

	m=4		m=8		m=16	
	i	λ_i	i	λ_i	i	λ_i
	3	0.1194	3	0.0837	5	0.1370
	4	0.5260	4	0.1132	3	0.1662
	9	0.2098	6	0.4681	5	0.6013
	10	0.1448	7	0.3349	10	0.0955
a	2		3		6	
Rate	0.4182		0.5462		0.5746	
E_b/N_0	9.76		8.06		7.29	
$(E_b/N_0)_{gap}$	0.44		0.37		0.41	

Fig. VI-5. Decoding Thresholds for IRA with an m -ary Accumulator

D CONCLUSION

We considered coding schemes for non-coherent *flash-signaling* over Ultra-wideband channels. Different code constructions were proposed and optimized using an exit chart based methodology. The performance of proposed codes was then measured using both an exit

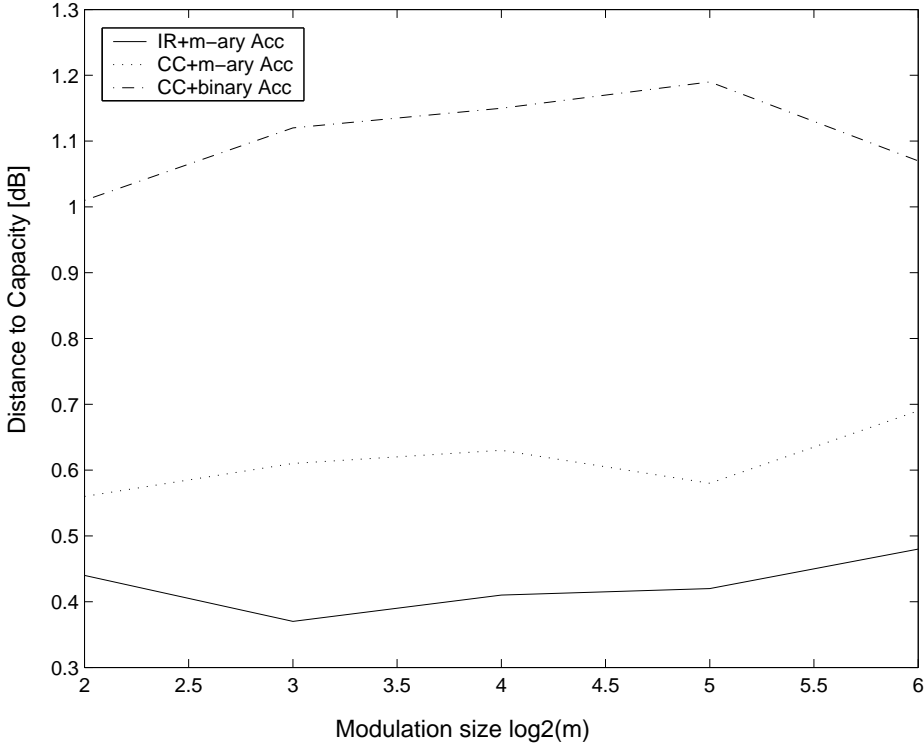


Fig. VI-6. Distance to Capacity

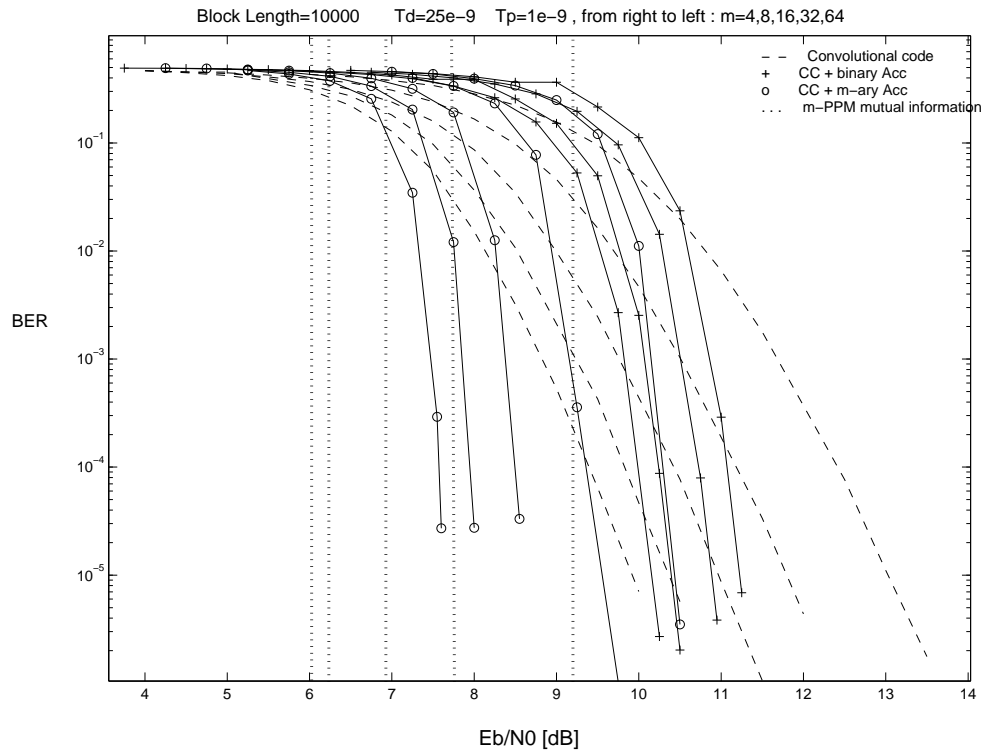


Fig. VI-7. Decoding simulations

chart based analysis and Monte Carlo simulations. The optimized were shown to perform close to information-theoretic limits.

Bibliography

- [1] Ross, G.F., “The transient analysis of multiple beam feed networks for array systems”, Ph.D. dissertation, Polytechnic Institute of Brooklyn, Brooklyn, NY, 1963. [6]
- [2] Ross, G.F., “The transient analysis of certain TEM mode four-port networks”, *IEEE Trans. Microwave Theory and Tech.*, Vol. MTT-14, Issue 11, pp. 528-547, 1966. [6]
- [3] Ross, G.F., “A time domain criterion for the design of wideband radiating elements”, *IEEE Trans. Antennas Propagat.*, Vol. 16, Issue 3, pp. 355, 1968. [6]
- [4] Bennett, C.L.; Ross, G.F., “Time-domain electromagnetics and its application” Proc. *IEEE* 66, 299-318, 1978. [6]
- [5] Harmuth, H.F., *Transmission of Information by Orthogonal Functions*, Second Edition Springer, New York, 1972. [6]
- [6] Harmuth, H.F., “Range-Doppler Resolution of Electromagnetic Walsh Waves in Radar”, *IEEE Trans. Electromagn. Compat*, EMC-17, 106-111, 1975. [6]
- [7] Harmuth, H.F., “Selective Reception of Periodic Electromagnetic Waves with General Time Variation”, *IEEE Trans. Electromagn. Compat*, EMC-19, 137-144, 1977. [6]
- [8] Harmuth, H.F., *Sequency Theory* Academic Press, New York 1977. [6]
- [9] Harmuth, H.F., *Nonsinusoidal Waves for Radar and Radio Communication* Academic, New York, 1981. [6]
- [10] Baum, C.E. et al (Eds.) “Ultra-Wideband, Short-Pulse Electromagnetics 3”, Plenum, New York, 1997. [6]
- [11] Bertoni, H.L.; Carin, L.; Felsen, L.B. (Ed.s) “Ultra-Wideband Short-Pulse Electromagnetics”, Plenum Press, 1993.

- [12] Carin, L.; Felsen, L.B., "Ultra-Wideband Short-Pulse Electromagnetics 2", Plenum, New York, 1995. [6]
- [13] FCC document 00-163, "Revision of part 15 commission rules ET Docket No. 98-153 regarding UWB transmission systems", adopted 2-14-2002. [6]
- [14] <http://www.ieee802.org/15/pub/TG3a.html>
- [15] <http://www.ieee802.org/15/pub/TG4a.html> [ix, 6, 7, 20, 62][8][8]
- [16] Win, M. Z. , Scholtz, R. A. , "Impulse radio: how it works " *IEEE Communications Letters*, Volume: 2 Issue: 2, pp. 36 -38, Feb. 1998. [11]
- [17] Win, M. Z. , Scholtz, R. A. , " Ultra-wide bandwidth time-hopping spread-spectrum impulse radio for wireless multiple-access communications " *IEEE Transactions on Information Theory* Volume: 48 Issue:4, pp. 679 -689, April 2000. [72]
- [18] Gassezadeh, S. S. , Tarokh, V. , "The Ultra-wideband Indoor Path Loss Model," IEEE P802.15 Working group, June 2002 . [21]
- [19] Saadane, R. ;Menouni, H. A. ;Knopp, R. ;Aboutajdine, D. "Empirical eigenanalysis of indoor UWB propagation channels" *IEEE Global Telecommunications Conference*, November 29-December 3, 2004, Dallas, USA. [13, 14]
- [20] Abou-Faycal, I. C. ; Trott, M. D. ; Shamai S. "The Capacity of Discrete-Time Memoryless Rayleigh-Fading Channels " *IEEE Transactions on Information Theory*, Vol. 47, Issue:5, May 2001, pp. 1290-1301. [10]
- [21] Pierce, J. N. , "Ultimate performance of M-ary transmission on fading channels" *IEEE Transactions on Information Theory* Volume: 12 Issue: 1, pp. 2-5, Jan. 1966. [9]
- [22] Medard M. ; Gallager R. G. , " Bandwidth scaling for fading multipath channels" *IEEE Transactions on Information Theory* Volume: 48 Issue: 4, pp. 840 -852, Apr. 2002. [20, 55]
- [23] Subramanian, V. G. ; Hajek, B. , "Broad-band fading channels: signal burstiness and capacity " *IEEE Transactions on Information Theory* , Volume: 48 Issue: 4 , pp. 809-827, Apr 2002. [10, 20, 55]
- [24] Porrat, D. ; Tse, D.N.C. , "Bandwidth scaling in ultra wideband communication" in *Allerton Conference on Communications, Control, and Computing*, Monticello, IL, USA, Oct. 2003. [-]
- [25] Pendergrass, M. , IEEE P802.15 Working group, "Empirically Based Statistical Ultra-Wideband Channel Model," April 2002. [14, 17]
-

- [26] Win, M. Z. ; Scholtz, R. A., "On the energy capture of ultrawide bandwidth signals in dense multipath environments " *IEEE Communications Letters*, Vol. 2, Issue: 9 pp. 245-247, 1998. [14]
- [27] Cramer, J. M. ; Scholtz, R. A. ; Win, M. Z., " Spatio-temporal diversity in ultra-wideband radio" *Wireless Communications and Networking Conference, IEEE*, Vol. 2, pp. 888-892, 1999. [14]
- [28] Verdu, S. , " Spectral efficiency in the wideband regime " *IEEE Transactions on Information Theory*, Vol. 48 Issue: 6 , June 2002 pp. 1319 -1343. [9, 10, 11, 64]
- [29] R. S. Kennedy, *Fading Dispersive Communication Channels*. John Wiley & sons, 1969. [9, 56]
- [30] T. M. Cover, J. A. Thomas, *Elements of Information Theory*. John Wiley & sons, 1991. [49, 67]
- [31] Telatar, I. E.; Tse, D. N. C. , "Capacity and mutual information of wideband multipath fading channels " *IEEE Transactions on Information Theory*, Vol. 46, Issue:4, pp. 1384-1400, 2000. [39, 56]
- [32] Gallager, R.G., *Information Theory and Reliable Communication*, Wiley and Sons, 1968. [13, 39, 76]
- [33] R. Papoulis, *Probability, Random Variables, and Stochastic Processes*. McGraw-Hill, 1984. [-]
- [34] C. W. Helstrom, *Elements of Signal Detection and Estimation*. PTR Prentice Hall, 1995. [13, 27]
- [35] A. Stuart J. Keith Ord, *Kendall's Advanced Theory of Statistics: Volume 1 Distribution Theory*. Halsted Press, 1994. [29, 78]
- [36] Proakis, J. ; *Digital Communications*. McGraw-Hill, 1995. [29, 78]
- [37] Telatar, I. E.; Tse, D. N. C. , "Capacity and mutual information of wideband multipath fading channels " *IEEE Transactions on Information Theory*, Vol. 46, Issue:4, pp. 1384-1400, Jul. 2000. [9, 20, 55, 56, 64]
- [38] Lapidoth, A. ; Shamai, S. , "Fading Channels: How Perfect Need *Perfect Side Information* Be?" *IEEE Transactions on Information Theory*, Vol. 48, Issue:5, pp. 1118-1134, May. 2002. [34]
-

- [39] Medard, M. ,“The Effect Upon Channel Capacity in Wireless Communications of Perfect and Imperfect Knowledge of The Channel” *IEEE Transactions on Information Theory*, Vol. 46, Issue:3, pp. 933-946, May. 2000. [34]
- [40] Caire, G. ; Shamai, S. ,“On the Capacity of Some Channels With Channel State Information ” *IEEE Transactions on Information Theory*, Vol. 45, Issue:6, pp. 2007-2019, Sep. 1999. [34]
- [41] Viswanathan, H. ,“Capacity of Markov channels with receiver CSI and delayed feedback” *IEEE Transactions on Information Theory*, Vol. 45, Issue:2, pp. 761-771, Mar. 1999. [34]
- [42] Duman, T. ;Salehi, M. ,“Optimal quantization for finite-state channels” *IEEE Transactions on Information Theory*, Vol. 43, pp. 758-765, Mar. 1997. [34]
- [43] Schuster, U.G.; Borgmann, M.; Bolcskei, H.; “Semicoherent PPM for wideband communications” in *Proc. International Symposium on Information Theory*, June 2004. [34]
- [44] Choi, J.D.; Stark, W.E., “Performance of UWB Communications with Imperfect Channel Estimation” *Journal on Selected Areas in Communications*, Vol. 20, Issue:9, Pp. 1754 - 1766, Dec. 2002. [34]
- [45] Wozencraft, J.M. ; Jacobs, I. M. , *Principles of Communication Engineering*, Wiley and Sons, 1965. [39]
- [46] Forney, G.D., Jr.; “The Viterbi Algorithm” in *Proc. IEEE* Vol.6, pp. 268-278, Mar. 1973. [39]
- [47] Bahl, L.R.; Cocke, J.; Jelinek, F.; Raniv, J.; “Optimal Decoding of Linear Codes for Minimizing Symbol Error Rate”*IEEE Transactions on Information Theory*, Vol. 20, pp. 268-278, Mar. 1973. [39]
- [48] Turin, G.L. , “The characteristic function of Hermitian quadratic forms in complex normal variables”, *Biometrika*, Vol. 47, pp. 199-201, 1960. [45]
- [49] Poor, H. V.; Verdu, S. ,“A Lower Bound on the Probability of Error in Multihypothesis Testing” *IEEE Transactions on Information Theory*, Vol. 41, Issue:6, pp. 1992-1994, Nov. 1995. [48]
- [50] Han, T. S.; Verdu, S. ,“Generalizing the Fano inequality” *IEEE Transactions on Information Theory*, Vol. 40, Issue:4, pp. 1247-1251, Jul. 1994. [35, 49]
- [51] Shannon, C. E. ,“Certain Results in Coding Theory for Noisy Channels” *Information and Control*, Vol. 1, pp. 6-25, Sept. 1957. [49]
-

- [52] Ye, L. ; Molisch, A.F.; Jinyun Z. ; “Practical approaches to channel estimation and interference suppression for OFDM based UWB communications” in *Proc. of the IEEE 6th Circuits and Systems Symposium on Emerging Technologies: Mobile and Wireless Comm.* Vol. 1, pp. 21-24, 31 May-2 Jun. 2004 [55]
- [53] Saberinia, E.; Tewfik, A.H.; “Pulsed and non-pulsed OFDM ultra wideband wireless personal area networks” in *Proc. of IEEE Conference on Ultra Wideband Systems and Technologies*, pp. 275 - 279, 16-19 Nov. 2003. [56]
- [54] Zhengyuan, X. ; Liu L. ; “Power allocation for multi-band OFDM UWB communication networks” in *Proc. IEEE 60th Vehicular Technology Conference, VTC2004-Fall* Vol. 1, pp. 368-372, 26-29 Sept. 2004. [56]
- [55] Wessman, M.-O.; Svensson, A.; Agrell, E.; “Frequency diversity performance of coded multiband-OFDM systems on IEEE UWB channels” in *Proc. IEEE 60th Vehicular Technology Conference, VTC2004-Fall* Vol. 2, pp. 1197-1201, 26-29 Sept. 2004. [55]
- [56] Saberinia, E.; Tewfik, A.H.; “Receiver structures for multicarrier UWB systems” in *Proc. Seventh International Symposium on Signal Processing and Its Applications* Vol. 1, pp. 313-316 1-4 Jul. 2003. [56]
- [57] Ghorashi, S.A.; Allen, B.; Ghavami, M.; Aghvami, A.H.; “An overview of MB-UWB OFDM” in *Proc.IEE Seminar on Ultra Wideband Communications Technologies and System Design* pp. 107-110, 8 Jul., 2004. [55]
- [58] Ramachandran, I.; Nakache, Y.-P.; Orlik, P.; Molisch, A.F.; Jinyun Zhang; “Symbol spreading for ultrawideband systems based on multiband OFDM” in *Proc. IEEE International Symposium on Personal, Indoor and Mobile Radio Communications, PIMRC* Vol. 2, pp. 1204-1209, 5-8 Sept. 2004. [56]
- [59] Balakrishnan, J.; Batra, A.; Dabak, A.; “A multi-band OFDM system for UWB communication” in *Proc. of IEEE Conference on Ultra Wideband Systems and Technologies* pp. 354-358, 16-19 Nov. 2003. [55]
- [60] Gupta, R.; Tewfik, A.H.; “Capacity of ultra-wideband OFDM” in *Proc. of The 57th IEEE Semiannual Vehicular Technology Conference, VTC 2003-Spring* Vol. 2, pp. 1420-1424, 22-25 Apr. 2003. [55]
- [61] Batra, A.; Balakrishnan, J.; Dabak, A.; “Multi-band OFDM: a new approach for UWB” in *Proc. of International Symposium on Circuits and Systems,ISCAS* Vol.5, pp. V-365-V-368 23-26 May 2004. [55]
-

- [62] Saberinia, E.; Tewfik, A.H.; "Outage capacity of pulsed-OFDM ultra wideband communications" in *Proc. of International Workshop on Ultra Wideband Systems, Joint UWBST & IWUWBS* pp. 323-327, 18-21 May 2004. [55]
- [63] Multi-band OFDM Physical Layer Proposal for IEEE 802.15 Task Group 3a. <http://www.ieee802.org/15/pub/TG3a.html>, Mar. 2004. [56]
- [64] Cheng Luo; Medard M. , "Performance of single-tone and two-tone frequency-shift keying for ultrawideband" *the Thirty-Sixth Asilomar Conference on Signals, Systems, and Computers*, Volume: 1 , PP. 701-705, Nov. 2002 [56, 58, 62, 64]
- [65] Bo Hu; Beaulieu, N.C.; "Accurate evaluation of multiple-access performance in TH-PPM and TH-BPSK UWB systems" *IEEE Transactions on Communications*, Vol. 52, Issue:10, pp. 1758 - 1766, Oct. 2004. [72]
- [66] Cassioli, D.; Mazzenga, F.; "Spectral analysis of UWB multiple access schemes using random scrambling" *IEEE Transactions on Wireless Communications* Vol. 3, Issue 5, pp. 1637 - 1647, Sept. 2004. [72]
- [67] Boubaker, N.; Letaief, K.B.; "Performance analysis of DS-UWB multiple access under imperfect power control" *IEEE Transactions on Communications*, Vol. 52, Issue:10, pp. 1459 - 1463, Sep. 2004. [72]
- [68] Laney, D.C.; Maggio, G.M.; Lehmann, F.; Larson, L.; "Multiple access for UWB impulse radio with pseudochaotic time hopping" *IEEE Journal on Selected Areas in Communications* Vol. 20, Issue 9, pp. 1692 - 1700, Dec. 2002. [72]
- [69] Somayazulu, V.S.; "Multiple access performance in UWB systems using time hopping vs. direct sequence spreading" *IEEE Wireless Communications and Networking Conference* Vol. 2, pp. 522-525, 17-21 March 2002. [72]
- [70] Niranjayan, S.; Nallanathan, A.; Kannan, B.; "Exact modeling of multiple access interference and BER derivation for TH-PPM UWB" *IEEE Wireless Communications and Networking Conference* Vol. 2, pp. 801-806, 13-17 March 2005. [72]
- [71] Pasand, R.; Khaleshosseini, S.; Nielsen, J.; Sesay, A.; "The capacity of asynchronous m-ary time hopping PPM UWB multiple access communication systems" *IEEE 60th Vehicular Technology Conference* Vol. 7, pp. 4745-4749, 26-29 Sept. 2004. [72]
- [72] Zhao, L.; Haimovich, A.M.; "The capacity of an UWB multiple-access communications system" *IEEE International Conference on Communications* Vol. 3, pp. 1964-1968, 28 April-2 May, 2002. [72]
-

- [73] Gezici, S.; Kobayashi, H.; Poor, H.V.; Molisch, A.F.; "Performance evaluation of impulse radio UWB systems with pulse-based polarity randomization in asynchronous multiuser environments" *IEEE Wireless Communications and Networking Conference* Vol. 2, pp. 908-913, 21-25 March 2004. [72]
- [74] Taha, A.; Chugg, K.M.; "A theoretical study on the effects of interference UWB multiple access impulse radio" *The Thirty-Sixth Asilomar Conference on Signals, Systems and Computers* Vol. 1, pp. 728-732, 3-6 Nov. 2002. [72]
- [75] Taha, A.; Chugg, K.M.; "On the power spectral density of wireless multiple-access UWB impulse radio under realistic propagation conditions" *IEEE 58th Vehicular Technology Conference* Vol. 2, pp. 1298-1302, 6-9 Oct. 2003. [72]
- [76] Canadeo, C.M.; Temple, M.A.; Baldwin, R.O.; Raines, R.A.; "Code selection for enhancing UWB multiple access communication performance using TH-PPM and DS-BPSK modulations" *IEEE Wireless Communications and Networking Conference* Vol. 1, pp. 678-682, 16-20 March 2003. [72]
- [77] Mucchi, L.; Marabissi, D.; Ranaldi, M.; Del Re, E.; Fantacci, R.; "Impact of synchronization errors and multiple access interference to the performance of UWB impulse radio systems" *IEEE Eighth International Symposium on Spread Spectrum Techniques and Applications* pp. 477-483, 30 Aug.-2 Sept. 2004. [72]
- [78] Hao Zhang; Gulliver, T.A.; "Pulse position amplitude modulation for time-hopping multiple access UWB communications" *IEEE Wireless Communications and Networking Conference* Vol. 2, pp. 895-900, 21-25 March 2004. [72]
- [79] Durisi, G.; Romano, G.; "On the validity of Gaussian approximation to characterize the multiuser capacity of UWB TH PPM" *IEEE Conference on Ultra Wideband Systems and Technologies: Digest of Papers* pp. 157-161, 21-23 May 2002. [72]
- [80] Yoon, Y.C.; Kohno, R.; "Optimum multi-user detection in ultra-wideband (UWB) multiple-access communication systems" *IEEE International Conference on Communications* vol.2, pp. 812-816, 28 April-2 May 2002. [-]
- [81] Qinghua Li; Rusch, L.A.; "Multiuser detection for DS-CDMA UWB in the home environment" *IEEE Journal on Selected Areas in Communications* Vol. 20, Issue 9, pp. 1701-1711, Dec. 2002. [-]
- [82] Ping Liu; Zhengyuan Xu; Jin Tang; "Minimum variance multiuser detection for impulse radio UWB systems" *IEEE Conference on Ultra Wideband Systems and Technologies* pp. 111-115, 16-19 Nov. 2003. [-]
-

- [83] Zhengyuan Xu; Ping Liu; Jin Tang; "Blind multiuser detection for impulse radio UWB systems" *IEEE Topical Conference on Wireless Communication Technology* pp. 453-454, 15-17 Oct. 2003. [-]
- [84] Ping Liu; Zhengyuan Xu; Jin Tang; "Subspace multiuser receivers for UWB communication systems" *IEEE Conference on Ultra Wideband Systems and Technologies* pp. 116-120, 16-19 Nov. 2003. [-]
- [85] Qinghua Li; Rusch, L.A.; "Hybrid RAKE / multiuser receivers for UWB" *Radio and Wireless Conference* pp. 203-206, Aug. 10-13, 2003. [-]
- [86] Souilmi Y. , Knopp R. , "Challenges in UWB Signaling for Adhoc Networking" *DI-MACS Workshop on Signal Processing for Wireless Transmission*, Oct. 2002. [-]
- [87] Yoshida, S.; Ohtsuk, T.; "Performance evaluation of adaptive internally turbo coded ultra wideband-impulse radio (AITC-UWB-IR) in multipath channels" *IEEE 60th Vehicular Technology Conference, VTC2004-Fall* Vol. 2, pp. 1179-1183, 26-29 Sept. 2004. [-]
- [88] Eshima, K.; Hase, Y.; Oomori, S.; Takahashi, F.; Kohno, R.; "M-ary UWB system using Walsh codes" *IEEE Conference on Ultra Wideband Systems and Technologies: Digest of Papers* pp. 37-40, 21-23 May 2002. [-]
- [89] Takizawa, K.; Kohno, R.; "Combined iterative demapping and decoding for coded UWB-IR systems" *IEEE Conference on Ultra Wideband Systems and Technologies: Digest of Papers* pp. 423-427, 16-19 Nov. 2003. [-]
- [90] Chunyu Bi; Hui, J.; Bodenheimer, L.; Spielberg, H.; "Embedded turbo coding in pattern position modulation for ultra wideband radio systems" *International Symposium on Information Theory*, pp. 515-515, 27 June-2 July 2004. [-]
- [91] Matsumoto, T.; Ochiai, H.; Kohno, R.; "Super-orthogonal convolutional coding with orthogonal pulse waveform for ultra wideband communications" *International Workshop on Ultra Wideband Systems Joint with Conference on Ultrawideband Systems and Technologies* pp. 202-206, 18-21 May 2004. [-]
- [92] Peleg, M.; Shamai, S.; "Efficient communication over memoryless Rayleigh fading channels with turbo coding/decoding" *Communication Theory Mini-Conference*, , 6-10 June 1999 PP. 83 - 88. [83]
- [93] Bennatan, A.; Burshtein, D.; "On the application of LDPC codes to arbitrary discrete-memoryless channels" *IEEE Transactions on Information Theory*, Vol. 50 , Issue: 3 , March 2004, PP. 417 - 438. [83]
-

-
- [94] A. Roumy; S. Guemghar; G. Caire; S. Verdu, "Design Methods for Irregular Repeat-Accumulate Codes" *IEEE Transactions on Information Theory*, Vol. 50, Issue:8, pp. 1711-1727, August 2004. [91, 92]
- [95] S. ten Brink and G. Kramer, "Turbo Processing for Scalar and Vector Channels" in *Proc. 3rd Int. Symp. Turbo Codes and Related Topics*, Brest, France, Sept. 2003, pp. 23-30. [91]
- [96] G. Caire; G. Taricco; E. Biglieri, "Bit-Interleaved Coded Modulation" *IEEE Transactions on Information Theory*, Vol. 44, Issue:3, pp. 927-946, May 1998. [86]
- [97] Sae-Young Chung; Richardson, T.J.; Urbanke, R.L., "Analysis of sum-product decoding of low-density parity-check codes using a Gaussian approximation" *IEEE Transactions on Information Theory* Vol. 47, Issue: 2, pp. 657 - 670, Feb 2001. [90, 91]
-

List of publications

CONFERENCES

- Souilmi, Y.; Knopp, R.; Caire, G.
On Code Construction for Flash-Signaling Ultra-Wideband Systems
IEEE International Conference on Ultra-Wideband (ICU 2005), Zurich, Switzerland 2005
- Souilmi, Y.; Knopp, R.
Generalized Multi-Carrier Signaling for Ultrawideband Systems
39th Annual Conference on Information Sciences and Systems CISS, Baltimore, USA 2005.
- Souilmi Y.; Knopp R.
Achievable rates for UWB peer-to-peer networks
IZS 2004, 18h International Zurich Seminar on Communications. February 18-20, 2004, Zurich, Switzerland
- Souilmi, Y.; Knopp, R.
On the achievable rates of ultra-wideband systems in multipath fading environments
IEEE International Symposium on Information Theory, Yokohama, Japan. June 29 - July 4, 2003. Pages: 387 - 387
- Anouar H.; Souilmi Y.; Bonnet C.
Self Balanced Receiver-Oriented MAC for Ultra-wide Band Ad hoc Networks
Mobihoc 2003, Annapolis, Maryland, USA June 1-3, 2003.
- Anouar H.; Souilmi Y.; Bonnet C.
Self-balanced receiver-oriented MAC for ultra-wide band mobile ad hoc networks
IWUWBS'2003 International Workshop on Ultra Wideband Systems, June 2-5, 2003, Oulu, Finland
- Souilmi, Y.; Knopp, R.
On the achievable rates of ultra-wideband PPM with non-coherent detection in

multipath environments

IEEE International Conference on Communications, ICC '03, 11-15 May 2003. Pages : 3530 - 3534 vol.5

- Souilmi Y.;Knopp R.

On achievable rates and coding for UWB systems

2003 Winter school on coding and information theory, February 24-27, 2003, Monte Verita, Switzerland

- Souilmi Y.;Knopp R.

On achievable rates and coding for UWB systems

2003 Winter school on coding and information theory, February 24-27, 2003, Monte Verita, Switzerland

- Souilmi Y.;Knopp R.

Challenges in UWB signaling for ad-hoc networking

Invited paper in DIMACS Workshop on Signal Processing for Wireless Transmission, October 7-9, 2002, Piscataway, USA

JOURNALS AND BOOK CHAPTERS

- Souilmi Y.; Knopp R.

On the Achievable Rates of Multiband Ultra-Wideband Systems: Ultra-Wideband Systems

International Journal of Wireless Information Networks, October 2003, vol. 10, iss. 4, pp. 211-219(9). Kluwer Academic/Plenum Publishers

- Souilmi, Y.; Knopp, R.

Challenges in UWB signaling for ad-hoc networking Multiantenna Channels: Capacity, Coding and Signal Processing

Editors: Gerard J. Foschini and Sergio Verdu, American Mathematical Society, ISBN: 082183407X , DIMACS Series in Discrete Mathematics and Theoretical Computer Science, Volume 62, November 1, 2003, pp 271-284

CURRICULUM VITAE for Younes Souilmi

Personal Data

Name	Younes Souilmi
Date of Birth	October the 6 th , 1978
Nationality	Moroccan
Address	Institut Eurecom, 2229 Route des Cretes, 06904 Sophia Antipolis (France)
Position	Ph. D. Student
Telephone	+33 (0) 4. 93.00.29 22
E-mail	souilmi@eurecom.fr

Education

Since October 2001	Ph.D. Thesis at the Eurecom Institute (Sophia Antipolis, France)/ENST Paris (France) under the supervision of Prof. Raymond Knopp. Research Topics: <ul style="list-style-type: none">-Information theoretic analysis of UWB signaling-Non-coherent receivers for UWB systems-Coding for UWB non-coherent systems-MAC protocols for adhoc UWB systems
Jan. 2001-March 2001	Doctoral studies in signal and communications at Université de Nice-Sophia Antipolis (Sophia Antipolis, France). Doctoral degree obtained with honors in July 2001.
March. 2000-July 2001	Postgraduate studies in communication systems at the Eurecom Institute (Sophia Antipolis, France). Specialization in Mobile Communications. Eurecom certificate obtained in October 2001.
Sept. 1998-March 2000	Postgraduate studies in communication systems at Telecom Bretagne (Brest, France). Engineering degree in telecommunication systems obtained in October 2001.
Sept. 1996-June 1998	Preparatory classes for French Engineering School entrance exams in Lycee Moulay Youssef (Rabat, Morocco).
June 1996	Baccalaureat S (specialized in mathematics) with honors in Lycee Moulay Youssef (Rabat, Morocco).

Work Experience

- Feb. 2004 – Present** Junior Researcher – NEWCOM project
Network of Excellence In Wireless Communications
Project B: Ultra-Wideband Communications Systems
Partners: Chalmers University, POLITO Torino, Thales, Supelec, CNIT, TUI, TUA, VUM, University of Bristol.
- Oct. 2001 – Oct 2004** Junior Researcher – ERABLE Project
“Etude de mise en réseau de terminaux avec communications directes par technique mono-canal à large bande passante, et plus particulièrement la technique UWB (Ultra Wide Band)”
National French grant
Partners: Thales Communications, MITSUBISHI, CNAM, COMSIS.
- Sept. 2003-Dec. 2003** Teaching assistant for *Digital Communications* course with Prof. Knopp at Eurecom Institute. Exercise and lab sessions.
- Sept. 2000-Jan. 2001** Six months internship at Panasonic Speech Technology Laboratory Inc., Santa Barbara, CA, USA, “Design and Implementation of a Joint Channel and Noise Equalization Algorithms for Robust Speech Recognition”. Supervisors: Luca Rigazio and J.C Junqua.
- Jan. 2001-July 2001** Project with IMRA, Sophia Antipolis, France, “Design and Performance Analysis of a Channel Equalization Algorithm Using Antenna Diversity for Mobile DVB Mobile Receiver”. Supervisor: Dirk Slock (Institut Eurecom)
-

Patents

- Souilmi Y. et al. "Methods and apparatus for blind channel estimation based upon speech correlation structure," U.S. Patent No. 6,687,672, February 3, 2004.
- Nguyen P., Rigazio L., Souilmi Y., Junqua J-C. "Method and apparatus for feature domain joint channel and additive noise compensation," JP2003303000, October 24, 2003.
- Souilmi Y. et al "Method and apparatus for feature domain joint channel and additive noise compensation," U.S. Patent No 2,002,165,712, December 7, 2002.
-

Skills

- | | |
|------------------------------|-------------------------|
| Programming Languages | C, Matlab, Maple, Latex |
| Operating Systems | Windows, Linux |
-

Languages

- | | |
|----------------|-------------------------|
| French | Fluent written and oral |
| English | Fluent written and oral |
| Arabic | Native language |
| Spanish | Beginner |
-

References

Dr Jean-Claude Junqua

AV Core Technology Development Center ACC

Matsushita Electric Industrial Co. Ltd

Phone: +81-6-6900-9676

Email: Junqua.jean-claude@jp.panasonic.com

Prof. Giuseppe Caire

Mobile Communications Departement

Institut Eurecom – Sophia Antipolis, France

Phone: +33 (0) 493002906

Email: caire@eurecom.fr

Prof. Raymond Knopp

Mobile Communications Departement

Institut Eurecom – Sophia Antipolis, France

Phone: +33 (0) 493002906

Email: knopp@eurecom.fr
